Thèse   **2011**   **Open Access**

This version of the publication is provided by the author(s) and made available in accordance with the copyright holder(s).

- -

Combination therapy and targeted drug delivery: strategies for enhanced photodynamic therapy

- -

Zuluaga Estrada, Maria Fernanda

How to cite

UNIVERSITÉ DE GENÈVE

FACULTÉ DES SCIENCES

Section des sciences pharmaceutiques
Technologie pharmaceutique

Docteur Norbert Lange

Combination Therapy and Targeted Drug Delivery:

Strategies for Enhanced Photodynamic Therapy

THÈSE

présentée à la Faculté des sciences de l'Université de Genève
pour obtenir le grade de Docteur ès sciences, mention sciences pharmaceutiques

par

Maria Fernanda Zuluaga Estrada

de

Bogota (Colombie)

Thèse N°:4339

Genève

Atelier de reproduction Repromail

2011

UNIVERSITÉ DE GENÈVE

FACULTÉ DES SCIENCES

Doctorat ès sciences
Mention sciences pharmaceutiques

Thèse de *Madame Maria Fernanda ZULUAGA ESTRADA*

intitulée :

"Combination Therapy and Targeted Drug Delivery : Strategies for Enhanced Photodynamic Therapy"

La Faculté des sciences, sur le préavis de Messieurs N. LANGE, docteur et directeur de thèse (Section des sciences pharmaceutiques), E. ALLEMANN, professeur ordinaire (Section des sciences pharmaceutiques), P. KUCERA, professeur (Ecole Polytechnique Fédérale de Lausanne – Faculté des sciences de la vie – Section des sciences de la vie - Lausanne, Suisse), et H. VAN DEN BERGH, professeur (Ecole Polytechnique Fédérale de Lausanne – Faculté des sciences de base – Institut des sciences et ingénierie chimiques – Lausanne, Suisse), autorise l'impression de la présente thèse, sans exprimer d'opinion sur les propositions qui y sont énoncées.

Genève, le 4 août 2011

Thèse - 4339 -

Le Doyen, Jean-Marc TRISCONE

N.B.- La thèse doit porter la déclaration précédente et remplir les conditions énumérées dans les "Informations relatives aux thèses de doctorat à l'Université de Genève".

A Dario et Maria Sonia

Remerciements

J'adresse tout d'abord mes remerciements à mon directeur de thèse, le Docteur Norbert Lange. J'ai été très chanceuse de travailler avec une personne comme toi, si enthousiaste pour la science, rempli de bonnes idées et toujours ouvert aux discussions scientifiques. Merci pour ton encadrement, pour m'avoir permis d'évoluer dans la recherche, pour toute la confiance que tu as mis dans mon travail et tes encouragements perpétuels. Je suis également reconnaissante de ta compréhension et ton inconditionnel soutien qui m'ont permis d'arriver à la fin à la soutenance de ma thèse.

Un grand merci au Professeur Robert Gurny de m'avoir accueillie dans son excellent groupe de recherche. Merci également à mon amie colombienne Angelica Vargas d'avoir été performante et avoir initié les collaborations entre votre laboratoire et les étudiants colombiens.

Merci à la Confédération Suisse pour m'avoir donné la bourse des étudiants étrangers pendant les deux premières années d'études et à Monsieur Lombard, représentant des étudiants boursiers de Genève.

Je remercie également Doris Gabriel de m'avoir transmis, sans réserve, toute sa connaissance sur la synthèse de conjugués et sur la PDT ainsi que pour ses conseils scientifiques incessants.

Merci aux membres du jury qui ont accepté d'évaluer mon travail de thèse : le Professeur Eric Allémann, le Professeur Pavel Kucera et le Professeur Huber van der Bergh.

Merci au support technique et administratif pour leur disponibilité et leur assiduité. Je suis particulièrement reconnaissante de Myrtha, pour m'avoir introduit la culture suisse et pour ses biscuits variés et délicieux. Aussi merci à Marco pour ses leçons de dance et ses innombrables services.

Ma gratitude s'adresse également à tous mes collègues ou ex-collègues FAGAL et FATEC avec qui j'ai vécu des moments inoubliables. Tout particulièrement avec Isabel, Sergio, Rocio, Barte, Angelica, Florence D., Magali, Adriana, Martinus, Emilie, Pol, Lutz, Marieke,

Table of Contents

Introduction

Due to the fascination of mankind for light, it has been used to treat disease for thousands of years [1-3]. Ancient civilizations employed light alone or in combination with various plant extracts for the treatment of psoriasis, vitiligo, skin cancer and other non-skin-related diseases [4]. However, the onset of modern light therapy began only about a hundred years ago pioneered by the Danish physician, Niels Finsen [5]. He found that red light can treat smallpox and ultraviolet light from the sun can cutaneous tuberculosis.

In 1900, the French neurologist, Jean Prime, reported that following oral administration of eosin intended to relief epilepsy induced dermatitis only in sun-exposed areas of skin [6]. In the same year, Oscar Raab, a German medical student working for Professor Herman von Tappeiner, noted that acridine red was more toxic to protozoan in the presence of light than in the dark [7]. Further experiments with other dyes resulted in similar observations and Raab speculated that this effect was triggered by energy transfer from light to the chemical entity and therefore mediated by fluorescence. A couple of years later, von Tappeiner and the dermatologist Albert Jesionek treated facial skin carcinomas with topically applied eosin and light [8]. Then, in 1907, von Tappeiner and Albert Jodlbauer introduced the term "photodynamic reaction" to describe these apparently fluorescence-based effects [9]. In 1909, after couple of years of hot scientific controversy, von Tappeiner, in contrast to former statements, affirmed that the presence of oxygen and the process of sensitization was more or less responsible for the photodynamic effect [10].

Today, the clinical use of this oxygen-dependent process is known as photodynamic therapy (PDT). PDT requires three elements: oxygen, light and a photosensitizer (PS) [11]. Fig. 1 illustrates the underlying principle. The PS is activated by light of an appropriate wavelength. Subsequently, it interacts with molecular oxygen or biomolecules to generate cytotoxic singlet oxygen and free radicals. Because of their short lifetime and consequently short radius of action, [12] cytotoxicity is mainly limited to the irradiated surface.
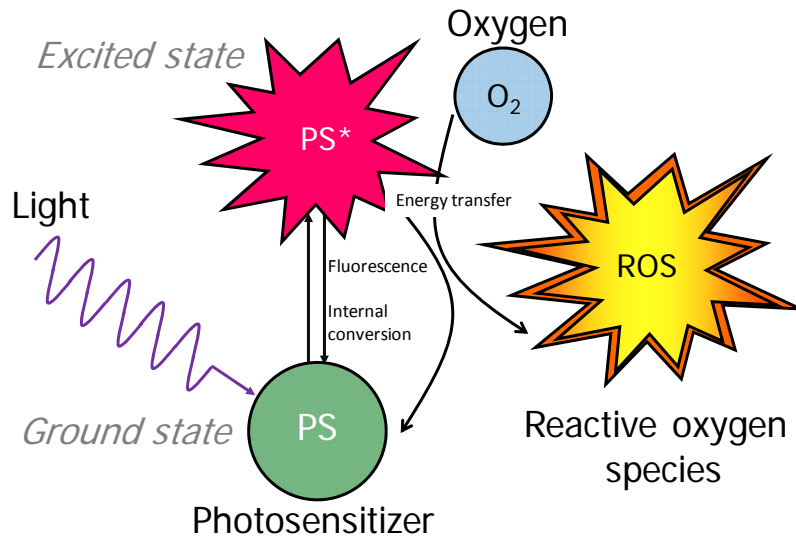
Figure 1. Mechanism of action of PDT. Light absorption promotes the activation of PS from a ground to an excited state. PS returns to the ground state through fluorescence photon emission or internal conversion. Alterternatively it can transfer energy to molecular oxygen to generate reactive oxygen species which, in turn, mediate cell and tissue damage.

PDT involves the systemic or topical administration of the PS, a period of time to allow enough PS accumulation in target tissue and maximum differentiation of PS accumulation between target tissue and normal tissue and, irradiation of the target tissue with light (Fig. 2).
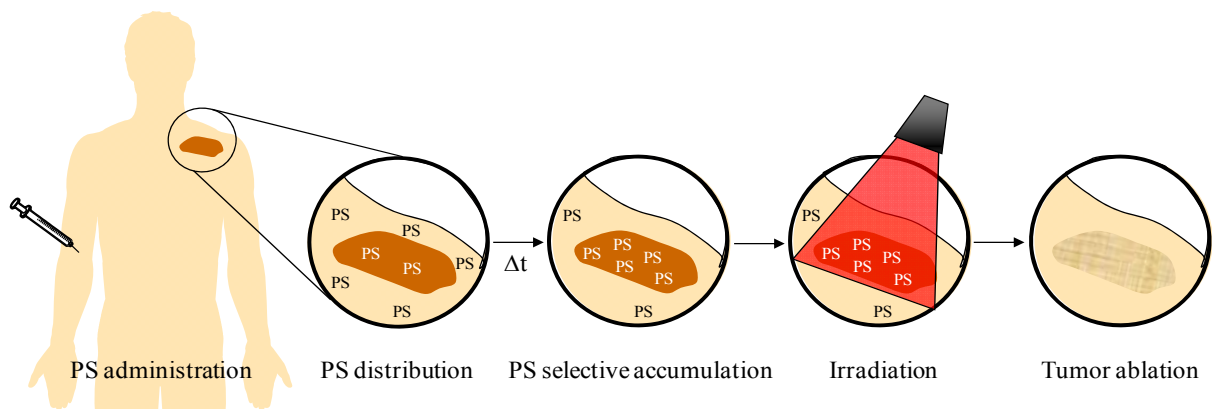
Figure 2. Typical PDT protocol. PS is administered systemically or topically. After a certain time, PS preferentially accumulates in diseased tissue and localized irradiation with light is performed. Areas that are simultaneously exposed to PS, light and oxygen (cellular or tissue oxygen) are predominantly ablated.

The efficacy of PDT strongly depends on the PS properties [4]. The ideal profile includes strong absorption in the red part of the visible spectrum, which allows for deeper light penetration; high quantum yield of triplet formation; high singlet oxygen quantum yield; low dark toxicity; and selectivity for tumor tissue versus healthy tissue.

The most extensively studied agents for PDT so far are porphyrin-based PS and precursurs thereof [3] (Fig. 3). 5-aminolevulinic acid (5-ALA) is a naturally occurring precursor in the heme biosynthetic pathway [12]. It is converted to the endogenous PS protoporphyrin IX, which can be activated by red, green and even blue light. Porphyrinoids are macrocyclic compounds with four or more pyrrole rings connected by methylen bridges [4]. According to the level of saturation of the porphyrinic macrocycle, porphyrins, chlorins and bacteriochlorins, are distinguished (Fig. 3).
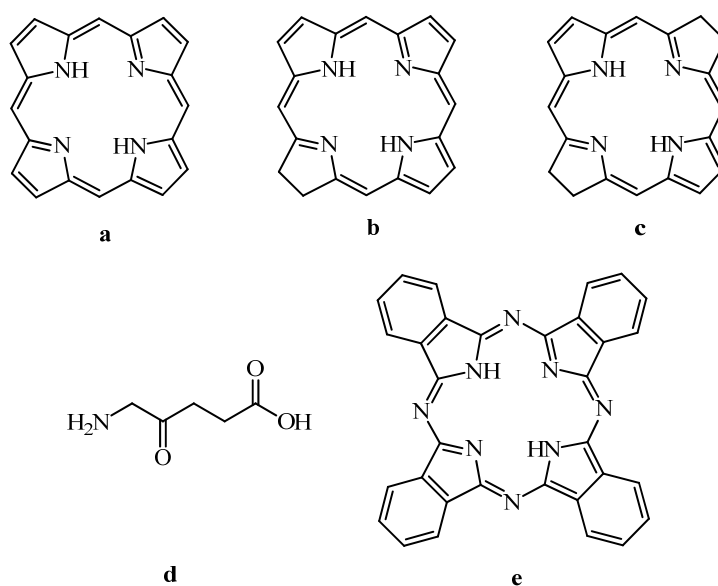
Figure 3. Skeleton of some agents used in PDT. (a) porphyrin, (b) chlorin, (c) bacteriochlorin, (d) 5-aminolevulinic acid, and (e) phthalocyanine.

Chlorins (2, 3-dihydroporphyrins) differ from their parent porphyrins by the presence of one reduced peripheral double bond causing a red shift in the so-called Q-bands and an increase in the red extinction coefficient. The tetrahydroporphyrin systems with two opposite reduced pyrrolic units are the basis for bacteriochlorins, with prominent absorption bands in the near-infrared (NIR), the 'ideal' region for PDT for maximum optical tissue penetration. Other

porphyrin-like PSs with strong absorption in the NIR region are phthalocyanines in which each pyrrolic ring is substituted by isoindol and the methylen bridges by nitrogen bridges [13].

Table 1 summarizes the most frequently used PS for the treatment of various types of cancer and other degenerative diseases.

Table 1. Some photosensitizers approved and in clinical trials [3,12,14,15]

Photosensitizer	Trade name	Potential indications	Activation wavelength
HpD, porfimer sodium	Photofrin®	Cervical, brain, esophageal, breast, head and neck, lung, bladder, and superficial gastric tumors; Bowen's disease	630 nm
m-THPC, temoporfin	Foscan®	Esophageal, prostate, pancreatic, and head and neck tumors	652 nm
BPD-MA verteporfin	Visudyne®	Age-related macular degeneration, pathologic myopia; Skin cancer	689 nm
HPPH,	Photochlor®	Skin and esophageal cancer	665 nm
Palladium-bacterio-pheophorbide	Tookad® Stake®	Prostate cancer	763 nm
5-ALA	Levulan®	Actinic keratoses; skin, head and neck, gynecological tumors; Photodetection of brain, head and neck, and bladder cancer	630 nm 375-400 nm
5-ALA-methylester	Medvix®	Actinic keratoses; skin cancer	635 nm
5-ALA benzylester	Benzvix®	Gastrointestinal cancer	635 nm
5-ALA hexylester	Hexvix®	Photodetection of bladder cancer	375-400 nm
Lutetium (III)-texaphyrin	Lutex®	Prostate, cervical, breast and brain cancer	732 nm
SnET2	Purlytin®	Kaposi's sarcoma; Skin, prostate, brain, and lung cancer	659 nm
NPe6 Taporfin sodium	Talaporfin®	Solid tumors, lung cancer, different malignancies of the skin	664 nm
Zinc phthalocyanine	CGP55847	Gastric cancer	670 nm
Silicon phthalocyanine	Pc 4®	Solid tumors from diverse origins	675 nm
Sulfonated aluminium phthalocyanine derivatives	Photosens®	Skin, breast, lung, head and neck, cervical cancer	675 nm

5-ALA, 5-aminolevulinic acid; BPD-MA, benzoporphyrin derivative-monoacid ring A; HPD, hematoporphyrin derivative; HPPH, 2-(1-hexyloxyethyl)-2-devinyl pyropheophorbide-alpha; mTHPC, meta-tetrahydroxy-phenylchlorin; NPe6, mono-L-aspartyl chlorin e6; SnET2, tin (IV) ethyl etiopurpurin.

Historically, hematoporphyrin prepared from hemoglobin was the first studied photosensitiser by Hausmann [3] and many others. This has led to the development of Hematoporphyrin derivative HpD a mixture of porphyrin-monomers, dimers and oligomers, and a partially purified version known as porfimer sodium [16].

This was the first PS to receive approval for PDT in 1999 in Canada and later in the USA and Europe, now commercialized under the name of Photofrin®. PDT with Photofrin® is indicated for patients with esophageal cancer, endobranchial non-small-cell lung cancer and high grade dysplasia in Barret esophagus. Temoporfin (Foscan®) recently got European approval for the treatment of head and neck cancer in patients who cannot be treated with other therapies. 5-ALA and its methyl- and hexyl-esters are commercialized under the names of Levulan®, Medvix® and Hexvix®, respectively. The two first PS precursors are approved for PDT of minimally to moderately thick actinic keratoses of the face and scalp in the USA and Europe. Hexvix® obtained marketing authorization in 2005 for the photodetection of urinary bladder cancer in Europe and since 2010 in the USA. Since 2001, verteporfin (benzoporphyrin derivative; Visudyne®) is indicated for the treatment of patients with predominantly classic subfoveal choroidal neovascularization (CNV) secondary to age-related macular degeneration (AMD), pathologic myopia or presumed ocular histoplasmosis in the USA and Europe.

So far, PDT of cancer or other degenerative diseases has given satisfactory and sometimes even spectacular results. However, only few of the numerous PS candidates tested preclinically have been introduced into clinical practice. Their application is restricted to specific indications. Two major reasons account for this: The suboptimal therapeutic outcome and low drug selectivity. The present work addresses these drawbacks using two different strategies: combination therapy (Part A, chapters 1 and 2) and targeted drug delivery (Part B, chapters 3, 4 and 5).

PART A. COMBINATION THERAPY

Chapter 1. Combination of Photodynamic Therapy with Anti-Cancer Agents

Published in Current Medicinal Chemistry 15(17), 1655-73, 2007

Because cancer involves multiple pathological processes [17], the use of combination therapies with different mechanisms of action might offer potential advantages. Several

preclinical studies and some clinical trials suggest that the use of PDT in combination with established treatments or with newly-developed modalities may be beneficial compared to the individual modalities [18-20]. To understand the rational of PDT in combination with other therapies, the first chapter introduces the reader to the main photobiological aspects of PDT, and then reviews the preclinical and clinical work on PDT in combination with other pharmacological approaches for the treatment of cancer including chemotherapy, angiogenesis inhibitors and immunotherapy.

Chapter 2. Synergies of VEGF Inhibition and Photodynamic Therapy in the Treatment of Age-related Macular Degeneration

Age related macular degeneration is the leading cause of irreversible central vision loss in the Western world in people older than 50 years of age [21]. Two distinct types of AMD are known as the dry and wet form of this disease [21]. In most cases disease onset starts with the dry form which may or may not develop into the wet form. In the dry form of the disease the retinal pigment epithelium less efficiently removes waste material and the so-called drusen develop. The induced slow degeneration, then leads to central vision loss. In the wet form, neovessels from the choroid intrude the retinal pigment epithelium in a process called choroidal neovascularisation (CNV). These newly formed vessels are highly leaky, leading to extravasation of blood, which progressively disrupts visual function. In the end result, a dense fibrovascular scar is formed that may cover the entire macular area.
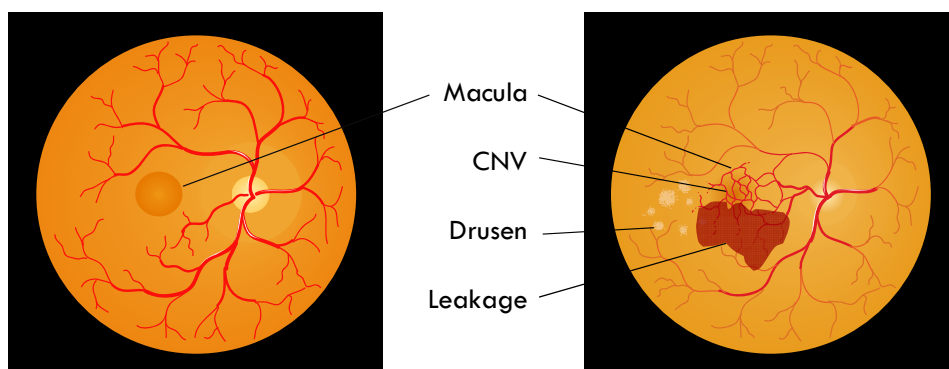
Figure 4. Squematic representation of retinal photographs. The left image corresponds to a healthy retina. The right image to the wet AMD characterized by CNV, sometimes drusen and, leaking fluid and blood.

While there is no treatment for the dry form, the wet form can currently be treated with three different therapeutic approaches: thermal laser, PDT and Anti-VEGF therapy [22]. PDT using a liposomal formulation of BPD-MA has shown to stabilize or slow vision loss [23]. However, inflammation, hypoxia as well as the expression of angiogenic factors including VEGF-A have been reported after PDT. In analogy with PDT in combination with conventional cancer treatments, we hypothesized that the combination of PDT and VEGF-A inhibiting agents would have a potential synergistic effect for the treatment of CNV and alter the progression of the disease. This chapter examines quantitatively the angiogenic response after PDT in the chick chorioallantoic membrane (CAM) model. Furthermore, the impact of an anti-VEGF agent on CAM vascularization subsequent to PDT is investigated.

PART B. TARGETED DRUG DELIVERY

In addition to their high lipophilicity, which often makes their formulation challenging, most PSs present unfavorable biodistribution and lack of sufficiently selective accumulation in tumors [24]. As a consequence, either partial or excessive destruction at the treated site (collateral damage to vital structures), long-lasting skin photosensitivity and, occasional systemic and metabolic disturbances is observed. Novel drug delivery systems are intended to circumvent these drawbacks. They take advantage of some unique characteristics of pathological tissues to increase the selectivity of PS to target tissue [18]. For instance, high to moderate molecular weight carriers such as liposomes [25], nanoparticles [26,27], low-density lipoproteins [28], micelles, and polymeric conjugates [29,30], can passively guide PS through the leaky vasculature of tumors. Once they have reached the target site a reduced clearance due to the impaired lymphatic drainage further increases the accumulation in abnormal tissues [31]. Another approach to enhance selectivity is to target upregulated cancer markers by the use of peptides [32], antibodies [33,34] or other high affinity ligands. In this way, PS is carried directly to the target by an active targeting mechanism.

Our approach consists of prodrugs that are designed to be passively delivered to the tumor and become phototoxic only as a result of the action of a pathology-related trigger (Fig. 5).
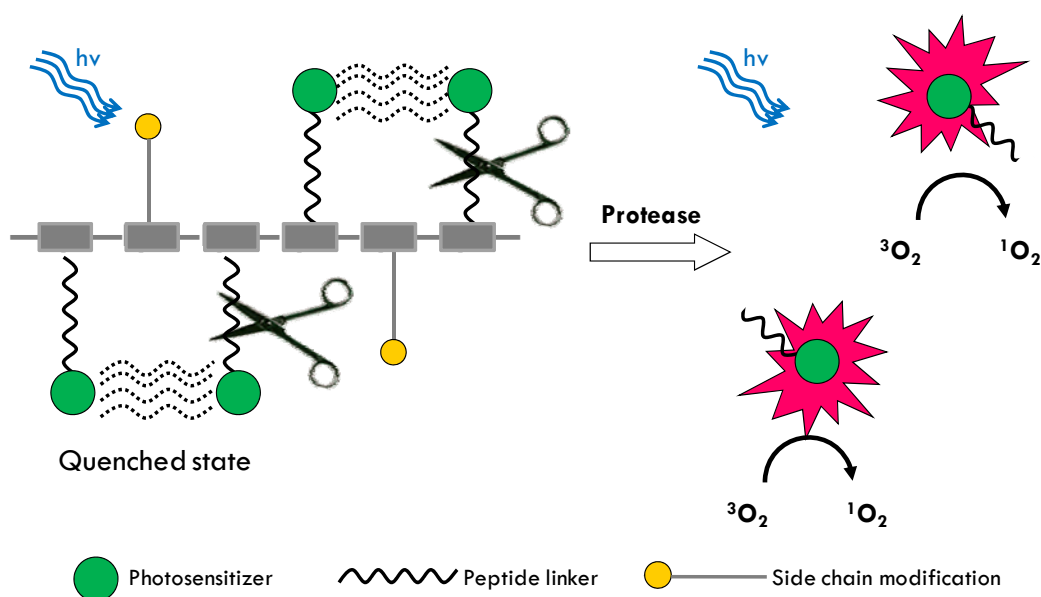
Figure 5. Principle of prodrug activation. Intramolecular energy transfer between closely positioned PS is assumed to efficiently depopulate irradiation-excited states, resulting in reduced fluorescence and energy transfer to molecular triplet oxygen. Enzymatic cleavage leads to the release of PS-peptidyl fragments, which, in turn, are free to diffuse and fully photoactive again.

In these prodrugs multiple photosensitizer units are covalently coupled to a polymeric backbone via protease-cleavable peptide linkers. Interaction between closely positioned PS moieties induces inter PS quenching. These initially non-photoactive compounds become more fluorescent and phototoxic after tumor specific enzymatic digestion of the peptide linkers and subsequent release of now active compounds.

Chapter 3. Urokinase-plasminogen-activator sensitive polymeric photosensitizer prodrugs: Design, synthesis and in vitro evaluation*

Published in Journal of Drug Delivery, Science and Technology, 19(1), 15-14, 2009

*The author of this thesis partially contributed to this manuscript (fluorescence increase after urokinase digestion, cellular activation and phototoxicity test).

Proteolytic degradation of the extracellular matrix is crucial for solid cancer development, invasion, and metastasis. During this process increased activities of several protease families,

such as metallo-, serine-, aspartyl, and cysteine proteases play important roles [35]. Of particular interest in this context is the extracellular serine protease urokinase-like plasminogen activator (uPA), which generates plasmin from the extracellular zymogen plasminogen [36]. Abundant expression of uPA in prostate cancer (PC) [37] makes this enzyme an interesting candidate for tissue-specific prodrug activation and highly selective PDT for this indication.

The deveolpment of a uPA-sensitive polymeric prodrug for PDT using an established minimal substrate serine-glycine-argenine//serine-alanine (SGR/SA), which is cleavable by uPA, is presented in this chapter. Different modifications to the moieties attached to the polymeric backbone were studied to evaluate their influence on fluorescence and singlet oxygen quenching capacity as well as on the restoration of phototoxicity upon proteolytic cleavage. The mechanism of cellular uptake, intracellular fate, and enzymatic activation on uPA-expressing DU-145 and PC-3 cells of prostate cancer origin were investigated for the most promising candidates.

Chapter 4. Modulating prostate cancer targeting of protease sensitive photosensitizer prodrugs by side chain modifications of the polymeric carrier

Submitted to Molecular Pharmaceutics

In the previous chapter it was shown that certain positively charged polymeric backbone carriers with selected side chains give a good compromise with respect to fluorescence quenching, ROS quenching, and solubility. The PS conjugates in combination with light proved to be efficient in killing prostate cancer cells expressing uPA *in vitro*. However, in a murine model for prostate cancer such compounds showed suboptimal biodistribution.

The current chapter is dedicated to the optimization of pharmacokinetics and biodistribution of the conjugate without significant loss of quenching capacity and solubility. New chemical modifications to the polymeric backbone induced changes in the molecular size and also in the net charge of the conjugates. These new conjugates were injected into PC-xenografted nude mice and the biodistribution was followed by fluorescence *in vivo* imaging. Preliminary PDT studies in the same model are also presented.

Chapter 5. Enhanced Selectivity of Photodynamic Therapy for the Treatment of Prostate Cancer

To be submitted to Cancer Research

Men diagnosed with low-risk PC confront a big dilemma of choice between radical prostectomy and active surveillance [38]. The first option provides cancer control but is frequently accompanied with genitourinary morbidity. In the second option, sexual and urinary function is preserved in exchange for psychological and health care cost. In recent years, focal therapy has been introduced as an intermediate option between these two extreme choices [39]. Ideally, in such therapy, cancer foci are selectively eliminated and, hence, normal prostate tissue and surrounding organs remain preserved. PDT is one of the modalities with the potential to achieve both: appropriate therapeutic outcome and minimal or no secondary effects [40]. However, clinical studies so far show that selectivity of PDT is still one of the features that has yet to be improved for this modality to be considered as standard of care for a focal treatment of PC or as salvage after PC recurrence.

In the previous chapter a prodrug with dual functionality, visualization of lesions in response to uPA activity and selective cytotoxicity effect upon irradiation with light, has been optimized. This chapter describes its phototoxic effect *in vitro* in PC-3 cancer cells and the *in vivo* response to PDT in comparison with administration of prodrug alone or light alone in a previously non-described *in vivo* model in PDT for PC using bioluminescent xenografts enabling non-invasive monitoring of the therapeutic outcome.

References

1. Ackroyd, R.;Kelty, C.;Brown, N.;Reed, M. The history of photodetection and photodynamic therapy. *Photochem. Photobiol.*, **2001**, *74*, 656.
2. Daniell, M. D.;Hill, J. S. A history of photodynamic therapy. *Aust. N. Z. J. Surg.*, **1991**, *61*, 340.
3. Dolmans, D. E. J. G. J.;Fukumura, D.;Jain, R. K. Photodynamic therapy for cancer. *Nat. Rev. Cancer*, **2003**, *3*, 380.
4. Sternberg, E. D.;Dolphin, D.;Bruckner, C. Porphyrin-based photosensitizers for use in photodynamic therapy. *Tetrahedron*, **1998**, *54*, 4151.
5. Finsen, N. R. *Phototherapy*. (Edward Arnold, 1901).
6. Prime, J. *Les accidents toxiques par l'eosinate de sodium*. (Jouve and Boyer, 1900).

7.   Raab, O. Uber die Wirkung fluoreszierender Stoffe auf Infusorien. *Zeitung Biol.*, **1900**, *39*, 3.

8.   von Tappeiner, H. J., A. . Therapeutische versuche mit fluoreszierenden stoffen. *Muench Med.Wochenschr.*, **1903**, *47*, 3.

9.   von Tappeiner, H. J., A. *Die sensiblilisierende Wirkung fluoreszierender Substanzen. Gesamte Untersuchungen uber die photodynamische. Erscheinerung.* (Voger, F. C., 1907).

10. Szeimies, R.-M.;Dräger, J.;Abels, C.;Landthaler, M. in *Comprehensive Series in Photosciences* Vol. Volume 2 (eds Rolf-Markus Szeimies Piergiacomo Calzavara-Pinton & Ortel Bernhard) 3 (Elsevier, 2001).

11. Bonnett, R.;Martinez, G. Photobleaching of sensitisers used in photodynamic therapy. *Tetrahedron*, **2001**, *57*, 9513.

12. Hopper, C. Photodynamic therapy: a clinical reality in the treatment of cancer. *Lancet Oncol.*, **2000**, *1*, 212.

13. Rio, Y.;Salome Rodriguez-Morgade, M.;Torres, T. Modulating the electronic properties of porphyrinoids: a voyage from the violet to the infrared regions of the electromagnetic spectrum. *Org. Biomol. Chem.*, **2008**, *6*, 1877.

14. Brown, S. B.;Brown, E. A.;Walker, I. The present and future role of photodynamic therapy in cancer treatment. *Lancet Oncol.*, **2004**, *5*, 497.

15. Huang, Z. A review of progress in clinical photodynamic therapy. *Technol Cancer Res Treat*, **2005**, *4*, 283.

16. Dougherty, T. J. A brief history of clinical photodynamic therapy development at Roswell Park Cancer Institute. *J. Clin. Laser Med. Surg.*, **1996**, *14*, 219.

17. Fitzgerald, J. B.;Schoeberl, B.;Nielsen, U. B.;Sorger, P. K. Systems biology and combination therapy in the quest for clinical efficacy. *Nat. Chem. Biol.*, **2006**, *2*, 458.

18. Dickson, E. F. G.;Goyan, R. L.;Pottier, R. H. New directions in photodynamic therapy. *Cell Mol. Biol.*, **2002**, *48*, 939.

19. Bradley, J.;Ju, M.;Robinson, G. S. Combination therapy for the treatment of ocular neovascularization. *Angiogenesis*, **2007**, *10*, 141.

20. Dougherty, T. J. *et al.* Photodynamic therapy. *J. Natl. Cancer Inst.*, **1998**, *90*, 889.

21. Pauleikhoff, D. neovascular age-related macular degeneration: Natural History and Treatment Outcomes. *Retina*, **2005**, *25*, 1065.

22. Kulkarni, A. D.;Kuppermann, B. D. Wet age-related macular degeneration. *Adv. Drug Deliv. Rev.*, **2005**, *57*, 1994.

23. Treatment of age-related macular degeneration with photodynamic therapy study, g. Acute severe visual acuity decrease after photodynamic therapy with verteporfin: case reports from randomized clinical trials-- TAP and VIP report no. 3. *Am. J. Ophthalmol.*, **2004**, *137*, 683.

24. Hsi, R. A.;Rosenthal, D. I.;Glatstein, E. Photodynamic therapy in the treatment of cancer: current state of the art. *Drugs*, **1999**, *57*, 725.

25. Derycke, A. S.;de Witte, P. A. Liposomes for photodynamic therapy. *Adv. Drug Deliv. Rev.*, **2004**, *56*, 17.

26. Zeisser-Labouebe, M.;Lange, N.;Gurny, R.;Delie, F. Hypericin-loaded nanoparticles for the photodynamic treatment of ovarian cancer. *Int J Pharm*, **2006**, *326*, 174.

27. Vargas, A.;Eid, M.;Fanchaouy, M.;Gurny, R.;Delie, F. In vivo photodynamic activity of photosensitizer-loaded nanoparticles: formulation properties, administration parameters and biological issues involved in PDT outcome. *Eur. J. Pharm. Biopharm.*, **2008**, *69*, 43.

28. Jori, G.;Reddi, E. The role of lipoproteins in the delivery of tumour-targeting photosensitizers. *Int. J. Biochem.*, **1993**, *25*, 1369.

29. Kopecek, J. Targetable polymeric anticancer drugs. Temporal control of drug activity. *Ann. N. Y. Acad. Sci.*, **1991**, *618*, 335.

30. Hamblin, M. R. *et al.* Polycationic photosensitizer conjugates: effects of chain length and Gram classification on the photodynamic inactivation of bacteria. *J. Antimicrob. Chemoth.*, **2002**, *49*, 941.

31. Maeda, H.;Wu, J.;Sawa, T.;Matsumura, Y.;Hori, K. Tumor vascular permeability and the EPR effect in macromolecular therapeutics: a review. *J. Control Release*, **2000**, *65*, 271.

32. Schneider, R. *et al.* Recent improvements in the use of synthetic peptides for a selective photodynamic therapy. *Anticancer Agents Med. Chem.*, **2006**, *6*, 469.

33. Chen, W. R.;Huang, Z.;Korbelik, M.;Nordquist, R. E.;Liu, H. Photoimmunotherapy for cancer treatment. *J Environ. Pathol. Toxicol. Oncol.*, **2006**, *25*, 281.

34. van Dongen, G. A.;Visser, G. W.;Vrouenraets, M. B. Photosensitizer-antibody conjugates for detection and therapy of cancer. *Adv. Drug Deliv. Rev.*, **2004**, *56*, 31.

35. Dano, K. *et al.* Cancer invasion and tissue remodeling--cooperation of protease systems and cell types. *APMIS*, **1999**, *107*, 120.

36. Sidenius, N.;Blasi, F. The urokinase plasminogen activator system in cancer: recent advances and implication for prognosis and therapy. *Cancer Metastasis Rev.*, **2003**, *22*, 205.

37. Cozzi, P. J. *et al.* Evaluation of urokinase plasminogen activator and its receptor in different grades of human prostate cancer. *Hum. Pathol.*, **2006**, *37*, 1442.

38. Ahmed, H. U.;Moore, C.;Emberton, M. Minimally-invasive technologies in uro-oncology: the role of cryotherapy, HIFU and photodynamic therapy in whole gland and focal therapy of localised prostate cancer. *Surg. Oncol.*, **2009**, *18*, 219.

39. Lindner, U.;Trachtenberg, J.;Lawrentschuk, N. Focal therapy in prostate cancer: modalities, findings and future considerations. *Nat. Rev. Urol.*, **2010**, *7*, 562.

40. Moore, C. M.;Hoh, I. M.;Bown, S. G.;Emberton, M. Does photodynamic therapy have the necessary attributes to become a future treatment for organ-confined prostate cancer? *B.J.U. Int.*, **2005**, *96*, 754.

PART A. COMBINATION THERAPY

Chapter 1. Combination of Photodynamic Therapy with Anti-Cancer Agents

Maria-Fernanda Zuluaga and Norbert Lange

Department of Pharmaceutics and Biopharmaceutics, School of Pharmaceutical Sciences, University of Geneva, University of Lausanne, 30 Quai Ernest-Ansermet, 1211 Geneva 4, Switzerland

ABSTRACT. Degenerative diseases such as cancer usually involve more than one pathological process. Therefore, attempts to combat such diseases with monotherapeutic approaches may not always do so efficiently. For this reason, the use of combination therapy with modalities that target different disease pathways represents an alternative strategy. Photodynamic therapy (PDT) has already been established as an alternative therapy for the treatment of various types of malignant disorders, including esophageal, lung and bladder cancer as well as other degenerative diseases. This technique involves the administration of a tumor localizing photosensitizer followed by its activation with light of a specific wavelength. In the presence of tissue oxygen, the photoactive sensitizer triggers a series of photochemical and photobiological processes that may lead to direct cancer cell damage, tumor microvascular occlusion and host immune response. Due to these multiple actions, PDT has increasingly gained recognition as a potential adjuvant for conventional cancer treatments. Several preclinical studies and some clinical trials suggest that the use of PDT in combination with established treatments or with newly-developed modalities may be of benefit as compared to the individual modalities. In this review, we briefly introduce the reader to the main photobiological aspects of PDT, and then discuss the use of PDT in combination with other pharmacological approaches for the treatment of cancer.

Keywords: Combination therapy; photodynamic therapy; chemotherapy; immunotherapy; angiogenesis inhibitors; cancer; synergies.

1. Introduction,

Most diseases of interest for contemporary drug development involve multiple, distinct pathological processes [1]. Therefore, the use of combination therapies with different mechanisms of action might offer potential advantages over a single therapy. This may explain why despite the pharmaceutical industry's crusade for single molecule blockbusters [2], combination therapies have increasingly received attention in the last few years. In this context, the ultimate goal of an association of two different therapeutic approaches is an enhancement or even synergistic effect as compared to each individual treatment without increasing the number of side effects. An extensive review on calculations of synergistic or additional effects based on experimental data has been published by Greco *et al.* [3]. Assessing the nature and intensity of agent interactions is universal and especially critical in the treatment of many human diseases. There are various approaches to determining synergy, antagonism, or additional effects of therapeutic compounds and the reader is referred to the above-mentioned reference. In the literature, most concentration effect models and curves are based on monotonically increasing effects. In clinical as well as preclinical studies, apparent toxic effects and, therefore, decreasing efficacy with increasing drug dose will make the assessment of synergy more complicated and will not be discussed in this review. Assuming that in a combinational treatment a drug is not interacting with itself, the problem of drug interaction is a three dimensional problem with the treatment efficacy as a function of two individual variables, i.e. the doses of each drug applied. In this context, most concepts are based on methodologies developed by Loewe and Muischnek in 1926 [4]. Graphically, these methodologies can be explained by so-called isobolograms (see Fig. 1). In these, each axis represents the concentration of each drug and the isoline in this plot represents the line of a given therapeutic effect, e.g. 50% growth inhibition, 25% of induction of protein expression, etc. As a prime example, Fig. 1 shows the graphical representation of such an isobologram for two hypothetical drugs that inhibit the growth of cancer cells *in vitro*. The isoline is the projection of 50% growth inhibition. From Fig. 1, it becomes clear that drugs 1 and 2 have a single effective concentration for 50% growth inhibition of 20 mg/mL and 100 mg/mL, respectively. If no interaction between both drugs exists, any combination of drug concentrations that fall on the connecting line between these two values should give a 50% growth inhibition (e.g. 10 mg /mL of Drug 1 and 50 mg/mL of Drug 2). However, if the efficacy of the combined treatment is higher or lower, the isoline for this combination should

fall under the straight line or vice versa, indicating synergy or antagonism, respectively. These graphic considerations can be put into a basic mathematical assessment approach:

$$1 = \frac{D_1}{ID_{X,1}} + \frac{D_2}{ID_{X,2}}$$

Whereas D_1 and D_2 represent the concentrations of each drug in the mixture, and $ID_{X,1}$ and $ID_{X,2}$ are the concentrations of each drug that result in X% of the inhibition when given alone. When the right hand side of the equation (equal to the combination index (CI) of Berenbaum [5] is less than 1, then synergism is indicated. However, if this value is higher than one, antagonism is indicated.
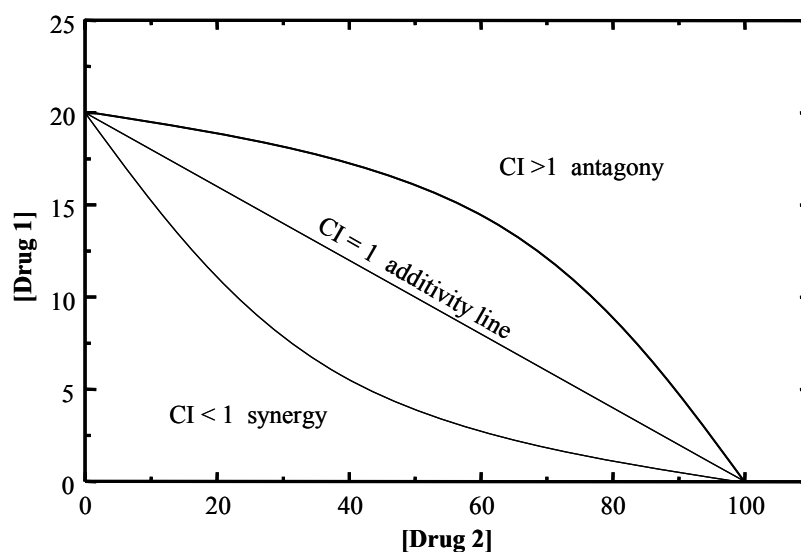
Figure 1. Determination of treatment interactions by isobolographic analysis. The predicted additivity of two drugs is calculated using a geometrical construct in which the predicted efficacy of two treatments together, to produce an identical effect, is graphically presented (additivity line). This line is constructed by connecting the two individual drug doses that produce a given effect (the isoeffect). Each point on the additivity line represents the issoeffect and correlates with a particular dose of both drugs. Each corresponding dose would give a certain level of effect, which if added together, would give the isoeffect, had the treatments occurred independently. From the isobologram, additivity of the observed treatment can be assumed if the treatment efficacy of any combination of drug concentrations falls on the additivity line. If the observed efficacy falls below the additivity line, the combined treatments are 'synergistic' and 'antagonistic' if they fall above.

Photodynamic therapy (PDT) has been recently evaluated as an adjuvant therapy to other therapeutic modalities, including surgery, hyperthermia, radiotherapy, immunotherapy, and chemotherapy as new approaches for the treatment of a variety of cancers and non-malignant disorders [6-8].

In PDT, two individually non-toxic components are combined to induce cellular effects in an oxygen-dependent manner [9]. The first component consists of a photosensitive molecule –a photosensitizer- that preferentially localizes to a target cell and/or tissue. The second involves the administration of light of a specific wavelength that activates the sensitizer. The excited sensitizer generates highly reactive singlet oxygen and other reactive oxygen species that trigger a complex cascade of photochemical reactions and photobiological events that eventually cause injury and death of targeted cells (see Fig. 2).
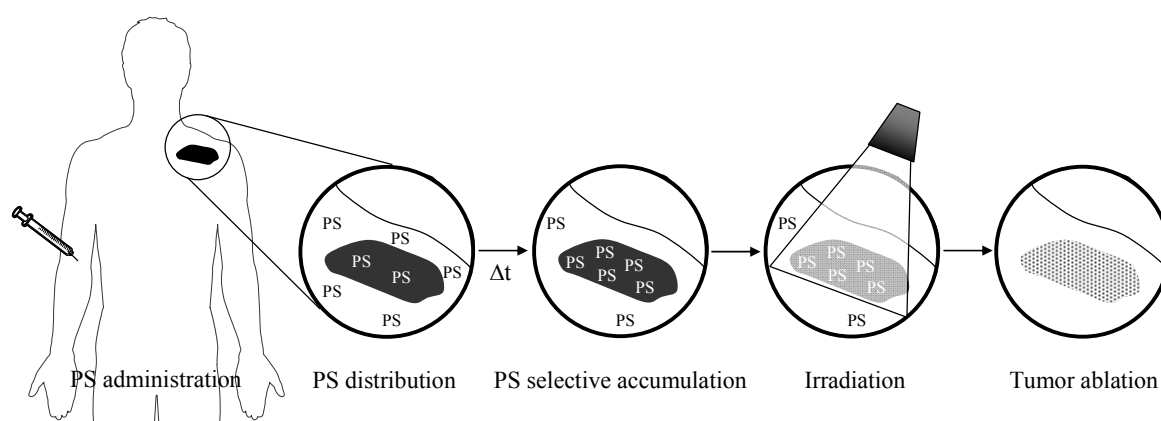
Figure 2. The principles of PDT. A photosensitizer (PS) is administered systemically (or topically). After a period to allow the PS to accumulate in the target tissue, irradiation with non-thermal light activates the PS. In the presence of cellular/tissular oxygen, the photoexcited sensitizer triggers the production of highly reactive singlet oxygen and/or other free radicals that may lead to cell/tissue damage.

In this review we first summarize the photobiological processes induced by PDT in order to provide the reader with the fundamentals for the use of PDT in a combinational approach. Then, we present state-of-the-art preclinical and clinical studies on combinations of PDT with other pharmacological approaches for cancer treatment with emphasis in four main categories: (1) PDT and chemotherapy; (2) PDT and pro-oxidant or oxidant enhancers; (3) PDT and angiogenesis inhibitors; and (4) PDT and immunotherapy.

2. Photobiology of PDT

The response of tumors to PDT depends on several factors, including those related to the experimental protocol (photosensitizer, dose, light dose and drug light interval) and those related to the tumor (cell type and its genetic and metabolic phenotype). Different characteristics of the photosensitizer, e.g. its chemical nature, hydrophobicity, overall charge, charge-to-mass ratio, and cellular uptake mechanisms, generally determine its biodistribution and intracellular localization [10]. In turn, this, together with the photosensitizer concentration, irradiation conditions and oxygen level in the tissue, will determine the biological response of tumoral cells. Upon excitation of the photosensitizer with light two principle photochemical pathways, known as Type I and Type II, will trigger this biological response (see Fig. 3).
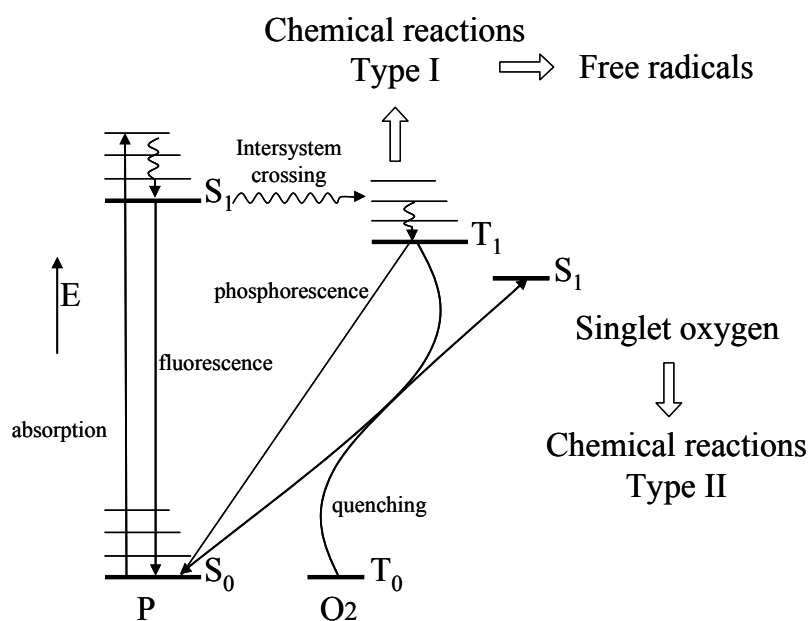
Figure 3. Modified Jablonski diagram of PDT sensitization. Irradiation with light of appropriate wavelength causes excitation of the photosensitizer from the ground state S_0 to a higher energy levels, e.g. the first excited singlet state S_1. The singlet excited photosensitizer can relax back to the ground state through fluorescence photon emission or internal conversion, or can undergo spin-forbidden intersystem crossing into the triplet state (T_1). From these two excited states (S_1, T_1) the excited sensitizer can react with a biomolecule or oxygen to produce radicals (Type I reaction). From the triplet state, the photoexcited molecule return to the ground state via phosphorescent photon emission, react with biomolecules or oxygen to produce radicals (Type I reaction) or interact with triplet ground state molecular oxygen, generating highly toxic singlet oxygen $^1O_2$ which, in turn triggers a cascade of reactive oxygen species producing reaction that can cause cellular damage.

In the Type I, the photosensitizer interacts with a biomolecule (or oxygen) resulting in hydrogen atom (or electron) transfer that leads to the production of radicals. In the Type II, singlet oxygen is generated as a result of energy transfer from the triplet exited state of the photosensitizer to the triplet ground state of molecular oxygen. Although these two pathways occur in the photosensitization process, it appears that the Type II predominates over the Type I, highlighting singlet oxygen as the principal actor for PDT-induced damage. Scheme 1, illustrates how different sorts of biomolecules react readily with this highly reactive molecule.
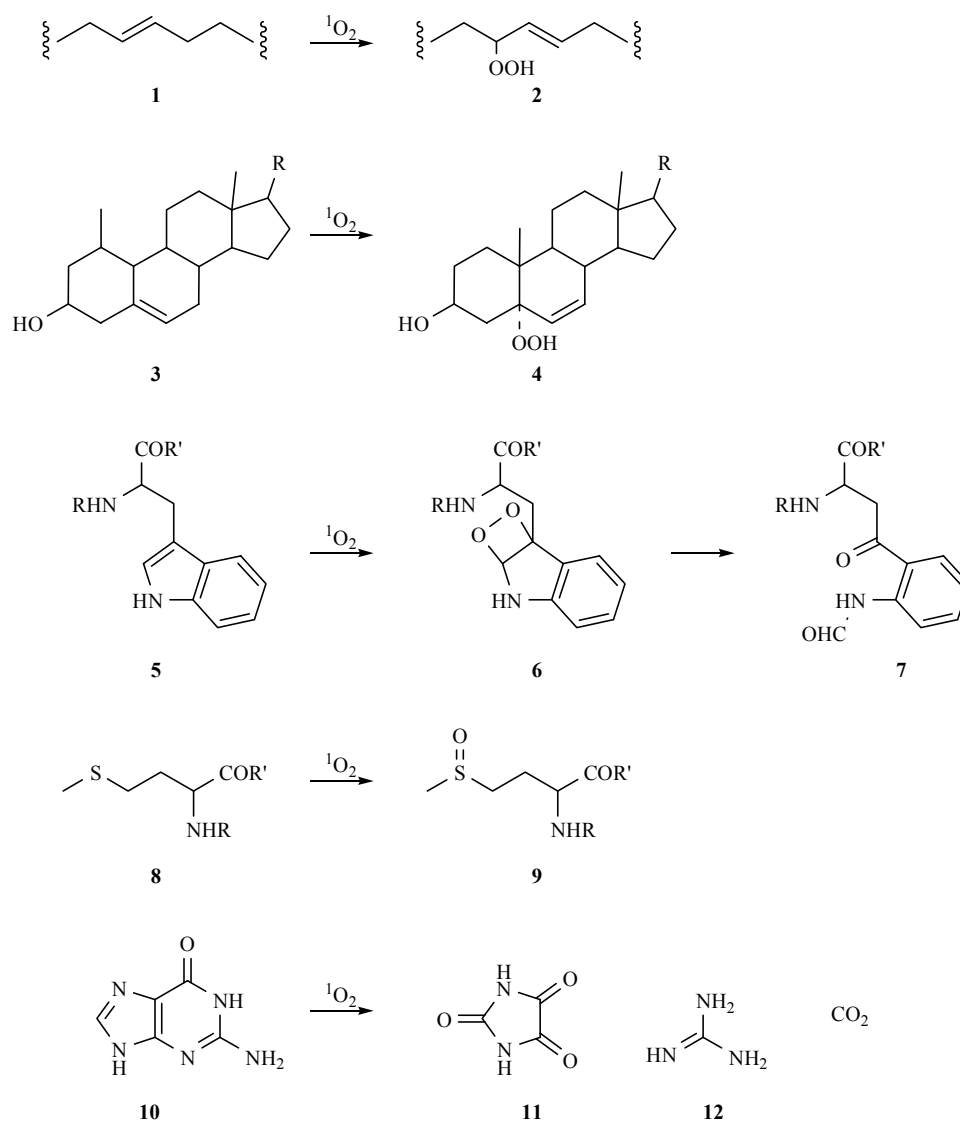
Scheme 1. Typical reactions of singlet oxygen with selected biomolecules: unsaturated lipid (1), cholesterol (3), tryptophan (5), methionine (8), and guanine (10).

Targets of PDT include tumor cells, vasculature of the tumor and normal tissue, as well as the host's immune system [6]. Therefore, the response to PDT commonly involves three main mechanisms (see Fig. **4**) whose contributions are dependent on the numerous factors previously mentioned [9-11].
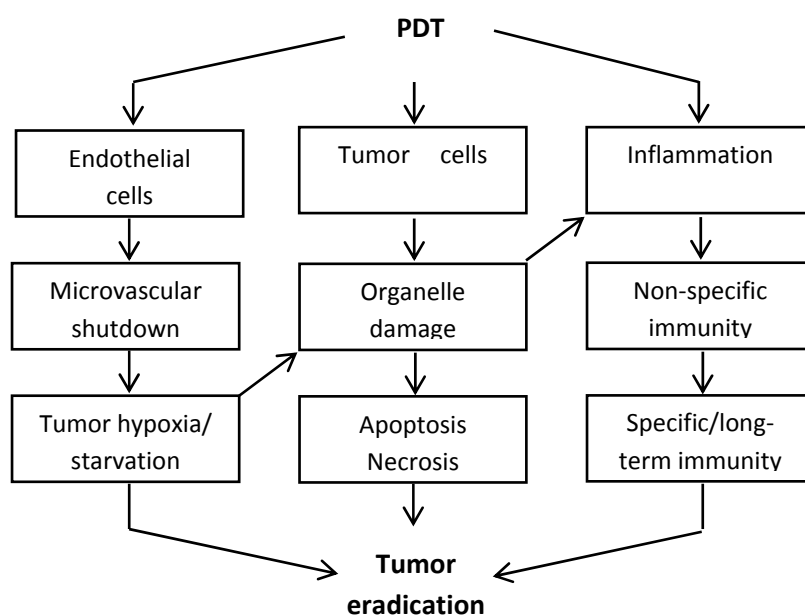
Figure 4. Mechanisms of PDT-mediated tumor destruction. PDT can kill tumor cells directly by apoptosis and/or necrosis, and indirectly through damage of the tumor associated vasculature and/or activation of the immune response against tumor cells.

First, PDT can kill tumor cells directly. Second, PDT can produce profound changes in the tumor vasculature leading to tumor infarction. Third, PDT can induce an inflammatory and immune response against tumor cells. The complex interaction of these components is required for long-term tumor control. Moreover, the response to PDT strictly depends on the localization of the photosensitizer within the cell following exposure, which, in turn, is dominated by the photosensitizer's structure and hydrophobicity. Fig. **5** shows the chemical structures of some photosensitizers that are relevant for the present review.
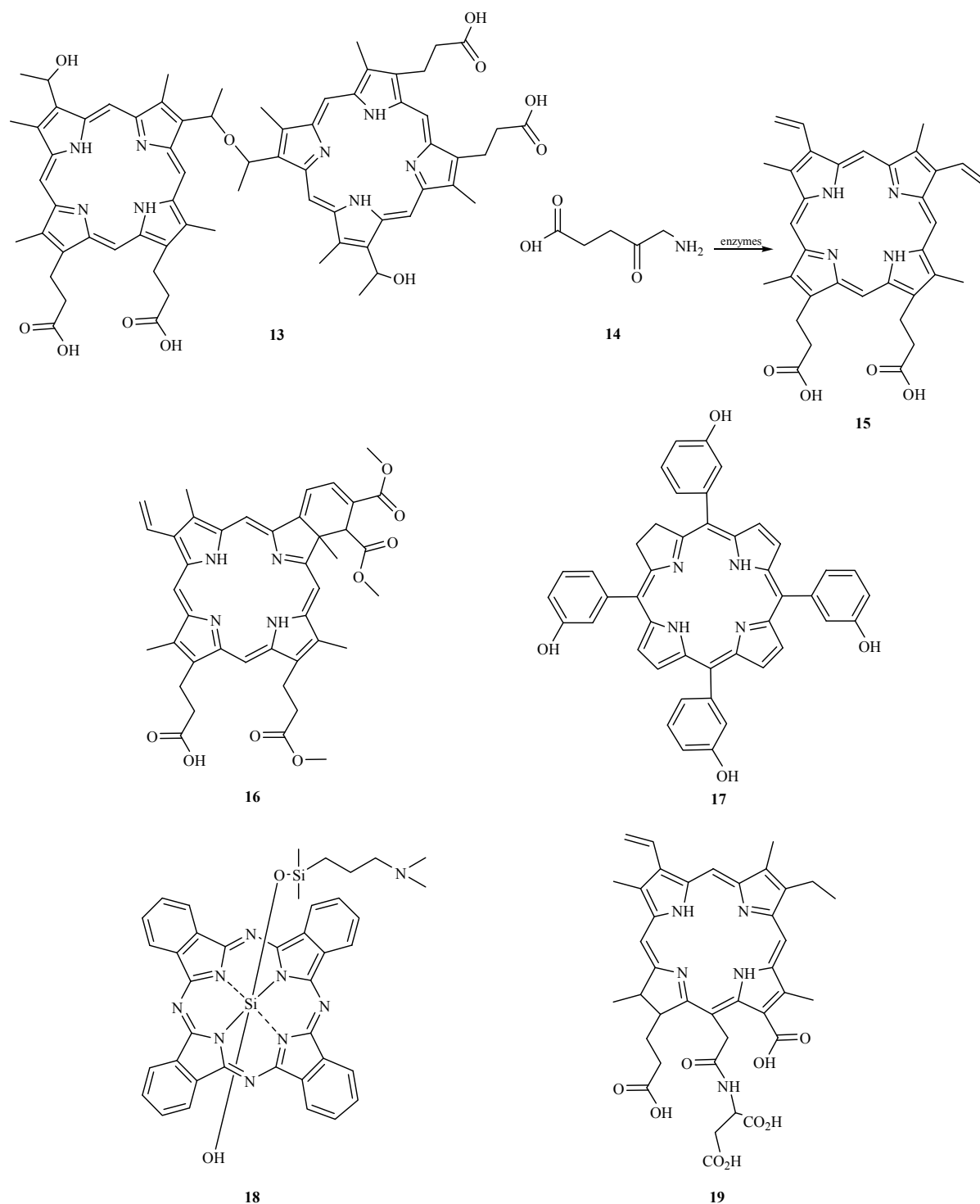
Figure 5. Structures of selected photosensitizers either clinically approved or in trials, which have been studied in combination therapy. Hematoporphyrin derivative (Photofrin®) (13), 5-aminolevulinic acid (Levulan®) ((14) is a prodrug of protoporphyrin IX (15). benzoporphyrin derivative (Visudyne®) (16), m-tetrahydroxyphenyl chlorine (Foscan®) (17), silicon phthalocyanine (18), monoaspartyl chlorine e6 (19), hexylpyropheophorbide a (20), palladium bacteriopheophorbide a (21), tin etiopurpurin (22), zinc phthalocyanine (23), lutetium texaphyrin (24), and, hypericin (25).

20

21

22

23

24

25
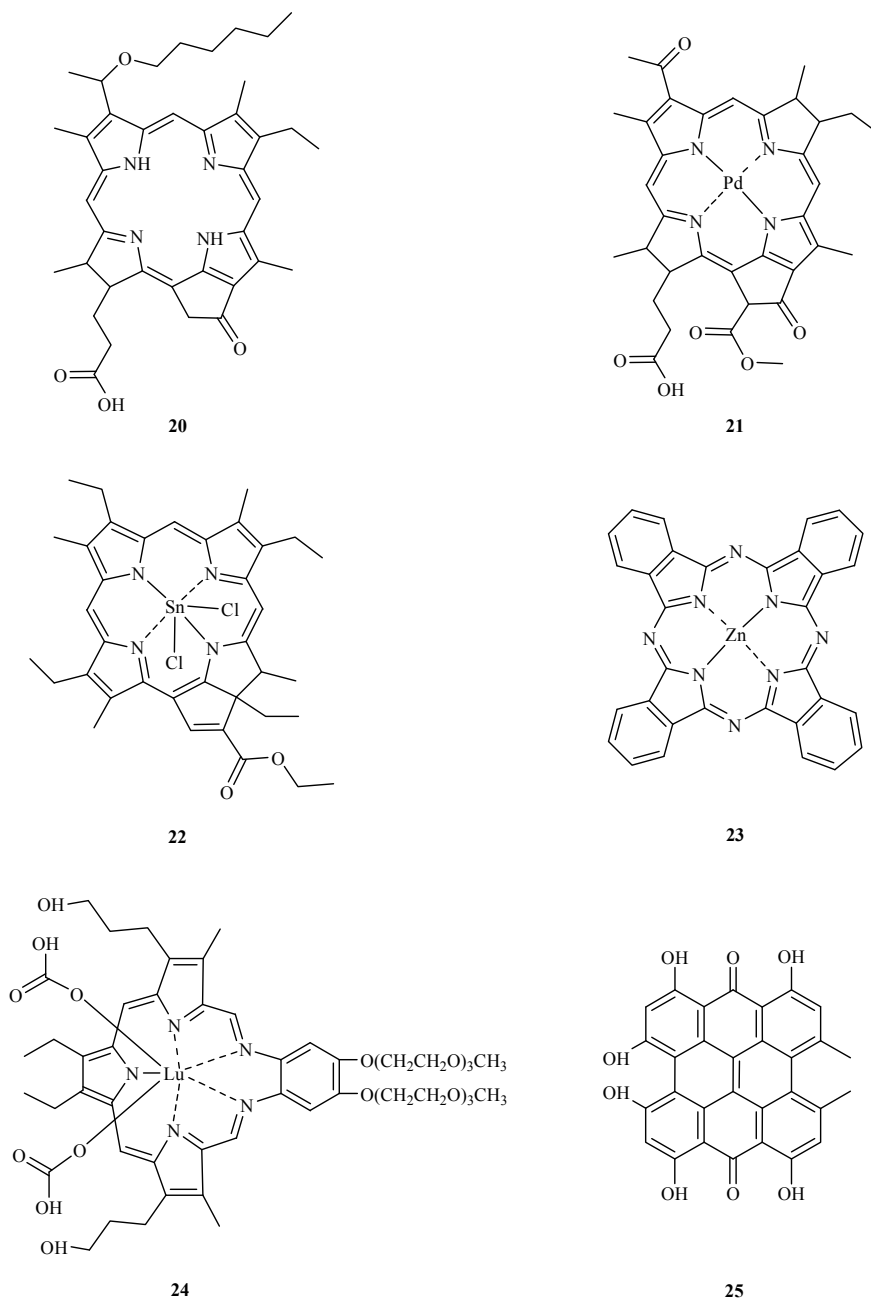
Fig. 5. Continued.

2.1. Direct damage and cell death

Photodynamic therapy *in vivo* reduces the number of clonogenic tumor cells through direct photodamage of cellular components, but complete tumor eradication is often not achieved, predominantly due to non-homogeneous distribution of the photosensitizer within the tumor and the limited availability of oxygen within the target tissue during irradiation [6,12]. Cellular damage seems to occur preferentially in the plasma membrane, membranous

organelles, and in particular, endoplasmic reticulum, golgi apparatus, lysosomes and mitochondria, microtubules, and the nucleus [10,13]. Direct photo-oxidation of membrane lipids may not be directly cytotoxic, but these oxidized lipids may serve as potent signals that trigger cell death. Lysosomal damage caused by PDT may not always be lethal since cytosolic inhibitors can inactivate enzymes released subsequent to lysosome disruption. However, this disruption may also release the photosensitizer initially localized in lysosomes, allowing its relocalization to more susceptible organelles such as the mitochondrial membrane or the nucleus. Mitochondria have been considered to be very susceptible targets for photodynamic damage because ATP, required to power cellular functions, is produced in these organelles [13]. Furthermore, mitochondrial damage has been closely related to the apoptotic effect of PDT due to the release of cytochrome c that triggers the onset of apoptosis [14,15]. As a consequence to PDT, the outer mitochondrial membrane potential has been shown to decrease, and subsequently, cytochrome c is released from the intermembrane site. Then, along with other apoptotic activating factors present in the cytoplasm, it directly activates the cascade of caspases that carry out the final stages of apoptosis. Microtubules are also vulnerable to PDT. However, irreversible depolymerization of tubulin, as well as microfilament disruption, is only observed at higher PDT doses. It has been suggested that DNA damage is not initially a major contributor to the PDT response presumably due to initial photosensitizer localization in the nuclear membrane. However, DNA lesions, such as single-strand breaks and/or alkali-labile sites, have been observed in various cells after PDT, which may imply the relocalization of the photosensitizer during illumination [10].

Tumor cells directly damaged by PDT undergo at least two types of cell death: apoptosis, and necrosis [11,13-15]. However, recent studies also suggest induction of autophagy as a third mechanism of PDT to kill cells [16]. Apoptosis is a normal physiological process controlled by intra- and extracellular signals that control tissue development and involution as well as tissue homeostasis. It is characterized by a common sequence of morphological and biochemical changes including condensation of chromatin and formation of membrane-enclosed vesicles. These vesicles confine a residual cell component, which, in turn, limits leakage of intracellular material, and thus prevents the onset of inflammation. Eventually, these apoptotic bodies are scavenged by phagocytes and cells die under immunological control. In contrast, necrosis is a violent and quick form of degeneration that results from high levels of cell damage. It is characterized by the destruction of organelles and disruption of the plasma membrane, leading to the release of intracellular content into the extracellular

compartment and tissue inflammation. Autophagy was originally characterized as a survival response to cellular stress. However, there are also experimental evidence that it is implicated as a death pathway [16]. In authophagy, cytosol and organelles become encased in vacuoles which fusionate with lysosomes for breakdown and eventual recycling of the resulting macromolecules.

Although PDT can lead to apoptosis, necrosis, autophagy, or a combination of these three outcomes, in many cases, PDT is highly efficient in inducing apoptosis [10]. However, it is not still clear if apoptosis induced by PDT *in vivo* is the result of direct damage, secondary to vascular occlusion and inflammation or a combination of both [10]. Furthermore, some studies suggest that apoptosis is not the process by which PDT-treated cells die, but rather the process by which lethally damaged cells are dismantled [14]. According to Kessel *et al.* [16], a similar role may hold for autophagy.

2.2. Vascular damage

Besides direct damage of disease associated cells, PDT can induce severe damage to tumor microvasculature leading to persistent post-PDT tumor hypoxia/anoxia and nutrient deficiency, which in turn is lethal to the tumor. The mechanism underlying the vascular occlusion by PDT differs widely with different photosensitizers [6,13,17], and has been recently reviewed by Krammer [18]. However, some of these effects include vessel constriction/collapse, macromolecular leakage, leukocyte adhesion, blood flow stasis, and thrombus formation. These are apparently linked to platelet activation and release of thromboxane, as well as damage to the vascular endothelium and production of nitric oxide by the endothelium. Endothelial cells normally produce a balance of vasodilating (i.e. prostacyclin and endothelium derived growth factors) and vasoconstrictive (endothelin-1) mediators that maintain a healthy vascular tone. PDT exposes the basement membrane to the blood serum, inducing cascades of eicosanoids and other inflammatory agents that switch the balance towards vasoconstriction. Platelet and neutrophils adhere to the vessel wall, roll toward the constriction and aggregate, at which point they migrate into the surrounding tissues following chemokine gradients. Conversely, expression of potent angiogenic factors, such as vascular endothelial growth factors (VEGF), cyclooxygenase-2 (COX-2), and metalloproteinases (MMPs), can be upregulated during PDT [9,19-21]. VEGFs are endothelial-cell-specific mitogens and survival factors that also cause increased vascular

permeability and recruit progenitor endothelial cells from the bone marrow [22]; COX-2 is an inducible isoform of prostaglandin-endoperoxide synthase considered an early response gene involved in inflammation and mitogenesis that mediates the production of prostaglandins (PG), which are powerful angiogenic mediators [23]; MMPs are zinc-containing endopeptidases that function in both physiological and pathological conditions, and are involved in tumor angiogenesis, invasion, and metastasis [24]. Although the mechanism involved in the upregulation of these three types of molecules is not completely clear, oxidative stress and tumor tissue hypoxia induced by PDT are thought to activate a number of transcription factors and signaling pathways that regulate their transcription [19,20,25]. The hypoxia inducible factor (HIF)-1α induced by PDT has been closely related to the activation of the *VEGF* gene [19], while the nuclear transcription factor (NF)-κB seems to play a major role in the PDT-induced COX-2 [20,25]. PDT has been shown to increase the expression of the extracellular matrix metalloproteinase inducer (EMMPRIN), and to block the tissue inhibitor of metalloproteinase (TIMP)-1, which results in an efficient stimulation of the production of MMPs [26].

2.3. Inflammatory and Immune effect of PDT

Photodynamically induced changes in the plasma membrane and the membrane of cellular organelles can trigger different events with far-reaching consequences [6,27]. PDT stimulates multiple signal transduction pathways simultaneously for both cell death and survival. Thus, cell fate is likely to be determined by the interaction of these pathways [10]. In fact, PDT is presumed to induce the release of a variety of lipid and secondary messengers (phospholipases C, A2, sphingomyelinase, PGE_2, NO), as well as calcium ions from intracellular stores. As a result, several protein kinase signaling cascades are activated, some of which seem to lead to cell death through apoptosis and inflammatory/immune responses, whereas others seem to promote cell survival. PDT is also a strong inducer of the expression of a range of stress response genes that are thought to enhance survival after oxidative stress through regulation of apoptotic cell death. Upregulation of glucose-regulated proteins, such as GRP78, can either protect or sensitize cells exposed to PDT, depending on the subcellular localization of the photosensitizer. Furthermore, the expression of cytokines - tumor necrosis factor (TNF); interleukin (IL) and granulocyte-colony-stimulating factor (G-CSF) - may promote either cell death or cell survival or an immune response *in vivo*.

PDT-mediated immune reactions are presumably a key contributor to final tumor eradication. In addition, differences in the nature and intensity of the inflammatory response between normal and cancerous tissues may contribute to the selectivity of PDT-induced damage [6,9]. Although inflammation is frequently accompanied by immunosuppressive effects, PDT appears to be able to tip the balance of agents that regulate the immune system towards either activation or suppression by the release of specific cytokines [13]. This is probably controlled by many complex factors including, but not limited to, the nature of the photosensitizer, light dose, and dose rate [13]. The mechanism by which PDT induces tumor immunity has been suggested by Korbelik [28]. The inflammatory signaling accompanied by the release of large quantities of cell debris, cytokines and other chemotactic agents, initiates and maintains the recruitment of leukocytes from the blood and amplifies their activity. Within minutes of light treatment, a massive regulated invasion of neutrophils is produced. Neutrophils can remain within tumor blood vessels and degranulate, releasing myeloperoxidases, lysosomal enzymes and toxic oxygen radicals that destroy endothelial and tumor cells. As neutrophils die, the release of their cellular contents induces chemotaxis of new waves of immune cells. Mast cells flood into the damaged tissue and release granules containing vasoactive agents and cytokines. In addition, monocytes and macrophages invade, proliferate, collect cell debris, and preferentially recognize and destroy pockets of surviving tumor cells. At the end of the inflammatory response, macrophages and monocytes can secrete immunosuppressive factors as a result of a transient reduction in the delayed-type contact hypersensitivity response, which downregulates the response and may hamper any future, specific immune response. Otherwise, macrophages and/or dendritic cells can be prompted to phagocytize large numbers of cancer cells damaged through photodynamic action. These tumor-associated cells serve as antigen presenting cells processing tumor-specific peptides and presenting them on their membranes in the context of major histocompatibility class II molecules. Presentation of tumor peptides, accompanied by intense accessory signals, creates conditions for the recognition of tumor antigens by CD4$^+$ helper T lymphocytes. These lymphocytes rapidly expand and become activated and, in turn, sensitize cytotoxic CD8$^+$ T cells to tumor-specific epitopes leading to fully developed tumor immunity. It is reported that B lymphocytes and natural killer cells (NK) also become activated and may contribute to PDT-elicited immune responses, but the role of these cells is still unclear [6]. Specific immune cells can, under reduced tumor burden, eliminate small foci of viable cancer cells that have escaped other PDT mediated anti-tumor effects [27]. Furthermore, their activity is not limited to the original PDT

treated site, but can include disseminated and metastatic lesions of the same cancer [28], which may be decisive in attaining long-term tumor control.

Due to its multiple physiological effects, PDT may be successfully combined with a variety of pharmacological protocols for achieving substantial gains in tumor destruction and long-term tumor control.

3. PDT and Chemotherapy

Cisplatin, doxorubicin and mitomycin C are three of the most extensively studied chemotherapeutic drugs used as single agents in the management of various cancers [29]. It is believed that their main mechanism to kill cancer cells relies on their binding to DNA and interfering with subsequent processes in cell replication, eventually leading to cell death. Despite the wide use of these drugs, their dose-limiting toxicities and the emergence of resistance have lead to the search for new approaches that minimize these two drawbacks. In this context, some *in vitro* and *in vivo* studies have revealed promising results. One of the first studies was performed by the group of Nahabedian [30]. They treated nude mice bearing RIF-1 and EMT-6 tumors with cisplatin, doxorubicin, hematoporphyrin derivative-mediated (HpD)-PDT or a combination of each drug and PDT. The RIF-1 tumors were only sensitive to doxorubicin and no additional anti-tumor effect was observed when combined with PDT. On the other hand, the EMT-6 tumors were moderately sensitive to PDT and mildly sensitive to both cisplatin and doxorubicin. While combining PDT and cisplatin did not result in an enhanced anti-tumor effect, the combination PDT and doxorubicin significantly enhanced the effect of PDT alone. The authors suggested that this enhancement corresponds either to an increased activity of doxorubicin alone, due to a photochemical reaction of the drug during PDT or to a secondary effect to the mild hyperthermia generated by irradiation. Although, their results did not evidence synergistic effects, a good tolerability for the combination regimen was demonstrated. Later, Canti *et al.* [31] administered the same cytotoxic agents followed by PDT with aluminum phthalocyanine (AlS$_2$Pc) to mice bearing L1210 leukemia and P388 lymphoma. Non-therapeutic drug doses were used. As expected, low doses of either doxorubicin or cisplatin were ineffective; however, in combination with PDT, a significant additive anti-tumor effect was observed. Furthermore, the combination of light treatment and drugs did not result in increased anti-tumor activity. The tumoricidal effect of interstitial PDT using Photofrin® combined with mitomycin C was also investigated in RIF-1 tumors by Baas

and co-workers [32]. While each treatment alone induced a small but significant tumor growth delay, the combination of mitomycin C with PDT further increased this delay. In these experiments, the light dose to obtain the same effect of Photofrin® alone was reduced by a factor of two when the cytostatic agent was given prior to PDT. In contrast, mitomycin C given immediately after illumination did not improve the effect of PDT. In another study, different photosensitizers, meso-tetrahydroxyphenylchlorin (*m*-THPC), bacteriochlorin a (BCA), and Photofrin® were compared in terms of tumor regrowth and cures in combination with mitomycin C [33]. The combination of mitomycin C with either *m*-THPC or BCA without illumination was not significantly different from the anti-neoplastic agent given alone. However, in agreement with the previously performed study, the use of *m*-THPC-PDT combined with mitomycin C allowed considerable reduction in the light or photosensitizer dose without affecting the therapeutic effect compared to *m*-THPC-PDT alone. For *m*-THPC-PDT, however, mitomycin C given immediately after illumination was equally effective as mitomycin C given 15 minutes before illumination, in contrast to the results found for PDT with Photofrin®, where the maximum benefit from the combination was obtained when the chemotherapeutic drug was given before illumination. This difference can be attributed to vascular occlusion during PDT with Photofrin®, which inhibits the access of mitomycin C to the tumor mass. BCA-PDT combined with mitomycin C did not result in a greater tumor response compared with PDT alone when the photosensitizer was given 15 minutes before illumination. However, when BCA was injected 1 hour before illumination, the association with mitomycin C resulted in a significant decrease in regrowth. Because both photosensitizer and chemotherapeutic agents were injected at the same time in these experiments, the BCA distribution within the tumor tissue was probably suboptimal for the shortest time interval.

On the other hand, several studies have evaluated the combination of anti-neoplastic drugs and PDT in various *in vitro* cell culture models [34-36] using different techniques to assess either cell viability or cell proliferation after treatment. The group of Kopecek [37] has assessed the interaction between doxorubicin and meso-chlorin e_6 monoethylene diamine (Mce$_6$) on human ovarian epithelial carcinoma OVCAR-3 *in vitro*. According to the isobolographic approach (see Fig. 6), doxorubicin and Mce$_6$-PDT appeared to act independently (additively) at doses above their ED$_{50}$ and synergistically when both agents were administered at 50% of their ED$_{50}$. Both the dose and effect isobole analyses confirmed the continuous action of doxorubicin, in contrast to the single effect of Mce$_6$-PDT, which is consistent with their suggested mechanisms. However, because *in vitro* studies do not allow

the assessment of either vascular or inflammatory/immune effects of PDT, these findings do not discard multiple mechanisms when Mce_6 is used as photosensitizer. In fact, this drug is one of the examples of a photosensitizer causing vascular damage leading to stasis shortly after the initiation of light treatment [17].
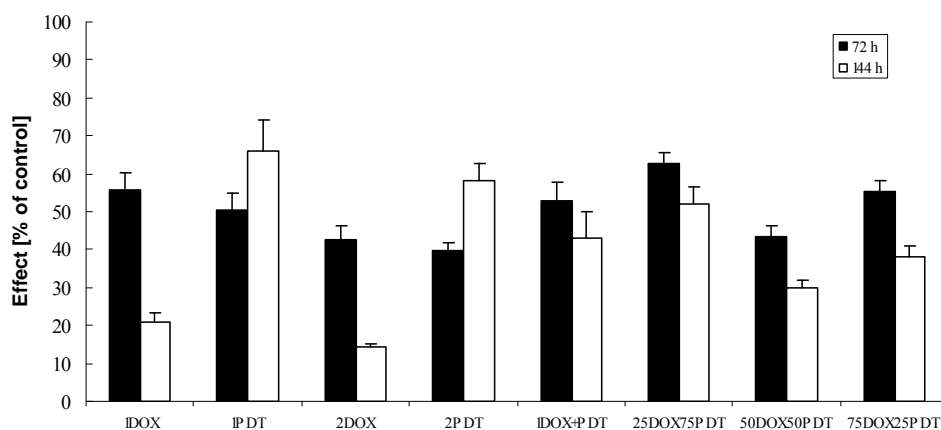
Figure 6. Dose-addition isobole analysis for the interaction between doxorubicin and PDT with Mce_6. MTT assay 72- and 144-hour assays. One ED_{50} doxorubicin (1DOX) and one ED_{50} Mce_6-PDT (1PDT) and twice the ED_{50} of doxorubicin (2DOX) and Mce_6-PDT (2PDT) are depicted for comparison. The expected results for the combination of 50% ED_{50} doxorubicin with 50% ED_{50} Mce_6-PDT = 100% ED_{50} are depicted as 1DOX+PDT. For the combination 25% ED_{50} doxorubicin with 75% ED_{50} Mce_6-PDT (25DOX75PDT) antagonism was noted. Synergy was observed for the combination 50% ED_{50} doxorubicin with 50% ED_{50} Mce_6-PDT (50DOX50PDT). Additivity persisted for 75% ED_{50} doxorubicin with 25% ED_{50} Mce_6-PDT (25DOX75PDT). Adapted from reference [37].

Nonaka and co-workers [34] studied the cytotoxic and apoptotic effect of a combination of cisplatin and PDT with Photofrin® on L5178 mouse lymphoma cells. A significantly increased number of apoptotic cells was demonstrated for the combined treatment compared to either treatment alone. This enhanced effect was shown to be synergistic and related to the effect of caspase-3 activity induced by both PDT and cisplatin through different pathways. Crescenzi *et al.* [35] investigated the effect of indocyanine green-(IG)-mediated-PDT combined with cisplatin on MCF-7 breast cancer cells. Single treatments were not lethal for MCF-7 cells, whereas in combination, the overall lethal output was potentiated. Isobolographic assessment of the combined treatments revealed additive and quasi-synergistic responses depending on cell viability tests. Later, the same group [36] used similar conditions

for H1299 lung cancer cells. In these experiments, monotherapies reduced the cell viability by approximately 50%, whereas the combined therapies did so by 92% as a result of their additive effects.

Cell culture models have also been used for the assessment of the cytotoxicity of Photofrin® II, a purified version of HpD, or 5-aminolaevulinic acid (5-ALA)-mediated PDT combined with mitomycin C. Some examples consist of human colon adenocarcinoma and bladder cancer cell lines [38-40]. The group of Ma [38,39] investigated the cytotoxic effects of mitomycin C in cultured WiDr human colon adenocarcinoma cell lines and then compared this single treatment to a combination treatment with Photofrin® II-PDT. The cytostatic agent additively increased the cell sensitivity to PDT. Upon increasing the concentration of the anti-neoplastic drug, the combined effect changed from additive to synergistic, as judged by isobologram analysis. This result can be related to the change in cell accumulation from late S and early G2 phase to mid and early S phase with increasing mitomycin C dose. Datta and co-workers [40] studied the effect of 5-ALA-mediated-PDT in combination with mitomycin C on the J82 bladder cancer cell line and a mitomycin C-resistant counterpart (J82/MMC). Cell viability assays demonstrated that the J82/MMC was not cross-resistant to PDT and suggested a higher sensitivity of J82/MMC to PDT than the parent cell line. For both cell lines, an enhanced effect occurred only when the cytostatic agent was given first. The type of interaction and the sequence of mitomycin C and 5-ALA-mediated-PDT was more deeply investigated by the same group [41] and will be discussed later.

Analogous results from *in vitro* and *in vivo* models have been reported, revealing a reduction in cell viability and tumor surface, respectively. Brophy and Keller [42] worked with Photofrin® II as the photosensitizer, doxorubicin as the cytotoxic agent, and H-MESO-1 cells and BDF1 hybrid male mice as the model. *In vitro,* PDT with Photofrin® II alone resulted in a 23% decrease in cell viability, while the addition of increasing doses of doxorubicin to PDT reduced cell viability by more than 60%. *In vivo*, a 50% reduction of tumor surface with further regrowth was observed for PDT alone, while no impact on tumor growth was evidenced for doxorubicin alone. The combination of both treatments resulted in 100% tumor necrosis with no tumor regrowth suggesting a more rapid, intense and prolonged response compared to each treatment given alone. Similarly, Kirveliene *et al.* [43] worked with MH-22A murine hepatoma cells and nude mice models and *m*-THPC-PDT. Single treatment with either *m*-THPC-PDT or doxorubicin resulted in increasing dose-dependent cytotoxicity against MH-22A cells. Cell viability after PDT in combination with doxorubicin was

significantly reduced under most conditions compared to individual treatments. Furthermore, *in vivo* data showed a significant reduction in tumor volume by both single treatments compared to the control group. *m*-THPC-PDT and doxorubicin in combination were more effective in inhibiting tumor growth than any of these two treatments alone. These two studies show evidence of a good correlation between *in vivo* and *in vitro* data: a higher anti-tumor activity of combined regimens against transplanted cancer cells corresponded with a higher cytotoxicity *in vitro*. However, the degree of statistical significance between the effects *in vivo* and *in vitro* differed to some extent.

There is good support that the combination of a cytotoxic drug and PDT might improve the overall outcome of the treatment of cancer. In spite of that, the relevance of the sequencing of the combining agents to the combination effect is still under evaluation. Table 1 summarizes the type of interaction found *in vitro* for cisplatin, doxorubicin, or mitomycin C in combination with PDT.

Table 1. In vitro interactions between conventional chemotherapeutic agents and PDT with different photosensitizers

Chemotherapeutic	Photosensitizer	Sequence	Interaction	Cell line	Reference
Cisplatin	Photofrin®	pre-PDT	synergistic	L5178	[34]
		pre-PDT	additive	H1299	[36]
	Indocyanine G	pre-PDT	from additive to synergistic	MCF-7	[35]
Doxorubicin	Photofrin® II	pre-PDT	synergistic	H-MESO-1	[42]
	Mce$_6$	pre-PDT	from additive to synergistic	OVCAR-3	[37]
	m-THPC	pre-PDT	antagonistic	MH-22A	[43]
		post-PDT	additive	MH-22A	[43]
Mitomycin C	Photofrin® II	pre-PDT	form additive to synergistic	WiDr	[39]
	5-ALA	pre-PDT	antagonistic	J82	[40]
		pre-PDT	synergistic	J82/MMC	[40]
		post-PDT	antagonistic	J82	[40]
		post-PDT	antagonistic	J82/MMC	[40]

French *et al.* [41] investigated the interaction of mitomycin C and 5-ALA-mediated PDT in both the J82 bladder cancer cell line and its mitomycin C-resistant counterpart, J82/MMC. Mitomycin C increased 5-ALA-induced protoporphyrin IX (PpIX) fluorescence in both cell lines in a dose-related manner. This interaction was greater in the J82/MMC than in the J82 cell line, presumably due to the higher mitochondrial density of the mitomycin C-resistant cell line. Isobolograms for both cell lines showed that the interaction was marginally synergistic for J28/MMC, while it was not necessarily additive for J28. The administration of mitomycin C after PDT resulted in an antagonistic effect compared to single treatments, while the opposite sequence appeared to be synergistic. Uehara *et al.* [44] treated C3H/HeNCrj mice transplanted with R-S1 mouse squamous cell carcinoma with Photofrin®-PDT in combination with cisplatin administered either after or before PDT. At suboptimal cisplatin doses, histological findings showed that the administration of cisplatin 3 hours before PDT was significantly different from other combinations such as cisplatin 1 hour before PDT and cisplatin immediately after PDT, as well as from each therapy alone. Compared to the control group, administration of cisplatin 3 hours before PDT was the only treatment resulting in a significant reduction of tumor volume at three, seven and 10 days. Therefore, the interval of administration between the anti-cancer drug and PDT greatly influences the therapeutic outcome.

In contrast to cisplatin, doxorubicin seems to enhance the PDT response against tumor cells when this cytostatic agent is administered after PDT. Kirveliene *et al.* [43] observed that the anti-tumoral activity against MH-22A was more pronounced when *m*-THPC-PDT was followed by doxorubicin. *In vitro* data showed that the difference between cytotoxic effects of doxorubicin and the combined treatment with doxorubicin before PDT was approximately 40%, while it exceeded 60% when doxorubicin was added after PDT. The contribution of combination was evaluated by analysis of variance. This analysis revealed an antagonistic component when doxorubicin was given first. This negative interaction was mainly explained in terms of reduction of the cellular uptake of the photosensitizer caused by the cytotoxic agent. On the other hand, when doxorubicin was added after PDT, the combined action resulted from the addition of the individual cytotoxicities of the anti-neoplastic agent and *m*-THPC-PDT. *In vivo*, the anti-tumor activity of PDT 15 minutes before doxorubicin regimen was higher than that of doxorubicin 24 hours before PDT. However, the statistical significance between these two sequences was not as high as it was observed *in vitro*.

Because of the few studies comparing data *in vitro* and *in vivo*, it is difficult to ascertain the best sequence of combining the treatments *in vivo*. *A priori*, the effect of either mitomycin C or cisplatin in combination with PDT is superior when the cytostatic agent is administered first, while the effect of combining doxorubicin plus PDT is superior when doxorubicin is subsequently applied to PDT. These phenomena can be explained by different considerations, i.e. increase in photosensitizer uptake (mitomycin C), decrease (doxorubicin) in the presence of the anti-cancer drug, sufficient distribution of the cytostatic agent (cisplatin) at the moment PDT is performed, and the action of both therapeutic approaches on cells in different phases of their cell cycle (mitomycin C, cisplatin). However, the complexity of the *in vivo* situation may lead to inconsistencies with *in vitro* findings in particular when factors such as sequencing and dosing of combined treatments are involved.

Similar to mitomycin C, other bioreductive drugs, which are produgs converted into potent cytotoxins under metabolic conditions of either low oxygen tension or in the presence of high levels of specific reductases [45], have been studied in combination with PDT. The association of such chemotherapeutic agents with PDT might circumvent the tumor resistance to PDT in hypoxic regions of tumors where insufficient oxygen is present. At the same time, this approach exploits the local hypoxia induced by PDT, therefore, enhancing the anti-tumor response of individual treatments. Misonidizole, one of the oldest bioreductive agents, was used by Gonzolez *et al.* [46] as an adjunctive therapy with HpD PDT to treat Dunning rat prostatic cancers. In these studies, the light dose in the PDT also produced a significant hyperthermia. An enhanced effectiveness on tumor growth was observed by combining PDT and hyperthermia induced effects with misonidizol compared to PDT or misonidizole alone. Later, Henry and Isaacs [47] studied the effect of PDT associated with a new generation of more potent bioreductive agents represented by the compound RSU1164 in the same model. Combination of RSU1164 with HpD-PDT was found to synergistically delay tumor growth. In fact, the bioreductive drug alone produced no significant effect on tumor growth suggesting an insufficient degree of tumor hypoxia to activate the agent. While PDT alone delayed tumor growth, the tumor size at 24 days in combination with RSU1164 was reduced by 50%. Furthermore, AlS$_2$Pc-mediated PDT in combination with bioreductive analogs of the RSU1164, the RSU1069 and its prodrug RB6145, was performed by Bremner *et al.* [48]. In RIF-1 experimental murine tumors, RSU1069 and RB6145 potentiated the effect of PDT when light was administered between 30 minutes and 6 hours after photosensitizer administration. Tumor cures were observed under optimal conditions. Bioreductive drugs

such as misonidazole, pimonidazole, metronidazole, nimorazole, RB6145, RSU1069, SR4233, mitomycin C, or RB90740 at their maximum tolerated doses were used in combination with PDT in the same model [49]. Although misonidazole also enhanced PDT, the results were less pronounced as compared to RSU1069 and RB6145. No potentiation of the PDT effect was observed in the combination with pimonidazole, metronidazole, and nimorazole. Due to systemic effects under anesthesia, the two latter were administered at lower doses than their reported maximum tolerated doses, which may partly explain this observations. For the agent SR4233, only a limited tumor growth inhibition effect was observed when tumor hypoxia was increased by either PDT or clamping in combination with AlS$_2$Pc or Photofrin$^®$-mediated PDT, presumably due to the rapid conversion of SR4233 into inactive metabolites under severely hypoxic conditions [50].

In a recent study, Hasan and co-workers [51] isolated and characterized cell lines resistant to ALA-mediated-PDT derived from a LM3 murine mammary adenocarcinoma. They found that the oxygen consumption was significantly increased in the resistant clones compared to LM3. Furthermore, subcutaneous injection of those clones to mice, showed a tumor growth delay and early necrosis in comparison to the parenteral cell line, which can be related to their increased oxygen consumption. According to the authors, not only PDT can induce in vivo chronic hypoxia due to the vascular shut-down but, also, surviving cells may be hypoxic by an independent mechanism and, therefore, can be preferential targets of bioreductive drugs.

Altogether, these studies suggest that combination therapy of bioreductive drugs and PDT may be of value in the treatment of cancer. Factors such as drug distribution within the tumor and the ability of the drugs to be reduced under the conditions caused by PDT have to be considered when choosing the bioreductive drug.

Another approach in the context of combination treatments consists of the use of conjugates between the photosensitizer and the chemotherapeutic agent. So-called porphyrin platinum conjugates (PPC) consist of a porphyrin derivative and a platinum fragment in the same molecule. The hypothesis for the use of such systems is based not simply on the combined effect of PDT and cytostatic activities, but also on the porphyrin-mediated targeting of tumors [52]. Brunner and co-workers [53,54] have obtained promising results with such conjugates compared to standard monotherapy and combination therapy. Initially, different PPCs were obtained from platinum complexes of a series of 1, 2-diamines and hematoporphyrin or 13, 17-bis(2-carbocyethyl)-3, 8 [bis-(ethyleneglycolmonoethyl ether) oxyethyl]-2, 7, 12, 18-

tetramethylporphin. Then, their activity against MDA-MB-231 mammary carcinoma cells was evaluated and compared to that of Cisplatin and PDT with Photofrin® either alone or in combination. Three of the tested conjugates were as active as or even more active than cisplatin in association with PDT, demonstrating the validity of this approach. One of these conjugates evaluated as a liposomal formulation showed a strongly concentration-dependent activity. A second generation of these conjugates (PPC II) was evaluated in two cell lines, the J82 bladder cancer cell line and the UROtsa established from a normal urothelium. One of these PPC II, a water-soluble conjugate, exceeded the sum of cell viability induced by HpD-PDT and cisplatin therapy. In addition, proliferation in J82 cells was more affected than in UROtsa cells, presumably due to the lower dark phototoxicity of this conjugate on the latter cell line enabling them to recover from the treatment.

Other strategies of selective tumor targeting in combined chemotherapy and PDT have been investigated by Kopecek and co-workers [37,55-57]. Based on the use of polymeric drug delivery systems for the improvement of the specificity of drug action, an N-(2-hydroxypropyl) methacrylamide (HPMA) copolymer bound doxorubicin and a HPMA copolymer-Mce$_6$ were assessed as individual therapies and in combination using a human epithelial ovarian carcinoma (OVCAR-3) xenograft model [37,57]. The incorporation of HPMA copolymers extended the narrow margin of safety evidenced for free Mce$_6$ and demonstrated both safety and efficacy of HPMA-doxorubicin conjugates. The combination therapy of HPMA-doxorubicin and HPMA-Mce$_6$-PDT was non-toxic and resulted in complete tumor ablation, while none of the monotherapies showed a complete response. Further *in vitro* studies on OVCAR-3 [58] showed that both HPMA copolymers required a 10-fold increase in drug concentration to show equivalency with free drugs. At ED$_{50}$, the efficacy profile administration of HPMA-doxorubicin followed HPMA-Mce$_6$, resulting in an enhanced long-term inhibition of OVCAR-3 cells as compared to HPMA-Mce$_6$ alone. The opposite sequence was not significantly different from HPMA-doxorubicin alone in terms of efficacy. *In vivo*, an enhanced tumor accumulation was achieved for both HPMA-Mce$_6$ (4-fold) and HPMA-doxorubicin (2-fold) as compared to free drug. In the same study, several single and multiple treatments were evaluated. The prolonged retention time of the photosensitizer conjugate within the tumor made multiple PDT irradiations feasible. Single HPMA-Mce$_6$-PDT combined with multiple HPMA-doxorubicin treatments exhibited a significantly greater effect than multiple HPMA-doxorubicin treatments alone. Multiple HPMA-Mce$_6$ photodynamic treatments were better therapy than single HPMA-Mce$_6$-PDT

treatment with multiple HPMA-doxorubicin injections. As expected, the best results were obtained when multiple HPMA-Mce$_6$-PDT were combined with multiple HPMA-doxorubicin treatments. Later, the same team also investigated the use of such metacrylamide-drug copolymers specifically targeted with monoclonal antibodies in a murine model [56]. The incorporation of the OV-TL 16 antibody enhanced accumulation in tumors by a factor of 13 with a concomitant increase in therapeutic efficacy of the combined immunoconjugate therapy. In addition, combined treatments of the antibody targeted drugs (HPMA-Mce$_6$-Ab-doxorubicin and HPMA-Mce$_6$-Ab-PDT) resulted in inhibition of tumor growth with more than three times longer remission in OVCAR-3 xenografts than was achieved with the corresponding non-targeted conjugates.

Due to their lack of selectivity, an undesirable consequence of the administration of conventional chemotherapeutic compounds is the observation of their toxicity in normal tissues with a high rate of cellular turnover [59]. Therefore, new anti-neoplastic agents have been developed to address this issue. An interesting new prototype is an ether lipid, edelfosine, a synthetic analogue of lysophosphatidylcholine that does not act directly on the formation and function of cellular replication, but modulates membrane properties and metabolism of phospholipids, resulting in a selective apoptotic response in tumor cells [60]. Both therapies, edelfosine and merocyanine 540 (MC540)-mediated-PDT, have been used separately as purging agents in clinical trials [61,62]. Recently, some authors reported their use in combination. Yamazaki and Sieber [63] evaluated their combined effect on L1210 murine leukemia cells, and, K562 and HL-60 human leukemia cells. A high degree of synergy between both treatment regimens was observed, in particular when the PDT preceded the anti-cancer lipid. Interestingly, edelfosine enhanced the antileukemic effect of MC540-PDT even on K562 cells, which are refractory to edelfosine as a single purging agent. Inactivation of normal murine granulocyte-macrophage progenitors was also enhanced. However, the potentiating effect of Edelfosine on the photoinactivation of normal bone marrow cells was small compared to that of leukemia cells. Siebe and co-workers [64,65] performed an initial assessment of the safety and efficacy of a similar two-step purging procedure (MC540-PDT followed by edelfosine). A variety of cell lines, moderately to minimally sensitive to MC540-PDT, were employed. The combination significantly depleted all tumor cells, while preserving a considerable percentage of normal cells. At low edelfosine concentration, the combined cytotoxic effect appeared to be additive, while at higher concentrations it led to

synergistic effects. In tumor cells, the transition from an additive to synergistic effect occurred at lower concentrations of edelfosine than in normal haematopoietic stem and progenitor cells.

A different study on potential combinations was reported by Tsujino and colleagues [66]. They studied the effect of amifosine and/or amphotericin B, drugs usually used concomitantly with chemotherapy, in the anti-tumor effect of MC540-PDT over leukemia cells, wild-type small cell lung cancer cells and cisplatin-resistant small cell lung cancer cells. The use of non-toxic concentrations of amifosine and amphotericin B, either alone or in combination, enhanced the photoinactivation of cancer cells by MC540. Amphotericin B also enhanced the effect of PDT on normal granulocyte-macrophage progenitors, whereas amifosine protected them against the cytotoxic action of PDT.

Other anti-neoplastic agents, so far less studied in combination with PDT, are the so-called inhibitors of the cellular energy metabolism such as lonidamine and levamisol. These molecules exert a powerful inhibitory effect on oxygen consumption, aerobic glycolysis and lactate transport and accumulation of neoplastic cells [67,68]. Shevchuk and co-workers [69,70] showed a potentiating anti-tumor action of 5-ALA-based-PDT when administered together with these agents. V79 Chinese hamster lung fibroblast cells were preincubated with lonidamine or levamisol jointly with 5-ALA for 4 hours prior to irradiation, or first treated with 5-ALA-based-PDT followed by the incubation with any of the two inhibitors 24 hours post irradiation. Only a minor dark cytotoxicity was observed by each inhibitor in combination with 5-ALA. However, both levamisol and lonidamine altered the efficacy of PDT most likely due to their interference with the biosynthetic pathway of heme. However, at low concentrations lonidamine synergistically enhanced the sensitivity of the cells to PDT, presumably due to its effect on either glycolysis or the respiration chain. On the other hand, levamisol induced a maximum of 1.5-fold increase in the PDT efficacy profile above which no further increase was induced. This synergistic interaction correlates well with the levamisol stimulation of 5-ALA-induced PpIX synthesis within the whole range of concentrations investigated. The administration of levamisol or lonidamine after PDT induced only an additive or slightly synergistic effect.

In spite of the promising results of these *in vitro* and *in vivo* studies, only a small number of clinical trials can be found in the literature. Jin and colleagues [71] reported a study in 144 patients with cardiac cancer in advanced stages. Patients were treated by HpD-PDT alone, Tegafur/uracil and mitomycin C in association (standard chemotherapy), or a combination of

both PDT and standard chemotherapy. For PDT, an intravenous injection of the photosensitizer 48-72 hours prior to treatment was used and multiple exposures were occasionally needed. The dosages for combined chemotherapy were variable, but a common schedule was Tegafur/uracil every day and mitomycin C every week. In patients receiving PDT plus chemotherapy, treatments were performed at the same time using the schedules mentioned above. No significant difference was observed with respect to the effect rate (complete remission plus partial remission) among the three groups. However, 19.5% of patients from the group with combination therapy showed complete remission compared to 5.5% and 8.3% for PDT and chemotherapy groups, respectively. None of the patients treated with PDT in combination with chemotherapy had liver or kidney function failure and only mild bone marrow depression was observed in this group. Moreover, no severe side effects, such as hemorrhage or perforation, were observed. This suggests that a combination of these two therapies with the proposed regimens is safe and may be beneficial.

In another trial, four patients with recurrent skin metastasis of a mammary carcinoma were administered low dose PDT using Photofrin® with or without previous infusion of a low dose mitomycin C [72]. The use of chemotherapy prior PDT allowed the reduction of the light dose by a factor of two, which may be useful to treat larger tumor areas. Moreover, the skin phototoxicity lasted maximally three weeks, which reduces the undesired prolonged cutaneous photosensitivity. A phase-1 study of sequential mitomycin C and 5-ALA-mediated-PDT administered to 22 patients with recurrent superficial bladder cancer was reported by Skyrme and colleagues [73]. Cumulative tumor recurrences were low, up to 11 at 24 months after PDT, compared to 29 in the 18 months before enrollment. No patient had evidence of progression to muscle-invasive disease. Additionally, the combined treatment was safe and well tolerated. No systemic or phototoxic side effects or reduction in bladder volume were reported. These results provide support of a new possibility for the treatment of superficial bladder cancer. Pass *et al.* [74] carried out a phase III randomized trial of surgery with and without intraoperative PDT and postoperative immunochemotherapy for malignant pleural mesothelioma (MPM). Surgical cryoreduction of the tumor was performed on 63 patients and those patients randomized to PDT received intraoperative PDT with Photofrin® as well. All patients received two cycles of immunochemotherapy after surgery (tamoxifen, interferon (IFN)-α and cisplatin). Intraoperative PDT did not result in any improvement of the treatment with respect to time to recurrence, recurrence patterns, and median survival, suggesting that first-generation intrapleural PDT is not beneficial to patients with MPM. Although this new

therapeutic intervention was not successful in this study, it is far too early to discard it as a technique for intrapleural cancer control.

Methotrexate is an anti-cancer agent that is currently used in combination with other chemotherapeutic compounds for the treatment of many types of mostly invasive cancers [75]. It impedes tetrahydrofolate synthesis to competitive binding to dihydrofolate reductase, which, in turn, inhibits the synthesis of purines needed for the synthesis of DNA and RNA. Recently, it has been shown that this mechanism mainly contributes to the cell differentiation in colon cancer cells [76], which, then, can up-regulate heme biosynthesis in some cells [77]. It has been already shown that agents stimulating cell differentiation such as DMSO positively influence 5-ALA induced PpIX synthesis [78]. In this context, Sinha *et al.* [79] have shown that pre-incubation of a human prostate cancer cell line with methotrexate and subsequent 5-ALA mediated PDT increased the efficacy of the PDT treatment significantly. Similar effects were observed with differentiation inducers such as retinoic acid and vitamin D [80].

4. PDT and pro-oxidant agents or oxidant enhancers

The use of antioxidants in cancer prevention is mostly justified through prevention of oxidative damage of DNA [81]. However, one of the most important biological effects after PDT is oxidative stress through radical oxygen species resulting in cell death. Interestingly, a number of antioxidants can also exhibit pro-oxidant activities, especially in the presence of catalytic metals [82]. In fact, some studies have shown an enhanced activity of PDT by the concomitant use of certain antioxidants. A detailed review on this topic including different antioxidants has been recently published by Jakus and Farkas [83]. Early studies of the effect of ascorbate on the photosensitization of red blood cells by porphyrins [84] and phthalocyanines [85] evidenced an increased photohemolysis and rate of cell lysis in a dose-dependent manner, suggesting that ascorbate acts as a reactant and not as a catalyst. Buettner and co-workers [82,86] investigated the use of iron and ascorbate in combination with Photofrin®-PDT on L1210 murine leukemia cells and human oral squamous cell carcinoma SCC-25 cells. PDT alone resulted in the production of membrane-derived free radicals. The pro-oxidant combination significantly enhanced the production of lipid radicals, 4- and 2-fold times when present during photosensitization or given after PDT, respectively. The dose effect curves of iron revealed that, with iron, an optimal concentration can be achieved, above

which no further increase in radical production can be observed. The increased radical production correlated with a decrease in cell survival for both cell lines. Furthermore, the photosensitizer dose could be reduced to one-third when using the pro-oxidant combination. In contrast, Frank et al. [81] found a potent antioxidant activity of ascorbic acid, protecting mitochondria and other cell structures from oxidative cell injury induced by 5-ALA-mediated-PDT. Ascorbic acid was found to significantly inhibit the cellular protein oxidation and lipid peroxidation as well as the amount of necrotic factors, i.e. FasL and TNF-α mRNA expression generated by 5-ALA-mediated-PDT. According to these studies, ascorbate might act as pro-oxidant at low concentrations and as an antioxidant at higher concentrations. However, concentration may not be the only indication for ascorbates anti- or pro-oxidant activity. In a recent study, Kramarenko and colleagues [87] investigated the influence of ascorbate on Visudyne®-PDT on HL-60 and U937 human leukemia cells. Cells were preincubated with Visudyne® and ascorbate either in combination or alone, and then irradiated. For HL-60 cells, combined treatment resulted in a 65% decrease in cell survival compared to 50% for PDT alone. In contrast, using the same conditions as were used for HL-60 cells, only minimal changes in survival of U937 cells were observed. Furthermore, the growth rate of HL-60 cells was considerably reduced (2.5-fold) by the ascorbate and PDT combined treatment as compared to non-treated cells, whereas growth curves for treated and non-treated U937 cells were not significantly different. Both cell lines are from the same myelomonocytic origin and, therefore, similar results were expected. However, HL-60 cells showed a high level of myeloperoxidase, an enzyme which upon activation, i.e. by H_2O_2, induces the formation of more reactive oxidants. In U937 cells, this enzyme activity was below the limit of detection. Data clearly showed that ascorbate enhances the production of H_2O_2 associated with PDT using Visudyne®, and thus activation of myeloperoxidase in HL-60 cells, increasing the overall cytotoxic effect.

In the same way, the efficiency of PDT jointly administered with other widely used antioxidants, i.e. butyl hydroxyanisole (BHA), α-tocopherol has been investigated [88,89]. Shevchuk et al. [88] studied the effect of BHA in either HpD- or Mec_6-based-PDT on Ehrlich ascites carcinoma (EAC). Co-incubation of EAC cells with BHA and any of the two photosensitizers, followed by irradiation, caused an antagonistic interaction. However, upon increase of BHA concentration to toxic levels, the cytotoxic effect shifted towards an additive enhancement of the overall outcome. In contrast, EAC cells were 10-fold more sensitive to BHA when pretreated with HpD-PDT, showing a synergistic interaction between both

treatments. Furthermore, *in vivo* studies showed an additive action of BHA on the tumoricidal effect of HpD-PDT presumably caused by impairment of mitochondrial respiration. In fact, incubation of cells with BHA alone resulted in a significant decrease (60%) in dehydrogenase activity and oxygen consumption as well as a significant increase (60%) in the rate of aerobic glycolysis and inhibition of the aerobic lactate production.

Bezdetnaya and co-workers [89] investigated the influence of α-tocopherol in the *m*-THPC-sensitized photoinactivation of both HT29 adenocarcinoma cells and MRC-25 normal fibroblasts. At low concentrations of α-tocopherol, no effect on *m*-THPC-induced photosensitization of HT29 cells was observed. At higher concentrations of α-tocopherol, however, efficacy of PDT was increased and the effect was synergistic at cytotoxic levels of the vitamin. No changes in the PDT-mediated cell survival profile of MRC-5 cells were observed by preincubation of cells with α-tocopherol prior PDT. These results were consistent with the effective incorporation of α-tocopherol by neoplastic cells and with the absence of its uptake by MRC-5 cells. The same group [90] carried out another study using a water-soluble α-tocopherol analogue, Trolox, in combination with *m*-THPC-PDT on HT29 xenografts in nude mice. The administration of Trolox before PDT resulted in a reduction of tumor growth by a factor of 1.5, whereas no significant differences were observed when administered post-PDT. Comparison of the contribution of the different pathways for the combination Trolox pre-PDT showed the singlet oxygen reaction due to PDT being dominant at the onset of the irradiation and then decreased as a result of the induced hypoxic conditions; this decrease is accompanied by an increase in the oxidized Trolox radical. Thus, the enhancement effect is likely due to the Trolox-mediated radical pathway working in concert with singlet oxygen while oxygen concentration is decreased in the course of PDT. An alternative to this photochemical mechanism may involve the capacity of antioxidants to induce tumor cell differentiation and to inhibit tumor growth.

Since tumor cells use the overexpression of glutathione (GSH) as a protective mechanism against PDT-induced formation of free radicals [91], decreasing intracellular GSH levels is another attractive option for increasing sensitization of tumor cells to PDT. *In vitro* studies by Miller and Henderson [92] showed an augmented response to PDT by buthionine sulfoximine (BSO), which inhibits the rate-limiting enzyme (γ-glutamylcysteine synthetase) in the pathway of glutathione biosynthesis. Concomitant BSO treatment given to four cell lines (CHO, V79, EMT6, RIF) resulted in an increase of PDT-induced cell death directly related to

the GSH-depletion by BSO. Later studies with BSO demonstrated that this compound also enhanced the effect of PDT with Photofrin® *in vivo* [93,94]. Drugs were administrated 24 hours prior to irradiation. The combined treatment resulted in a significant increase in tumor regression. Additionally, when animals were treated with BSO, the GSH level in neoplastic cells was half of that in normal cells, suggesting that BSO selectively enhances the tumor response to PDT.

5. PDT and angiogenesis inhibitors

As shown previously, PDT mechanisms include apoptotic and necrotic responses and indirect cell death through microvascular injury, leading to inflammation and hypoxia. On the other hand, PDT also induces expression of angiogenic and cell survival signals including VEGF, COX-2, and MMP [19,20,25,26]. This might ultimately lead to neovascularization and in some instances tumor recurrence. Therefore, researchers have investigated the potential impact of inhibitors of these stress signals on the therapeutic outcome of PDT.

Recently, we have shown that PDT-induced vascular occlusion is partially reversible and can lead to reperfusion of previously occluded blood vessels and formation of new blood vessels [95]. Conversely, this relapse was found to be reduced by the coadministration of compounds acting against VEGF (see Fig. **7**), which clearly demonstrates the benefit of PDT in association with VEGF inhibitors.

Ferrario and co-workers [19] confirmed that PDT with Photofrin® induced the expression of HIF-1α and increased the protein target levels of HIF-1α target gene - *VEGF* - within a transplantable BA mouse mammary carcinoma. In the same study, tumor-bearing mice were treated with PDT followed by 10 daily doses of two anti-angiogenic peptides, either IM862 or EMAP-II. The latter induces apoptosis in growing capillary cells and prevents vessel in-growth, while IM8662 inhibits the production of VEGF and activates NK cells. Both combinations resulted in the potentiation of tumoricidal action of PDT. In fact, the anti-angiogenic agents on their own did not produce any tumor cure or regression, but increased the response of cancer cells to PDT by a factor of two. A recent study of Ferrario and Gomer [96] studied the effect of Avastin, a novel anti-angiogenic monoclonal antibody already approved for the treatment of colon and rectal cancer, on the sensitization of malignant cells to PDT with Photofrin®. Avastin was chronically administered to tumor-bearing mice

immediately after irradiation. An overexpression of human VEGF rather than host cell derived mouse VEGF was detected within tumors after PDT implying that tumor cells were the origin of most of the detectable VEGF. Avastin combined with PDT resulted in a statistically significant increased number of long-term tumor cures compared to individual treatments. A tumor cure rate of 55% was obtained with the combined treatment regimen, whereas PDT alone and Avastin alone showed only 22% and 10% cure rates, respectively. Interestingly, this enhancement of anti-tumor activity was not accompanied by any observable increase in normal tissue toxicity.
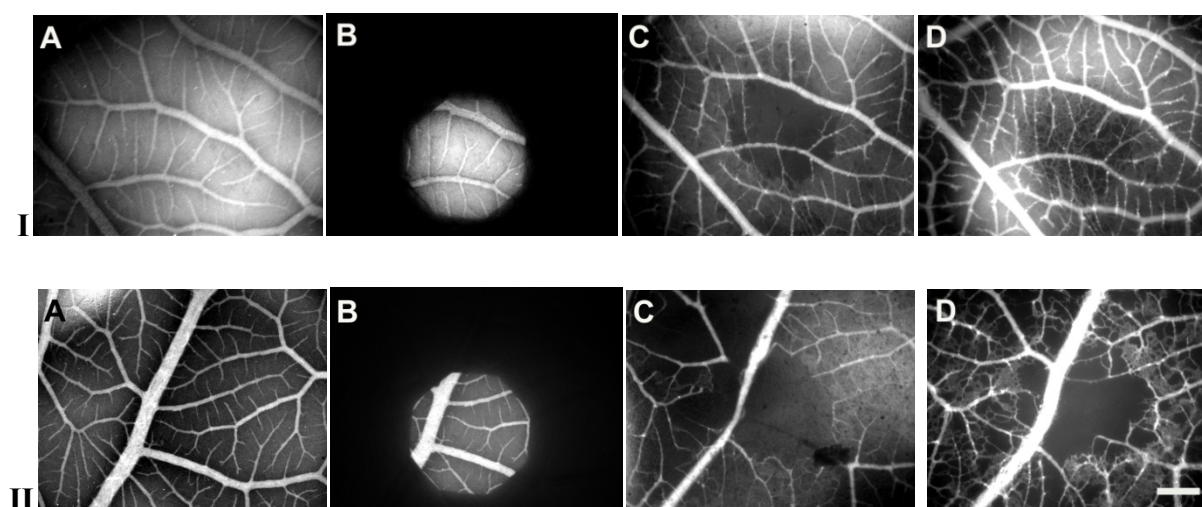
Figure 7. Comparative damage on chorioallantoic membrane vasculature produced by PDT alone and PDT in combination with anti-angiogenic treatment. (I) PDT using intravenously applied BPD-MA (0.25 mg/Kg embryo), (II) PDT using intravenously applied BPD-MA (0.25 mg/Kg embryo) followed by anti-VEGF therapy using topically applied sFlt-1 (1μg/embryo) 6 hours post-PDT. (A) Photosensitizer fluorescence angiography before irradiation (BPD-MA: λ_{ex} = 400–440 nm; λ_{em} > 610 nm). (B) Photosensitizer fluorescence angiography during BPD-MA-PDT (λ_{ex} = 400–440 nm; λ_{em} > 610 nm). Diameter of the irradiated area: 1.8 mm; irradiation condition: 30 J/cm^2, 1 minute after photosensitizer injection. (C) Sulforhodamine 101 fluorescence angiography (λ_{ex} = 510–560 nm; λ_{em} = 625-675 nm) 24 hours after PDT. (D) Sulforhodamine 101 fluorescence angiography (λ_{ex} = 510–560 nm; λ_{em} = 625-675 nm) 48 hours after PDT. Contrast medium (Lipidem) injected under the chorioallantoic membrane. Damage score on the irradiated area after 24 h: (IC) BPD-MA-PDT: 4, (IIC) BPD-MA-PDT/sFlt-1: 5; after 48 h: (ID) BPD-MA-PDT: 0, (IID) BPD-MA-PDT/sFlt-1: 4. White bar = 500 μm.

Dimitroff *et al.* [97] evaluated the anti-angiogenic and anti-tumor efficacy of two tyrosine kinase (RTK) inhibitors, PD166285 and PD173074, in C3H mice transplanted with murine mammary 16c tumor cells. The anti-cancer activity after oral administration of RTK inhibitors following PDT with hexylether pyropheophorbide-a (HPPH) was compared to that of PDT

alone. PDT treatment showed no significant decrease in tumor growth when compared to control mice. However, combining HPPH-PDT and follow-up treatment for 14 days with PD166285 displayed a dramatic increase in tumor-free interval. In addition, both RTK inhibitors significantly decreased the tumor regrowth (from 2- to 3-fold) when combined with PDT. Only mice from the combination groups exhibited tumor cures. In general, tumor regrowth was observed by one week after withdrawal from the treatment, suggesting the need for treatment maintenance. Some side effects, i.e. hyperkeratosis and neurotoxicity at high doses of PD166285, were observed for the combination with HPPH-PDT, while no noticeable toxicities were manifested with HPPH-PDT combined with PD173074 treatment. Zhou *et al.* [98] evaluated other RTK inhibitors, SU5416 and SU6668S, in combination with hypericin-mediated-PDT on human nasopharyngeal carcinoma CNE2 xenografts. Although, differences in tumor growth among individual and combined treatments were not statistically significant, SU6668 in combination with PDT seemed to be more effective. This observation suggests that SU6668 works better than SU5416 to inhibit tumor regrowth, which may be explained by the fact that SU6668 blocks VEGF, FGF and, PDGF receptors while SU5416 is highly specific for VEGF-receptor 2. Conversely, after withdrawal, the tumor regrowth rate was higher for SU6668 than for SU5416, which is in agreement with previous *in vitro* studies showing the latter as a long-lasting inhibitor of VEGF-dependent proliferation in cells [99].

Hasan and co-workers [100] studied the effect of TNP-470, an anti-angiogenic peptide which strongly inhibits vascular endothelial cell proliferation and migration by blocking methionyl aminopeptidase-2, on subcurative benzoporphyrin derivative monoacid ring A (BPD-MA)-PDT. This study showed that subcurative PDT in an orthotopic model of prostate cancer increases not only VEGF secretion but also the incidence of lymph node metastases. Prostate weight and prostate volume were significantly reduced by the chronic administration of TNP-470 after PDT compared to the control group. TNP-470 given before PDT did not result in any significant differences. Interestingly, animals in the control group and animals receiving either PDT alone, TNP-470 alone, or PDT pretreated with TNP-470 had a weight loss, whereas the weight of animals receiving TNP-470 after PDT did not change. These results showed that, if the angiogenic action of VEGF is blocked by TNP-470, tumor growth, lymph node metastasis, and, disease-related toxicity are reduced.

Another potent vascular targeting agent, the 5, 6 Dimethylxanthenone-4-acetic acid (DMXAA), has been also shown to selectively enhance PDT activity against mouse tumors [101,102]. Experimental evidence suggests that DMXAA increases tumor vascular

permeability both directly and through the induction of other vasoactive mediators, such as TNF-α [103]. In a first study on PDT combined with DMXAA, Bellnier *et al.* [101] investigated the effect of administering a low dose DMXAA prior to PDT with Photofrin® in a transplanted murine RIF-1 tumor model. Cultured RIF-1 cells were mostly resistant to DMXAA and TNF-α. However, the combinational treatment with PDT resulted in the reduction of tumor size as well as in a significant delay in regrowth and was both timing and sequence dependent. DMXAA was ineffective when administered after PDT, but effective when given a few hours before PDT. Furthermore, at low doses of Photofrin®, the effect on normal tissue of DMXAA combined with PDT was similar to that of PDT alone. According to these studies, DMXAA and not PDT was responsible for the increased expression of TNF-α after treatment indicating that this factor was primary responsible for the enhanced anti-tumor activity of PDT at low photosensitizer doses.

In a later study, the same research group [102] treated BALB/c mice bearing Colon-26 tumors with HPPH-PDT and DMXAA. Four different treatment regimens inducing different patterns of cellular, immune, and vascular responses were compared. The photosensitizer and the vascular permeability enhancer were administered 24 and 2 hours before irradiation, respectively. This time, an *in vivo* assessment of the tumor vascular response by magnetic resonance imaging and the fluorescein exclusion assay were included. PDT and DMXAA significantly enhanced the permeability of tumors when given as single treatments. However, the changes in vascular permeability induced by PDT did not predict tumor curability. In contrast, high-dose DMXAA or the combination of PDT and low-dose DMXAA, showed a common pattern of vascular permeability that was associated with long-term cure rates of more than 70%. Moreover, the therapeutic effects of DMXAA alone or in combination with PDT were largely confined to the tumor, whereas treatments with PDT increased the vascular permeability in both the tumor and peritumoral tissue. Although the doses of DMXAA and PDT in the combination regimen had virtually no anti-tumor activity when used separately, the combination of both at ineffective doses seemed to induce significant vascular damage which correlated with the enhanced tumor cure rate.

Due to its important role in inflammation and mitogenesis [104], PDT-induced expression of COX-2 would potentially impede the efficacy of PDT. Thus, COX-2 inhibition following PDT represents another alternative for the treatment of cancer. In addition, COX-2 overexpression has been reported for some types of cancer, such as colon, lung, and breast cancer [105-107]. Therefore, considerable attention has been paid to the potential effect of

selective COX-2 inhibitors in combination with PDT against malignant cells in recent years. Ferrario and co-workers [20] showed the efficacy of PDT using Photofrin® followed by administration of multiple doses of the COX-2 inhibitor NS-398 in RIF tumors in C3H/HeJ mice. The tumor response was not affected by the administration of NS-398 alone or low PDT doses. However, combination of PDT with the inhibitor treatment resulted in statistically significant increases in tumor cures even at low PDT doses. Although the mechanism by which COX-2 inhibition enhances PDT responsiveness remains unclear, the NS-398 reduced the induction of PGE_2 and VEGF synthesis after PDT. These results are in agreement with Harvey and co-workers [108], who tested the effect of mono-L-aspartyl chlorine e6 (NPe_6)-PDT followed by NS-398 treatment on C57BL/6NCr mice bearing Colon-38 tumors. Unexpectedly, NS-398 did not potentiate the effect of PDT using a fractionated dosing regimen of the photosensitizer, presumably because the observed effect was already maximal with PDT alone.

In a subsequent paper, Ferrario *et al.* [109] showed that COX-2 also decreased the PDT-induced expression of the proinflammatory mediators IL-1β and TNF-α, and increased PDT-treated tumor levels of the anti-inflammatory cytokine, IL-10. PDT with Photofrin® together with NS-398 or celecoxib, a FDA approved COX-2 specific inhibitor, was tested on mouse mammary carcinoma cells and tumor-bearing mice. Both inhibitors, at non-cytotoxic concentrations, increased *in vitro* cellular photosensitization in a dose-dependent manner. This increase was directly related to an increased level of apoptosis. *In vivo*, multiple doses of either NS-398 or celecoxib in combination with PDT quadrupled the cure rate of PDT alone. In contrast, the enhancement to PDT responsiveness was predominantly assigned to the inhibition of expression of angiogenic and inflammatory molecules by COX-2 inhibitors and not to an increase of the apoptotic activity as it was seen in the cell culture studies.

In contrast, Makowski *et al.* [110] found that neither NS-398 nor other COX-2 inhibitors (rofecoxib and nimesulide) were capable of sensitizing C-26 tumor cells to Photofrin®-mediated-PDT-induced damage. According to the authors, because NS-398 used by Ferrario *et al.* [20] was given chronically after PDT, it seems possible that the potentiating effects were indirect and resulted from independent anti-tumor effects of the inhibitor. Later experiments allowed them to confirm that the administration of COX-2 inhibitors before PDT did not influence the effectiveness of PDT and that effectively superior vascular and tumor damage is obtained with the chronic administration of COX-2 inhibitors after PDT. Differences between sequencing suggest that COX-2 inhibitors potentiate the anti-tumor effects of PDT through

inhibition of angiogenesis interacting with the reconstruction of blood vessels damaged by PDT.

Expression of COX-2 in lesions of the skin and oral cavity was reported by Akita *et al.* [111]. The authors studied the effect of 5-ALA-mediated-PDT in combination with nimesulide in two human oral squamous cell carcinoma cell lines, HSC-2 and HSC-4. The inhibitory effect of the combined treatment was superior to the individual treatment for the HSC-2, which overexpresses COX-2, while in HSC-4 cells no statistically significant differences were observed, presumably due to low levels of COX-2 expression. In fact, the interaction of 5-ALA-mediated-PDT with nimesulide in HSC-2 was demonstrated to be synergistic, supporting the hypothesis of independent mechanism of action.

Yee *et al.* [112] evaluated multiple-dose celecoxib as adjuvant treatment to improve the anti-tumor responsiveness of nasopharyngeal carcinoma bearing mice. Whereas PDT alone, inhibitor alone and the inhibitor given 24 hours post-PDT regimen were not significantly different in terms of tumor growth, the difference between PDT alone and in combination with the inhibitor given already 6 hours post-PDT was of borderline significance. Furthermore, simultaneous downregulation of COX-2, HIF-1α, VEGF A isoforms 165 and 121 occurred *in vivo* only when celecoxib was administered 6 hours post-PDT. Again, these results implicate that timing and sequence of the administration is crucial for effective tumor control in combination therapy.

There is experimental evidence of upregulation of inducible COX-2 after hypericin-mediated PDT induced by the selective activation of the mitogen-activated protein kinase (MAPK) p38 α and β at the protein and mRNA levels [113]. Therefore, an early blocking of the PG release through p38 MAPK inhibition might be useful as adjunctive therapy to PDT. Furthermore, the inhibition of the alpha isoform has been reported to block the release of VEGF and suppress tumor-promoted endothelial cell migration [114]. Hendrickx and colleagues [113] showed that the use of PD169316, a pyridinyl imidazole p38α MAPK inhibitor, improved the effectiveness of hypericin-PDT against human cervix carcinoma (HeLa) cells and human transitional cell carcinoma of the bladder (T-24), by blocking upregulation of COX-2 as well as by sensitizing cells to apoptosis. Unlike COX-2 inhibitors, the p38 MAPK inhibitor also interfered with apoptotic cell death in photodamaged cells. However, this difference does not exclude the validity of the use of COX-2 inhibitor for improving the anti-cancer efficacy of PDT as the inhibition of the COX-2-dependent synthesis of growth-promoting factors clearly

surpasses the anti-apoptotic role of the enzyme. In the same study [114], the response of HY-based PDT combined with either the COX-2 inhibitor NS398 or the p38 MAPK inhibitor PD169316 were compared. Although endothelial cell migration was blocked to a similar extent by both inhibitors, inhibition of p38α MAPK pathway was more effective in suppressing VEGF synthesis. Moreover, experiments including wild type and p38α knockout mouse embryonic fibroblasts clearly showed a balance towards cell death for p38α-deficient cells, which was not achievable by selective COX-2 inhibition by NS398. Altogether, these results imply that inhibition of p38 MAPK might be a more promising cancer treatment strategy than COX-2 inhibition.

An additional, but less studied, strategy consists of the administration of PDT in combination with MMP inhibitors since such enzymes are reported to be expressed after PDT and related to tumor angiogenesis, growth, invasion, and metastatic potential [115]. Ferrario *et al.* [26] evaluated the anti-tumor activity to Photofrin®-based-PDT with subsequent chronic administration of prinomastat, a potent synthetic MMP inhibitor, in BA bearing mice. The combination of PDT plus MMP inhibitor resulted in a significant difference in long-term cure rate compared to PDT alone. Tumors treated with prinomastat alone exhibited a modest reduction in growth, but no decrease in tumor size or long-term cures. Furthermore, skin damage by PDT with or without the MMP inhibitor was similar, which suggests that MMP expression does not modulate PDT-mediated normal skin phototoxicity. This study shows preliminary evidence of the potential advantageous therapeutic outcome for cancer treatment by using PDT and MMP inhibitors.

6. PDT and Immunotherapy

As mentioned above, anti-tumor immunity has been shown to be stimulated after PDT by the acute inflammatory response, generation of tumor-specific antigens, and induction of heat-shock proteins [116]. Treatment regimens using PDT and immunostimulating treatments are therefore likely to constitute an effective combination for various types of cancer. A common strategy to such combination is to sustain and/or amplify PDT-induced immunity against the treated cancerous lesion. Table 2 summarizes the predominant mechanisms of interaction between PDT and immunotherapy. Herein, the term "immunotherapy" will be used for all biological therapeutic agents that use the body's immune system, either directly or indirectly,

to fight cancer or to lower treatment-associated side effects. Combinations of PDT with some biological therapies including cytokine therapy, microbial adjuvants, and regulatory T cells and adoptive cellular therapies have already been addressed in a recent review on PDT and anti-tumor immunity [117].

Combination of PDT with several cytokines has shown to enhance PDT anti-tumor effect. Hall *et al.* [118] found a synergistic interaction of PDT with Photofrin® concomitant with IFN-α in T24 human bladder cancer cells. They showed that the PDT doses had to be doubled in order to achieve the same amount of cell death of IFN-α given 24 hours post-PDT. Moreover, at high photosensitizer doses, the combined treatment allowed to reduce the light dose by a factor of three. Although the effect of IFN-α alone was dose-dependent, an increase of the IFN-α dose in the combination treatment did not result in a significant improvement. Altogether, these results suggest that the use of combined PDT and IFN-α may be able to significantly reduce the dose of light, which in turn may reduce the side effects without decreasing the efficacy.

Table 2. Potential mechanisms of interaction between PDT and immunotherapy

- Upregulation of leukocyte adhesion molecules

- Potentiation of neutrophils and macrophages

- Induction of secondary cytokines

- Activation of dendritic cells, facilitation of the presentation of tumor antigens released following PDT, and induction of adaptative immunity

- Activation of CD4+ helper T-lymphocytes and sensitization of CD8+ cytotoxic T-lymphocytes

- Downregulation of CD4+CD25+ T-regulatory cells and potentiation of immunity

- Activation of B lymphocytes and natural killer cells

- Inactivation of remaining viable tumor cells through adaptative immunity

- Decrease of immunosuppressive effect induced by PDT

Dima and colleagues [119] evaluated IL-2 together with cyclophosphamide, another immunostimulant, in combination with Photofrin® II-PDT. Wistar rats with ascites tumor cells were treated with both individual and combination therapies. Fractionated irradiation and multiple doses of IL-2 and cyclophosphamide entrapped in liposomes were used. PDT in combination with low doses of cyclophosphamide and IL-2 regimen was found to considerably reduce not only the tumor volume, but also the mortality of animals by more than 1.5-fold compared to local treatment with only PDT. Furthermore, the mitogenic response and cytotoxic activity of spleen lymphocytes were significantly increased by the associated therapy compared to PDT, IL-2, or cyclophosphamide alone. In the same way, Photofrin® II-PDT has been investigated in association with recombinant human TNF-α in SM-F adenocarcinoma DBA/2 bearing mice [120]. Administration of TNF-α a few hours before suboptimal PDT doses resulted in a tumor area reduction of 57% compared to 21% of TNF-α alone. However, when standard doses of PDT were used, the interaction between PDT and the biologically active agent appeared to be additive. The administration of TNF-α immediately before irradiation seemed to be less effective than its administration a few hours before. No difference in normal tissue damage was observed between PDT combined with TNF-α a few hours before the irradiation regimen and PDT alone. In contrast, normal cells exhibited an increased photosensitization when TNF-α was given immediately before light administration, but not as high as that displayed by cancer cells. Although the mechanism of interaction during this combination treatment remains unclear, the authors suggest that the interaction may occur directly on the tumor cells or in the tumor parenchyma. While PDT induces the formation of singlet oxygen and superoxide anion radicals, TNF-α may involve the production of reactive oxygen species produced by neutrophils, tumor cells, or macrophages, both resulting in cellular damage. Alternatively, the effect may take place at the tumor vasculature, which both modalities damage severely.

According to several studies, neutrophils are essential for anti-tumor efficacy PDT [121] and therefore, administration of macrophage activating factors might improve such effectiveness. In a study carried out by Krosl and co-workers [122], genetically modified cells were engineered to produce murine granulocyte-colony-stimulating factor (GM-CSF). Then, mice transplanted with murine squamous cell carcinoma, a poorly immunogenic tumor, were treated with these modified cells and either Photofrin®-PDT or BPD-MA-PDT. For both combined regimens, cells were injected 48 hours before, immediately after, or 48 hours after irradiation. Complete tumor ablation was observed with all regimens. The combined

Photofrin®-PDT combined with GM-CSF doubled the tumor-free period and increased survival of tumor-bearing mice compared to PDT alone. Although PDT regimens with BPD-MA seemed to be less effective than with Photofrin®, similar results were obtained when comparing monotherapy and combination therapy. Approximately 50% of animals receiving BPD-MA-PDT combined with GM-CSF remained tumor-free, while tumor regrowth was observed for all animals without GM-CSF treatment.

Later, Golab *et al.* [123] evaluated the cytotoxicity of PDT with Photofrin® in association with an intensive treatment with G-CSF in colon (C-26) and Lewis lung (3LL) carcinoma *in vivo*. The results showed a significant reduction of tumor growth and prolongation of the survival time of tumor-bearing mice using the associated regimen. About 33% of C-26-bearing mice treated with PDT in combination with G-CSF showed complete remission. Interestingly, tumors were rejected when mice were rechallenged with C-26 cells, but not other tumor cells suggesting the development of specific immunity against the treated tumor. Histopathology, immunohistochemical and TUNEL staining of tumors demonstrated more intensive neutrophil infiltration and multiple apoptotic cells in the combined regimen compared to PDT alone. Co-administration of G-CSF and PDT synergistically stimulated bone marrow and spleen myelopoiesis increasing the number of active neutrophils. Furthermore, PDT increased vascular permeability facilitating tumor infiltration.

Preparations of microbial stimulators have been shown to improve the immune response to particular antigens, but are not always effective in reversing tumor progression. Therefore, microbial stimulators of innate immunity have been proposed as adjunctive therapy to other treatment modalities such as PDT. Myers *et al.* [124] investigated the interaction of HpD-PDT and *Corynebacterium parvum* in a murine transitional cell carcinoma (MBT-2) model. A low dose of *C. parvum* significantly improved the cancer cells sensitization to PDT, while PDT reduced the benefit obtained with high doses of the microbial adjuvant. However, high doses of the *C. parvum* given post-PDT resulted in a significant greater effect than the low dose of *C. parvum* before PDT. Similarly, Cho *et al.* [125] assessed the interaction of PDT and intravesical drugs, including some cytostatic agents and Bacillus Calmette-Guerin (BCG) in the same model. The associations were well tolerated and improved the cytotoxic effect of individual treatments. Korbelik and co-workers [126,127], evaluated combined regimens of either BCG or mycobacterium cell-wall extract (MCWE) treatment combined with PDT mediated by six clinically relevant photosensitizers: Photofrin®, BPD-MA, *m*-THPC, Mce$_6$, lutetium texaphyrin, and zinc phthalocyanine (ZnPC). The PDT doses used in all cases were

chosen to achieve strong tumor reduction response, but low levels of permanent tumor cures. Irrespective of the photosensitizer, beneficial effects on PDT-mediated cures were obtained using both bacterial strains. According to flow cytometry-based analysis of cellular populations found in excised EMT6 tumor, the association of PDT and MCWE enhanced the infiltration of neutrophils when given after PDT. Deeper investigations of the effect of BCG adjuvant to PDT showed that treatments with BCG pre- and post-*m*-THPC-PDT effectively reduced the incidence of tumor recurrence and tumor cures. Again, irrespective of the photosensitizer, the use of BCG as adjuvant therapy enhanced the cure rate of PDT-treated tumors, but not tumor recurrence after the tumor-free period, except ZnPC which resulted in no tumor recurrence. In contrast to MCWE, BCG administration did not affect significantly PDT-induced accumulation of activated myeloid cells, but apparently increased immune memory T cells in tumor-draining lymph nodes indicating that the interaction may take place in later events involved in preventing tumor recurrence.

Among other immunostimulants investigated by the group of Korbelik [128] as adjuvant therapies to PDT, sonifilan, a β-D-glucan obtained from the Aphyllophoral fungus Schizophyllum commune, has been proven to be of particular interest. The administration of sonifilan before PDT to tumor-bearing mice resulted in an increased Photofrin® retention in cancer cells and a three times higher PDT response. In contrast, the administration of sonifilan after PDT was not beneficial with respect to tumor growth. Glycated chitosan was another immunostimulant that was evaluated as adjuvant to PDT. This agent, administered immediately after PDT with Photofrin® to EMT6 tumor-bearing mice, provided significant improvement in the long-term survival of these animals [129].

Other microbial preparations have been evaluated as adjuvant treatments to PDT. Uehara and co-workers [130] investigated the anti-tumor effect of PDT when combined with a streptococcal preparation (OK-432) in a murine model. The PDT activity against NR-S1 mouse squamous cell carcinoma was improved by OK-432 in particular when administered a few hours before PDT, while OK-432 alone did not produce a significant effect on the neoplastic cells *in vivo*. The combined regimen resulted in an important immune reaction evidenced as intense hemorrhage and marked infiltration of inflammatory cells into the necrotic area. However, the number of neutrophils was not increased by the treatment. Moreover, mice treated with the PDT combined with OK-432 tended to survive longer than those treated with any of the two therapies alone.

Adoptive cellular therapies constitute another interesting combination for PDT. Mature dendritic cells are professional antigen-presenting cells and the most effective inducers of adaptative immunity which is not the case of immature dendritic cells [131]. Jalili *et al.* [132] evaluated the tumor sensitization to Photofrin®-based-PDT in association with the administration of immature dendritic cells in C-26 bearing BALB/c mice. Dendritic cells co-cultured with PDT-treated C-26 cells resulted in efficient endocytosis (50%) of tumor cells and/or remnants tumor cells as compared to dendritic cells co-cultured with non-PDT-treated cancer cells (3%). In addition, the increased secretion of IL-2 by dendritic cells co-cultured with PDT-treated C-26 cells unequivocally showed that immature dendritic cells became functional after their interaction with damaged tumor cells. *In vivo*, dendritic cells administered to C-26 tumor were capable to reach local and, to a lesser extent, distant lymph nodes. Cytotoxicity of lymph node cells towards tumor cells was only detectable with tumors treated with dendritic cells combined with PDT. Moreover, spontaneous cytotoxicity (attributed to NK cells) was present in all of the treated groups, whereas specific cytotoxicity (attributed to $CD8^+$ T cells) was markedly increased (5-fold) by the administration of dendritic cells alone or in combination with PDT. Altogether, these findings support the strong reduction of tumor growth in mice receiving PDT in association with dendritic cells.

Korbelik and Sun [133] reported a study of *m*-THPC-PDT in combination with a biological therapy involving a genetically altered NK92MI cell line to produce IL-2. The interaction was investigated in NOD-scid mice bearing SiHa and HT-29 tumors. Low doses of NK92MI cells were effective enhancers of the anti-tumor response to PDT when administered pertumorally, while no obvious benefit was observed when administered intravenously. In contrast, at higher concentrations NK92MI cells given immediately after PDT substantially increased the cure rates of PDT-treated tumors, irrespective to the administration route. Although similar cure rates were observed in both SiHa and HT-29 tumors, *in vitro* cytotoxicity assays showed that NK92MI cells were more aggressive against SiHa cells than HT-29 cells. Treatment with NK92MI alone did not lead to cures of subcutaneous tumors under comparable experimental conditions. Furthermore, immunocompatibility studies in immunocompetent BALB/c recipients bearing PDT-treated EMT6 tumors showed a clear therapeutic benefit, which indicates that the adoptively transferred cells were not destroyed before exerting their anti-tumor action. The enhancement produced by adjunctive NK92MI may be simply due its cytotoxic activity on the remaining foci of viable malignant cells not destroyed by PDT.

However, the interaction between pathways stimulated by PDT and NK92MI cell activity may also have a synergistic character that requires further elucidation.

A further biological therapy involves the administration of antibodies against cancer cells or cancer-associated targets. However, to the best of our knowledge, few experiments combining this modality with PDT have been reported. Del Carmen and colleagues [134] studied C225, a monoclonal antibody against the epidermal growth factor receptor (EGFR), as an adjunctive therapy to BPD-MA-PDT. A challenging model, NIH:OVCAR-5 bearing mice, was chosen for this study. Although the overexpression of EGFR is associated with the development of ovarian cancer resistant to chemotherapy and immunotherapy, the combinatory regimen showed increased anti-tumoral activity. C225 adjuvant to PDT resulted in a 7- or 4-fold reduction of tumor burden compared to C225 or PDT alone as well as improvements in survival time. *A priori*, this synergistic response may reflect the fact that the individual monotherapies target non-overlapping molecular pathways. C225 blockade of EGFR activity prevents cancer cells that overexpress EGFR from aberrantly entering S phase, which in turn makes them more vulnerable to PDT. An alternative explanation is that C225 mitigates the enhanced activation of EGFR after PDT and suppresses downstream survival signals. Because recurrent epithelial ovarian cancer is rarely curable, this approach may offer a new possibility to women suffering from this disease.

Although promising results of PDT-combined regimens with immunotherapy have been observed, so far, few studies have been performed in humans. Szygula *et al.* [135] reported a pilot study of 14 patients with Transitional cell carcinoma (TCC) of the urinary bladder. Patients were subjected to 5-ALA-mediated-PDT with subsequent BCG-therapy after the previous transurethral resection of bladder tumor (TUR-BT). In 10 cases, neither macroscopic recurrence nor cytologic signs of cancer or pre-cancerous lesions has been noted in a 2-year follow-up. From this group, total response was observed in eight patients (normal urothelium or urocystitis were found during control examinations) and partial response in two (diagnosed with low or high-grade dysplasia in microscopic examination). Tumor recurrence was observed in four patients (cancer cells in excised specimens). Although the number of patients included in this trial was small, these preliminary results show that the association of TUR-BT, 5-ALA-mediated-PDT and BCG might improve the efficacy of urinary bladder cancer therapy.

7. Conclusions

Chemotherapy as an option for the treatment of cancer represents some inconveniences including dose-limiting toxicity and treatment resistance. Furthermore, other therapies such as immunotherapy may not be totally effective as single treatment modality. This has led to the search for more effective therapeutic agents or mechanism-based combination therapies that overcome these drawbacks and, thus offer cancer patients more safe and effective treatments.

So far, PDT has been shown to be a useful and well-tolerated therapy for different diseases. Moreover, a large body of *in vitro* and *in vivo* evidence has been accumulated demonstrating the potential benefits of combination therapies including PDT in association with other pharmacological therapies over monotherapy for the treatment of several types of cancer. These results are mainly supported on the multiple mechanisms of action of PDT which usually single drugs do not exhibit. PDT in combination with chemotherapeutic agents has shown not only to increase the direct damage to the targeted cells by cytotoxic agents, but also to affect the tumor microvasculature and, in some cases, induce a host immune response against cancer cells. On the other hand, the final PDT outcome could be reduced by PDT-induction of potent angiogenic factors. The use of anti-angiogenic agents has been shown to counteract the PDT-induced angiogenesis and cell proliferation that otherwise could lead to disease recurrence. Although PDT can stimulate the host immune response, it can also induce the expression of some immune suppressor factors. Some immunologic agents have resulted in an enhancement of the PDT-induced host immune response against cancer cells or overcome PDT-induced immune suppression.

Despite the increased number of preclinical reports, there are still considerable efforts to undertake in terms of clinical trials for assessing the risk-benefit of such PDT-combined treatments in order to establish them as alternative or first choice treatments for malignant disorders.

References

1. Fitzgerald, J.B.; Schoeberl, B.; Nielsen, U.B.; Sorger, P.K. *Nat. Chem. Biol.*, **2006**, *2,* 458.

2. Frantz, S. *Nature*, **2005**, *437,* 942.

3. Greco, W.R. and Parsons, J.C. *Pharmacol. Rev.*, **1995**, *47,* 331.

4. Loewe, S. and Muischnek, H. *Naunyn Schmiedebergs Arch. Exp. Pathol. Pharmakol.*, **1926**, *114,* 313.

5. Berenbaum, M.C. *Clin. Exp. Immunol.*, **1977**, *28,* 1.

6. Dougherty, T.J.; Gomer, C.J.; Henderson, B.W.; Jori, G.; Kessel, D.; Korbelik, M.; Moan, J.; Peng, Q. *J. Natl. Cancer Inst.*, **1998**, *90,* 889.

7. Gudgin Dickson, E.F.; Goyan, R.L.; Pottier, R.H. *Cell. Mol. Biol. (Noisy -le-grand)*, **2002**, *48,* 939.

8. Bradley, J.; Ju, M.; Robinson, G. *Angiogenesis*, **2007**, *10,* 141.

9. Dolmans, D.E.J.G.; Fukumura, D.; Jain, R.K. *Nat. Rev. Cancer*, **2003**, *3,* 380.

10. Oleinick, N.L. and Evans, H.H. *Radiat. Res.*, **1998**, *150,* S146-S156.

11. Castano, A.P.; Demidova, T.N.; Hamblin, M.R. *Photodiag. Photodyn. Ther.*, **2005**, *2,* 1.

12. Castano, A.P.; Demidova, T.N.; Hamblin, M.R. *Photodiag.Photodyn. Ther.*, **2005**, *2,* 91.

13. Macdonald, I.J. and Dougherty G.J. *J. Porphyrins Phtalocyanines*, **2000**, *5,* 105.

14. Oleinick, N.L.; Morris, R.L.; Belichenko, I. *Photochem. Photobiol. Sci.*, **2002**, *1,* 1.

15. Agostinis, P.; Buytaert, E.; Breyssens H.; Hendrickx, N. *Photochem. Photobiol. Sci.*, **2004**, *3,* 729.

16. Kessel, D.; Vicente, M.G.H.; Reiners, J.J. *Laser Med. Surg.*, **2006**, *38,* 482.

17. Fingar, V.H. *J. Clin. Laser Med. Surg.*, **1996**, *14,* 323.

18. Krammer, B. *Anticancer Res.*, **2001**, *21,* 4271.

19. Ferrario, A.; von Tiehl, K.F.; Rucker, N.; Schwarz, M.A.; Gill, P.S.; Gomer, C.J. *Cancer Res.*, 2**000**, *60,* 4066.

20. Ferrario, A.; von Tiehl, K.; Wong, S.; Luna, M.; Gomer, C.J. *Cancer Res.*, **2002**, *62,* 3956.

21. Gomer, C.J.; Ferrario, A.; Luna, M.; Rucker, N.; Wong, S. *Laser Surg. Med.*, **2006**, *38,* 516.

22. Coultas, L.; Chawengsaksophak, K.; Rossant, J. *Nature*, **2005**, *438,* 937.

23. Taketo, M.M. *J. Natl. Cancer Inst.*, **1998**, *90,* 1529.

24. Coussens, L.M.; Fingleton, B.; Matrisian, L.M. *Science*, **2002**, *295,* 2387.

25. Volanti, C.; Hendrickx, N.; Van Lint, J.; Matroule, J.Y.; Agostinis, P.; Piette, J. *Oncogene*, **2005**, *24,* 2981.

26. Ferrario, A.; Chantrain, C.F.; von Tiehl, K.; Buckley, S.; Rucker, N.; Shalinsky, D.R.; Shimada, H.; DeClerck, Y.A.; Gomer, C.J. *Cancer Res.*, **2004**, *64,* 2328.

27. Canti, G.; De Simone, A.; Korbelik, M. *Photochem. Photobiol. Sci. , 2002, 1, 79-80*, **2002**, *1,* 80.

28. Korbelik, M. *J. Clin. Laser Med. Surg.*, **1996**, *14,* 329.

29. Scartozzi, M.; Galizia, E.; Verdecchia, L.; Berardi, R.; Chiorrini, S.; Cascinu, S. *Expert Opin. Pharmacother.*, **2007**, *8,* 797.

30. Nahabedian, M.Y.; Cohen, R.A.; Contino, M.F.; Terem, T.M.; Wright, W.H.; Berns, M.W.; Wile, A.G. *J. Natl. Cancer Inst.*, **1998**, *80,* 739.

31. Canti, G.; Nicolin, A.; Cubeddu, R.; Taroni, P.; Bandieramonte, G.; Valentini, G. *Cancer Lett.*, **1998**, *125,* 39.

32. Baas, P.; Michielsen, C.; Oppelaar, H.; van Zandwijk, N.; Stewart, F.A. *Int. J. Cancer*, **1994**, *56,* 880.

33. van Geel, I.P.; Oppelaar, H.; Oussoren, Y.G.; Schuitmaker, J.J.; Stewart, F.A. *Br. J. Cancer*, **1995**, *72,* 344.

34. Nonaka, M.; Ikeda, H.; Inokuchi, T. *Cancer Lett.*, **2002**, *184,* 171.

35. Crescenzi, E.; Varriale, L.; Iovino, M.; Chiaviello, A.; Veneziani, B.; Palumbo, G. *Mol. Cancer Ther.*, **2004**, *3,* 537.

36. Crescenzi, E.; Chiaviello, A.; Canti, G.; Reddi, E.; Veneziani, B.M.; Palumbo, G. *Mol. Cancer Ther.*, **2006**, *5,* 776.

37. Peterson, C.M.; Lu, J.M.; Gu, Z.W.; Shiah, J.G.; Lythgoe, K.; Peterson, C.A.; Straight, R.C.; Kopecek, J. *J. Soc. Gynecol. Invest.*, **1995**, *2,* 772.

38. Ma, L.W.; Steen, H.B.; Moan, J.; Berg, K.; Peng, Q.; Saether, H.; Rimington, C. *Int. J. Biochem.*, **1992**, *24,* 1807.

39. Ma, L.W.; Moan, J.; Berg, K.; Peng, Q.; Steen H.B. *Radiat. Res.*, **1993**, *134,* 22.

40. Datta, S.N.; Allman, R.; Loh, C.; Mason, M.; Matthews, P.N. *Br. J. Cancer*, **1997**, *76,* 312.

41. French, A.J.; Datta, S.N.; Allman, R.; Matthews, P.N. *BJU Int.*, **2004**, *93,* 156.

42. Brophy, P.F. and Keller, S.M. *J. Surg. Res.*, **1992**, *52,* 631.

43. Kirveliene, V.; Grazeliene, G.; Dabkeviciene, D.; Micke, I.; Kirvelis, D.; Juodka, B.; Didziapetriene, J. *Cancer Chemoth. Pharm.*, **2006**, *57,* 65.

44. Uehara, M.; Inokuchi, T.; Ikeda, H. *J. Oral Maxil. Surg.*, **2006**, *64,* 390.

45. Phillips, R.M. *Expert Opin. Inves. Drugs*, **1998**, *7,* 905.

46. Gonzolez, S.; Arnfield, M.R.; Meeker, B.E.; Tulip, J.; Lakey, W.H.; Chapman, J.D.; McPhee, M.S. *Cancer Res.*, **1986**, *46,* 2858.

47. Henry, J.M. and Isaacs, J.T. *J. Urology*, **1989**, *142,* 165.

48. Bremner, J.C.; Adams, G.E.; Pearson, J.K.; Sansom, J.M.; Stratford, I.J.; Bedwell, J.; Bown, S.G.; MacRobert, A.J.; Phillips, D. *Br. J. Cancer*, **1992**, *66,* 1070.

49. Bremner, J.C.; Bradley, J.K.; Adams, G.E.; Naylor, M.A.; Sansom, J.M.; Stratford, I.J. *Int. J. Radiation Oncology Biol. Phys.*, **1994**, *29,* 329.

50. Baas, P.; Oppelaar, H.; Stavenuiter, M.; van Zandwijk, N.; Stewart, F.A. *Int. J. Radiation Oncology Biol. Phys.*, **1993**, *27,* 665.

51. Casas, A.; Perotti, C.; Ortel, B.; Di Venosa, G.; Saccolitti, M.; Batlle, A.; Hasan, T. *Int. J. Oncol.*, **2006**, *29,* 397.

52. Osterloh, J. and Vicente, M.G.H. *J. Porphyrins Phthalocyanines*, **2002**, *6,* 305.

53. Brunner, H. and Schellerer, K.-M. *Inorg. Chim. Acta*, **2003**, *350,* 39.

54. Lottner, C.; Knuechel, R.; Bernhardt, G.; Brunner, H. *Cancer Lett.*, **2004**, *203,* 171.

55. Shiah, J.G.; Sun, Y.; Peterson, C.M.; Straight, R.C.; Kopecek, J. *Clin. Cancer Res.*, **2000**, *6,* 1008.

56. Shiah, J.G.; Sun, Y.; Kopeckova, P.; Peterson, C.M.; Straight, R.C.; Kopecek, J. *J. Control. Release*, **2001**, *74,* 249.

57. Peterson, C.M.; Lu, J.M.; Sun, Y.; Peterson, C.A.; Shiah, J.G.; Straight, R.C.; Kopecek, J. *Cancer Res.*, **1996**, *56,* 3980.

58. Lu, J.M.; Peterson, C.M.; Guo-Shiah J.; Gu, Z.W.; Peterson, C.A.; Straight, R.C.; Kopecek, J. *Int. J. Oncol.*, **1999**, *15,* 5.

59. Grajate, C. and Mollinedo, F. *Curr. Drug Metab.*, **2002**, *3,* 491.

60. Harguindey, S.; Pedraz, J.L.; Canero, R.G.; Katin, M. *Apoptosis*, **2000**, *5,* 87.

61. Vogler, W.R.; Berdel, W.E.; Olson, A.C.; Winton, E.F.; Heffner, L.T.; Gordon, D.S. *Blood*, **1992**, *80,* 1423.

62. Traul, D.L.; Anderson, G.S.; Bilitz, J.M.; Krieg, M.; Sieber, F. *Photochem. Photobiol.*, **1995**, 62, 790.

63. Yamazaki, T. and Sieber, F. *Bone Marrow Transplant.*, **1997**, *19,* 113.

64. Anderson, G.S.; Tsujino, I.; Miyagi, K.; Sampson, R.; Sieber, F. *J. Photoch. Photobio. B*, **2003**, *69,* 87.

65. Anderson, G.S.; Miyagi, K.; Sampson, R.W.; Sieber, F. *J. Photoch. Photobio. B*, **2002**, *68,* 101.

66. Tsujino, I.; Miyagi, K.; Sampson, R.W.; Sieber, F. *Photochem. Photobiol.*, **2006**, *82,* 458.

67. Di Cosimo, S.; Ferretti, G.; Papaldo, P.; Carlini, P.; Fabi, A.; Cognetti, F. *Drugs Today*, **2003**, *39,* 157.

68. Guminska, M.; Kedryna, T.; Marchut, E. *Biochem. Pharmacol.*, **1986**, *35,* 4369.

69. Shevchuk, I.; Chekulayev, V.; Moan, J.; Berg, K. *Int. J. Cancer*, **1996**, *67,* 791.

70. Chekulayev, V.; Shevchuk, I.; Chekulayeva, L.; Kahru, A. *J. Photoch. Photobio. B*, **1997**, *41,* 11.

71. Jin, M.L.; Yang, B.Q.; Zhang, W.; Ren, P. *J. Photoch. Photobio. B*, **1992**, *12,* 101.

72. Baas, P.; van Geel, I.P.; Oppelaar, H.; Meyer, M.; Beynen, J.H.; van Zandwijk, N.; Stewart, F.A. *Br. J. Cancer*, **1996**, *73,* 945.

73. Skyrme, R.J.; French, A.J.; Datta, S.N.; Allman, R.; Mason, M.D.; Matthews, P.N. *BJU Int.*, **2005**, *95,* 1206.

74. Pass, H.I.; Temeck, B.K.; Kranda, K.; Thomas, G.; Russo, A.; Smith, P.; Friauf, W, ; Steinberg, S.M. *Ann. Surg. Oncol.*, **1997**, *4,* 628.

75. Iaffaioli, R.V.; Milano, A.; Caponigro, F. *Ann. Oncol.*, **2007**, *18,* 153.

76. Singh, R.; Fouladi-Nashta, A.A.; Li, D.; Halliday, N.; Barrett, D.A.; Sinclair, K.D. *J. Cell. Biochem.*, **2006**, *99, 146*.

77. Shinjyo, N. and Kita, K. *Biochem.Bio. Res. Co.*, **2007**, *358,* 130.

78. Malik, Z.; Lugaci, H.; Hanania, J. *Exp. Hematol.*, **1988**, *16,* 330.

79. Sinha A.K.; Anand, S.; Ortel, B.J.; Chang, Y.; Mai, Z.; Hasan, T.; Maytin, E.V. *Br. J. Cancer*, **2006**, *95,* 485.

80. Ortel, B.; Sharlin, D.; O'Donnell, D.; Sinha, A.K.; Maytin, E.V.; Hasan, T. *Br. J. Cancer*, **2002**, *87,* 1321.

81. Frank, J.; Flaccus, A.; Schwarz, C.; Lambert, C.; Biesalski, H.K. *Free Radical Bio. Med.*, **2006**, *40,* 827.

82. Buettner, G.R. and Jurkiewicz, B.A. *Radiat. Res.*, **1996**, *145,* 532.

83. Jakus, J. and Farkas, O. *Photochem. Photobiol.*, **2005**, *4,* 694.

84. Girotti, A.W.; Thomas, J.P.; Jordan, J.E. *Photochem. Photobiol.*, **1985**, *41,* 267.

85. Rosenthal, I. and Ben Hur, E. *Int. J. Radiat. Biol.*, **1992**, *62,* 481.

86. Kelley, E.E.; Domann, F.E.; Buettner, G.R.; Oberley, L.W.; Burns, C.P. *J. Photoch. Photobio. B*, **1997**, *40,* 273.

87. Kramarenko, G.G.; Wilke, W.W.; Dayal, D.; Buettner, G.R.; Schafer, F.Q. *Free Radical Bio. Med.*, **2006**, *40,* 1615.

88. Shevchuk, I.; Chekulayev, V.; Chekulayeva, L. *J. Photoch. Photobio. B*, **1998**, *45,* 136.

89. Melnikova, V.; Bezdetnaya, L.; Belitchenko, I.; Potapenko, A.; Merlin, J.L.; Guillemin, F. *Cancer Lett.*, **1999**, *139,* 89.

90. Melnikova, V.O.; Bezdetnaya, L.N.; Brault, D.; Potapenko, A.Y.; Guillemin, F. *Int. J. Cancer*, **2000**, *88,* 798.

91. Wang, H.P.; Qian, S.Y.; Schafer, F.Q.; Domann, F.E.; Oberley, L.W.; Buettner, G.R. *Free Radical Bio. Med.*, **2001**, *30,* 825.

92. Miller, A. and Henderson, B. *J. Natl. Cancer Inst.*, **1986**, *77,* 505.

93. Jiang, F.; Lilge, L.; Belcuig, M.; Singh, G.; Grenier, J.; Li, Y.; Chopp, M. *Laser Surg. Med.*, **1998**, *23,* 161.

94. Jiang, F.; Robin, A.M.; Katakowski, M.; Tong, L.; Espiritu, M.; Singh, G.; Chopp, M. *Laser Med. Sci.*, **2003**, *18,* 128.

95. Zuluaga, M.F.; Mailhos, C.; Robinson, G.; Shima, D.T.; Gurny, R.; Lange, N. *Invest. Ophthalmol. Vis. Sci.*, **2007**, *48,* 1767.

96. Ferrario, A, and Gomer, C.J. *J. Environ. Pathol. Toxicol. Oncol.*, **2006**, *25,* 251.

97. Dimitroff CJ; Klohs W; Sharma A; Pera P; Driscoll D; Veith J; Steinkampf R; Schroeder M; Klutchko S; Sumlin A; Henderson B; Dougherty TJ; Bernacki R *Invest New Drugs*, **1999**, *17,* 121.

98. Zhou, Q.; Olivo, M.; Lye, K.Y.; Moore, S.; Sharma, A.; Chowbay, B. *Cancer Chemoth. Pharm.*, **2005**, *56,* 569.

99. Mendel, D.B.; Schreck, R.E.; West, D.C.; Li, G.; Strawn, L.M.; Tanciongco, S.S.; Vasile, S.; Shawver, L.K.; Cherrington, J.M. *Clin. Cancer Res.*, **2000**, *6,* 4848.

100. Kosharskyy, B.; Solban, N.; Chang, S.K.; Rizvi, I.; Chang, Y.; Hasan, T. *Cancer Res.*, **2006**, *66,* 10953.

101. Bellnier, D.A.; Gollnick, S.O.; Camacho, S.H.; Greco, W.R.; Cheney, R.T. *Cancer Res.*, **2003**, *63,* 7584.

102. Seshadri, M.; Spernyak, J.A.; Mazurchuk, R.; Camacho, S.H.; Oseroff, A.R.; Cheney, R.T.; Bellnier, D.A. *Clin. Cancer Res.*, **2005**, *11,* 4241.

103. Joseph, W.R.; Cao, Z.; Mountjoy, K.G.; Marshall, E.S.; Baguley, B.C.; Ching, L.M. *Cancer Res.*, **1999**, *59,* 633.

104. Moran, E.M. *J. Environ. Pathol. Toxicol. Oncol.*, **2002**, *21,* 193.

105. Kinoshita, T.; Takahashi, Y.; Sakashita, T.; Inoue, H.; Tanabe, T.; Yoshimoto, T. *BBA Mol. Cell Biol. L*, **1999**, *1438,* 120.

106. Singh, B. and Lucci, A. *J. Surg. Res.*, **2002**, *108,* 173.

107. Petkova, D.K.; Clelland, C.; Ronan, J.; Pang, L.; Coulson, J.M.; Lewis, S.; Knox, A.J. *Resp. Med.*, **2004**, *98,* 164.

108. Harvey, E.H.; Webber, J.; Kessel, D.; Fromm, D. *Am. J. Sur.*, **2005**, *189,* 302.

109. Ferrario, A.; Fisher, A.M.; Rucker, N.; Gomer, C.J. *Cancer. Res.*, **2005**, *65,* 9473.

110. Makowski, M.; Grzela, T.; Niderla, J.; Lazarczyk, M.; Mroz, P.; Kopee, M.; Legat, M.; Strusinska, K.; Koziak, K.; Nowis, D.; Mrowka, P.; Wasik, M.; Jakobisiak, M.; Golab, J. *Clin. Cancer Res.*, **2003**, *9,* 5417.

111. Akita, Y.; Kozaki, K.; Nakagawa, A.; Saito, T.; Ito, S.; Tamada, Y.; Fujiwara, S.; Nishikawa, N.; Uchida, K.; Yoshikawa, K.; Noguchi, T.; Miyaishi, O.; Shimozato, K.; Saga, S.; Matsumoto, Y. *Br. J. Dermatholog.*, **2004**, *151,* 472.

112. Yee, K.K.; Soo, K.C.; Olivo, M. *Int. J. Mol. Med.*, **2005**, *16,* 993.

113. Hendrickx, N.; Volanti, C.; Moens, U.; Seternes, O.M.; de Witte, P.; Vandenheede, J.R.; Piette, J.; Agostinis, P. *J. Biol. Chem.*, **2003**, *278,* 52231.

114. Hendrickx, N.; Dewaele, M.; Buytaert, E.; Marsboom, G.; Janssens, S.; Boven, M.V.; Vandenheede, J.R.; de Witte, P.; Agostinis, P. *Biochem. Bioph. Res. Co.*, **2005**, *337,* 928.

115. Bergers, G.; Brekken, R.; McMahon, G.; Vu, T.H.; Itoh, T.; Tamaki, K.; Tanzawa, K.; Thorpe, P.; Itohara, S.; Werb, Z.; Hanahan, D, *Nat. Cell Biol.*, **2000**, *2,* 737.

116. Hunt, D.W. and Chan, A.H. *Drugs*, **1999**, *2,* 231.

117. Castano, A.P.; Mroz, P.; Hamblin, M.R. *Nat. Rev. Cancer*, **2006**, *6,* 535.

118. Hall, D.; Nyseo, U.O.; Riggs, D.; Jackson, B.; Lamm, D.L. *P. Soc. Photo-Opt. Inst.*, **2001**, *4156,* 208.

119. Dima, V. F.; Ionescu, M. D.; Balotescu, C.; Dima, V. S. *P. Soc. Photo-Opt. Inst.*, **2003**, *5287,* 159.

120. Bellnier, D.A. *J. Photoch. Photobio. B.*, **1991**, *8,* 203.

121. Nowis, D.; Stoklosa, T.; Legat, M.; Issat, T.; Jakobisiak, M.; Golab, J. *Photodiag. Photodyn. Ther.*, **2005**, *2,* 283.

122. Krosl, G.; Korbelik, M.; Krosl, J.; Dougherty, G.J. *Cancer Res.*, **1996**, *56,* 3281.

123. Golab, J.; Wilczynski, G.; Zagozdzon, R.; Stoklosa, T.; Dabrowska, A.; Rybczynska, J.; Wasik, M.; Machaj, E.; Olda, T.; Kozar, K.; Kaminski, R.; Giermasz, A.; Czajka, A.; Lasek, W.; Feleszko, W.; Jakobisiak, M. *Br. J. Cancer*, **2000**, *82,* 1485.

124. Myers, R.C.; Lau, B.H.; Kunihira, D.Y.; Torrey, R.R.; Woolley, J.L.; Tosk J. *Urology*, **1989**, *33,* 230.

125. Cho, Y.H.; Straight, R.C.; Smith, J.A. Jr. *J. Urol.*, **1992**, *147,* 743.

126. Korbelik, M. and Cecic, I. *J. Photoch. Photobio. B*, **1998**, *44,* 151.

127. Korbelik, M.; Sun, J.; Posakony, J.J. *Photochem. Photobiol.*, **2001**, *73,* 403.

128. Krosl, G. and Korbelik, M. *Cancer Lett.*, **1994**, *84,* 43.

129. Chen, W.R.; Huang, Z.; Korbelik, M.; Nordquist, R.E.; Liu, H. *J. Environ. Pathol. Toxicol. Oncol.*, **2006**, *25,* 281.

130. Uehara, M.; Sano, K.; Wang, Z.L.; Sekine, J.; Ikeda, H.; Inokuchi, T. *Cancer Immunol. Immunother.*, **2000**, *49,* 401.

131. Guermonprez, P.; Valladeau, J.; Zitvogel, L.; Thery, C.; Amigorena, S. *Annu. Rev. Immunol.*, **2002**, *20,* 621.

132. Jalili, A.; Makowski, M.; Switaj, T.; Nowis, D.; Wilczynski, G.M.; Wilczek, E.; Chorazy-Massalska, M.; Radzikowska, A.; Maslinski, W.; Bialy, L.; Sienko, J.; Sieron, A.; Adamek, M.; Basak, G.; Mroz, P.; Krasnodebski, I.W.; Jakobisiak, M.; Golab, J. *Clin. Cancer Res.*, **2004**, *10,* 4498.

133. Korbelik, M. and Sun, J. *Int. J. Cancer*, **2001**, *93,* 269.

134. del Carmen, M.G.; Rizvi, I.; Chang, Y.; Moor, A.C.E.; Oliva, E.; Sherwood, M.; Pogue, B.; Hasan, T. *J. Natl. Cancer Inst.*, **2005**, *97,* 1516.

135. Szygula, M.; Pietrusa, A.; Adamek, M.; Wojciechowski, B.; Kawczyk-Krupka, A.; Cebula, W.; Duda, W.; Sieron, A. *Photodiag. Photodyn. Ther.*, **2004**, *1,* 241.

Chapter 2. Synergies of VEGF Inhibition and Photodynamic Therapy in the Treatment of Age-related Macular Degeneration

Maria-Fernanda Zuluaga[1], Carolina Mailhos[2], Gregory Robinson[2], D T. Shima[2], Robert Gurny[1], and Norbert Lange[1]

[1]Department of Pharmaceutics and Biopharmaceutics, School of Pharmaceutical Sciences, University of Geneva, University of Lausanne, 30 Quai Ernest-Ansermet, 1211 Geneva 4, Switzerland

[2] Eyetech Research Center, 35 Hartwell Ave., Lexington, MA 02421, USA.

ABSTRACT. Photodynamic therapy (PDT) and the administration of compounds acting against vascular endothelial growth factor (anti-VEGF) are approved for the treatment of choroidal neovascularization (CNV) secondary to age-related macular degeneration (AMD). Experimental evidence that the combined use of both treatment options may improve therapeutic outcome is presented. Fertilized chick eggs were incubated until day 12 of embryo development (EDD12) and treated by PDT using two different photosensitizing agents (liposomal formulation of BPD-MA; *m*-THPP encapsulated in polymeric nanoparticles) and were visualized using an epifluorescence microscope. Vascular occlusion of the treated zones of the chorioallantoic membrane (CAM) was assessed by fluorescence angiography, 24 and 48 hours post treatment. Alternatively, PDT treated areas were exposed to a soluble VEGF receptor antagonist (sFlt-1) 6 hours following treatment and were analyzed. Vascular occlusion in the PDT treated areas was observed with both photosensitizers 24 hour following treatment. Reperfusion of preexisting blood vessels and first signs of revascularization were visible already 48 hours post PDT. Topical administration of sFlt-1 to the treated areas augmented the occlusion and limited the subsequent angiogenesis in a dose-dependent manner. The combined use of PDT and agents targeting angiogenic cytokines may synergistically improve therapeutic outcome after combined treatment in patients with CNV secondary to AMD.

1. Introduction

The treatment of the «wet» form of age-related macular degeneration (AMD) can be achieved by three proven therapies [1]. Although thermal laser treatment is still used for the nonspecific coagulation of choroidal neovascularization (CNV) at extrafoveal sites [1], more directed agents include photodynamic therapy (PDT) and anti-VEGF therapy. These agents provide benefits through more specific inhibition of disease- associated neovascularization with minimal damage to retinal vessels, normal choriocapillaries, retinal pigment epithelium, and adjacent photoreceptors.

In liposomal benzoporphyrin derivative monoacid ring A-mediated PDT, the photosensitizer BPD-MA is applied intravenously, followed by irradiation of the diseased site with 689-nm light. Activation of the photosensitizer then leads to the local production of reactive oxygen species that trigger vascular occlusion through a complex cascade of molecular, cellular, and physiological events [2]. Because of the predominantly vascular localization of the photosensitizer directly after administration, collateral damage to neighboring tissues is not extensive. This treatment modality, approved for predominantly classic wet AMD, has been shown in several clinical trials to stabilize or slow vision loss [3-7].

Because the expression of angiogenic stimuli, such as vascular endothelial growth factors (VEGFs), basic fibroblast growth factors (bFGFs), and the angiopoietins, is involved in the pathogenesis of CNV associated with AMD [8-11], another option to treat this disease is the local administration of agents that interfere with the activity of these cytokines. VEGF is a major stimulator of angiogenesis [12]. Consequently two anti-VEGF agents, pegaptanib sodium and ranibizumab, have recently demonstrated convincing results in pivotal phase 3 studies. While the latter is a humanized antibody fragment that binds to all VEGF isoforms, pegaptanib sodium is a pegylated 28-base RNA oligonucleotide that binds specifically to the heparin-binding VEGF-A isoform. Both agents are administered intravitreally with minimal complications.

In PDT, microvascular injury induces inflammation and hypoxia and the expression of angiogenic and survival molecules including VEGF-A, which could lead to CNV persistence and recurrence. For that reason, it is likely that multiple rounds of AMD retreatments are necessary [13]. Because PDT and anti-VEGF therapy act on CNV according to different mechanisms, their combinational use might represent a benefit for patients undergoing treatment of AMD. This combination therapy is extremely promising, particularly if VEGF-

A-inhibiting agents are used after PDT, because PDT is able to remove unwanted CNV whereas anti-VEGF therapy will alter the progression of the disease and maintain the PDT effect.

To elucidate PDT/anti-VEGF combination therapy, we studied the angiogenic response after PDT in the chick chorioallantoic membrane (CAM) model with two different photosensitizers and the influence an anti-VEGF agent on CAM vascularization after PDT. Liposomal-formulated BPD-MA was used as a reference photosensitizer for the treatment of CNV and *m*-THPP encapsulated in nanoparticles to elucidate whether formulation, pharmacokinetics or photochemical properties have an influence on potential synergistic effect.

2. Materials and Methods

2.1. Materials

The following materials were used: recombinant human soluble VEGF R1 (sFlt-1)/Fc chimera (R&D Systems Europe Ltd (Abingdon, OX, UK); liposomal benzoporphyrin derivative monoacid ring A (BPD-MA; Visudyne®; Novartis, Basel, Switzerland); poly(D, L-lactide-*co*-glycolide) (PLGA) with a copolymer ratio of 50:50 and a molecular weight of 12 kDa (Resomer; RG502; Boehringer Ingelheim, Ingelheim, Germany); meso-tetra (*p*-hydroxyphenyl)porphyrin (*m*-THPP; Aldrich, Steinheim, Germany); poly(vinyl alcohol) 87.7% hydrolyzed with a molecular weight of 26 kDa (Mowiol® 4-88; Hoechst, Frankfurt/Main, Germany); D(+)-Trehalose dihydrate and phosphate-buffered saline (PBS; Sigma-Aldrich, Taufkirchen, Germany); sulforhodamine 101 and ethanol 99.8 (Fluka, Buchs, Switzerland); Lipidem 10% (Vifor SA, Geneva, Switzerland). All chemicals were of analytical grade and used without further purification.

2.2. Microscope set-up

Fluorescence imaging of CAM vessels was performed with a Retriga EX camera (QImaging, Burnaby, BC, Canada) fitted to a fluorescence microscope (Eclipse 600 FN; Nikon, Tokyo, Japan) equipped with an objective CFI achromat magnification of 4x, a numerical aperture of 0.10 and a working distance of 30 mm. Illumination was provided by a filtered 100-W mercury arc lamp. Light doses were measured with a calibrated FieldMaster power meter

(Coherent, Santa Clara, CA). For the studies with *m*-THPP, the microscope was equipped with a fluorescence cube (BV- 2A; Nikon). This cube is composed of a 420 CWL filter, which provides excitation wavelengths between 400 and 440 nm, a dichroic mirror (455 nm), and a long path filter (470 nm). An additional band path filter (D650/50m; Chroma Technology Corp., Rockingham, VT) was added. For the studies with BPD-MA, a fluorescence cube composed of a 420 CWL filter, a dichroic mirror (455 nm), and a long path filter (610 nm) was assembled. The fluorescence of sulforhodamine 101, was detected with a cube (G- 2B; Nikon) composed of a D535/50x excitation filter, a dichroic mirror (575 nm), and a long path filter (610 nm). An additional band path filter (D650/50m; Chroma Technology Corp.) was added. Digital imaging, data display, and storage were performed with commercial hardware (Macintosh; Apple, Cupertino, CA) connected to the CCD camera and the software (OpenLab 3.15; Improvision Ltd, Coventry, UK).

2.3. Nanoparticle preparation

Nanoparticles loaded with *m*-THPP were prepared using the emulsification-diffusion technique, as described by Vargas et al. [14] The mean diameter of the freeze-dried nanoparticles, determined by photon correlation spectroscopy (Zetasizer 5000, Malvern, Worcestershire, UK), was 123 ± 13 nm with a polydispersity index of 0.2. A photosensitizer loading of 7.3% (wt/wt) was determined spectrophotometrically with a spectrometer (Cintra 40; GBS, Victoria, Australia) using a calibration curve established at 688 nm.

2.4. Egg incubation

Fertilized hen eggs (Animalerie universitaire, University of Geneva, Geneva, Switzerland) were placed into an incubator (MG 200; Savimat, Chauffry, France) set at 37 °C and a relative humidity (RH) of 65%. Until EDD 4, eggs were automatically rotated. Then, a 3-mm hole was drilled into the eggshell at the narrow apex and was covered with an adhesive tape. Eggs were then incubated without rotation until the CAM assay on EDD 12.

2.5. Chick chorioallantoic membrane (CAM) preparation and injection procedure

The CAM assay was adapted from Lange et al. [15] with minor modifications. All assays were performed at least 5 times, unless otherwise specified. On EDD 12, the hole in the eggshell was enlarged to a diameter of 2 to 3 cm, allowing access to the CAM vasculature. Chick embryos were placed under the objective of the fluorescence microscope. For m-THPP doses of 0.6 and 1.2 mg/Kg body weight of chick embryo in PBS and for BPD-MA, 0.20 and 0.25 mg/Kg doses in water were used. Formulations were injected into one of the principal blood vessels of the CAM through a 33-gauge needle fitted to a 100-µl syringe (Hamilton, Reno, NV).

2.6. Photodynamic therapy and assessment of vascular occlusion

CAM was irradiated with light doses of 15, 25 or 30 J/cm2 at 400 to 440 nm 1 minute after IV administration of photosensitizer. The surface of the irradiated CAM area was 1.8 mm^2. Before PDT, a silicone O-ring (Apple Rubber Products INC., Lancaster, NY) was placed to frame the region on which PDT was performed. Subsequently, the aperture in the shell was carefully covered with a plastic film (Parafilm; Pechiney Plastic Packaging, Chicago, IL), and treated eggs were maintained in the dark for 24 hours in the incubator (37 °C, 65% RH). Then, 20 µl sulforhodamine 101 in NaCl 0.9% (0.5 mg/mL) were injected into chick embryos to document vascular occlusion after PDT. The same procedure was carried out 48 hours after PDT to determine the potential neovascularization of the treated area. To improve visualization of the vascular bed at 48 hours, the contrast medium (Lipidm 10%; Vifor SA) was injected under the chorioallantoic membrane. Comparison of vessel fluorescence before and after PDT (24 and 48 hours) allowed an evaluation of vessel occlusion using an arbitrary damage scale proposed by Lange et al. [15] presented in Table 1.

2.7. Anti-VEGF therapy

After the hole in the eggshell was enlarged to a diameter of 2 to 3 cm on EDD 12, a silicone O-ring was placed on the CAM, the aperture in the shell was carefully covered with a plastic film, and the eggs were maintained for 6 hours in the incubator (37°C, 65% RH). Next, 10 µl sFlt-1 solution in PBS (0.50, 0.75, 1.00 or 2.00 µg/embryo) was topically applied inside the

O-ring, and the shell was covered again with a plastic film. After 24 and 48 hours, fluorescence angiography of the irradiated area with sulforhodamine 101 was performed, as described.

Table 1. Evaluation of PDT-induced damage on CAM vessels

Damage scale*	Criterion
0	No damage
1	Partial closure of capillaries of diameter <10 μm
2	Closure of capillary system, partial closure of blood vessels of diameter <30 μm and size reduction of larger blood vessels
3	Closure of vessels of diameter <30 μm and partial closure of higher order vessels
4	Total closure of vessels of diameter <70 μm and partial closure of larger vessels
5	Total occlusion of vessels in the irradiated area

Intermediate values were found when different scores were averaged.

2.8. Photodynamic therapy and Anti-VEGF therapy synergies and damage assessment

After photosensitizer injection and irradiation under the conditions mentioned, treated eggs were maintained in the dark for 6 hours in an incubator (37°C, 65% RH). sFlt-1 solution (10 μl) was topically applied, and fluorescence angiography of the irradiated area with sulforhodamine 101 was performed 24 and 48 hours after PDT. Comparison of vessel fluorescence before and after PDT and both PDT and VEGF treatments allowed an evaluation of vessel damage using the same arbitrary damage scale.

2.9. Statistical analysis

Nonparametric analysis was performed to compare the effect of single treatment PDT and anti-VEGF and combined-treatment PDT/anti-VEGF by means of the Kruskal-Wallis or Jonckheere test, followed by post-hoc multiple comparison.

3. Results

3.1. Photodynamic therapy and damage assessment

The CAM model used to study AMD consists of controlling the CAM vasculature before, during, and 24 hours after the desired therapy. However, to assess undesirable effects such as reperfusion and repeat neovascularization in PDT, the CAM vasculature was also assessed 48 hours after the therapy. The effect of PDT after 24 hours and 48 hours with m-THPP-loaded nanoparticles (drug dose, 0.60 and 1.20 mg/Kg embryo) and BPD-MA liposomes (drug dose, 0.20 and 0.25 mg/Kg) on the vascular system of the CAM using 30 J/cm^2 as light dose are summarized in Fig. 1. All conditions resulted in dose-dependent vasculature occlusion after 24 hours. However, reperfusion of occluded vessels after 48 hours led to a considerable decrease in damage score. Formation of new vessels was particularly evident at 30 J/cm^2 (data not shown for other light doses). Optimal conditions to study antiangiogenesis activity were achieved using drug doses of m-THPP 1.2 mg/Kg embryo (Fig. 1A) and BPD-MA 0.25 mg/Kg embryo (Fig. 1B), respectively. These conditions resulted in strong vascular occlusion after 24 hours after PDT and in neovascularization and reperfusion of larger vessels (> 70 µm) after 48 hours.

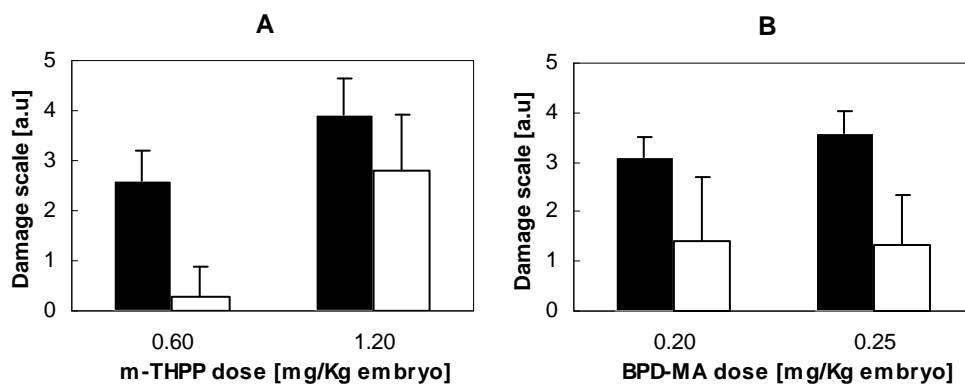*Figure 1. Vascular occlusion is induced by photosensitizing agent. Vascular damage induced by (A) m-THPP and (B) BPD-MA in the CAM as a function of photosensitizer concentration, 24h (■) and 48h (□) after PDT. Light dose, 30 J/cm². Mean ± S.D. (n ≥ 5).*

Fig. 2 shows the typical sequence of a CAM assay. It consisted of injection of a photosensitizer (Fig. 2A), followed by PDT (Fig. 2B) and sulforhodamine 101 angiography

24 hours after PDT (Fig. 2C). In addition to the standard sequence, another sulforhodamine 101 angiography with a contrast medium was again performed, this time 48 hours after PDT (Fig. 2D).
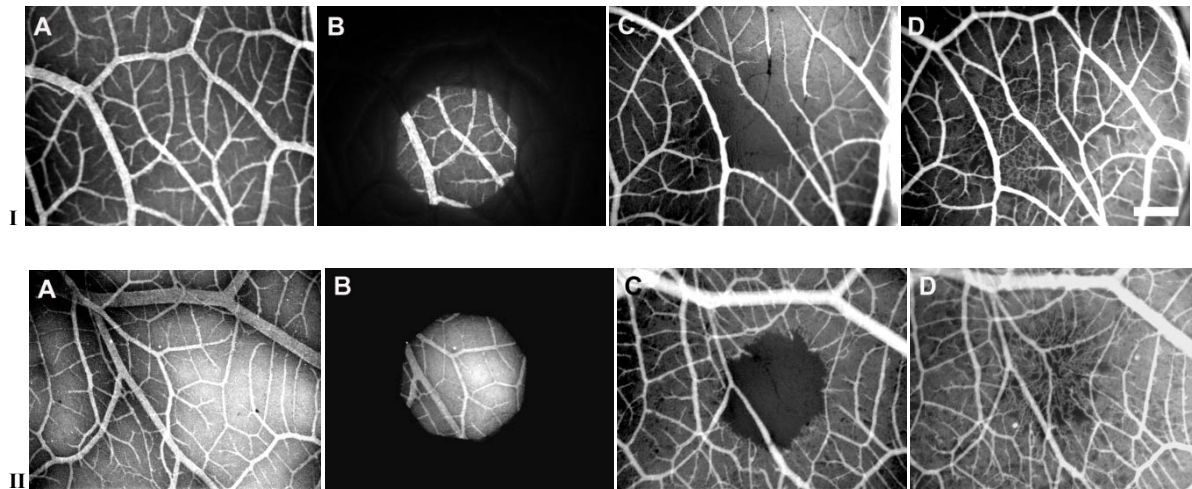
Figure 2. Assessment of vascular occlusion after photodynamic therapy. Fluorescence angiographies of PDT on CAM vasculature using intravenously applied (I) m-THPP nanoparticles (1.20 mg/Kg embryo), (II) BPD-MA (0.25 mg/Kg embryo). (A) Photosensitizer fluorescence angiography before PDT. (B) Photosensitizer fluorescence angiography during PDT. Diameter of the irradiated area, 1.8 mm; irradiation condition, 30 J/cm^2 1 minute after photosensitizer injection. (C) Sulforhodamine 101 fluorescence angiography 24 hours after PDT. (D) Sulforhodamine 101 fluorescence angiography 48 hours after PDT. Damage scores after 24 hours: (IC) m-THPP-PDT, 3; (IIC) BPD-MA-PDT, 4. Damage score after 48 hours: (ID) m-THPP-PDT, 1; (IID) BPD-MA-PDT, 0. White bar: 500 μm.

With the use of *m*-THPP under the conditions described here, total closure of the capillary system and blood vessels with diameters smaller 30 μm and size reduction of larger blood vessels were observed after 24 hours (Fig. 2IC). However, 48 hours after PDT, previously reduced vessels regained their original sizes, and some vessels that appeared to be occluded were reperfused (Fig. 2ID). Furthermore, the entire region was recovered by newly formed, smaller blood vessels (diameter, < 20 μm) that were morphologically different from those outside the treated areas. Similarly, high vascular occlusion 24 hours after PDT was found for BPD-MA (Fig. 2IIC), as was the regrowth of previous vasculature and the formation of new morphologically different vessel after 48 hours (Fig. 2IID). Therefore, regardless the photosensitizer, signs of vascular reperfusion and neoangiogenesis could be observed 48 hours after PDT in the CAM.

3.2. Anti-VEGF therapy

Anti-VEGF-induced changes were followed 24 hours and 48 hours after topical administration by fluorescence angiography. Autofluorescence of vessels of the CAM area exposed to drug was also recorded before administration for comparison. Fig. 3 illustrates the closure of blood vessels to different extents with varying doses of sFlt-1.
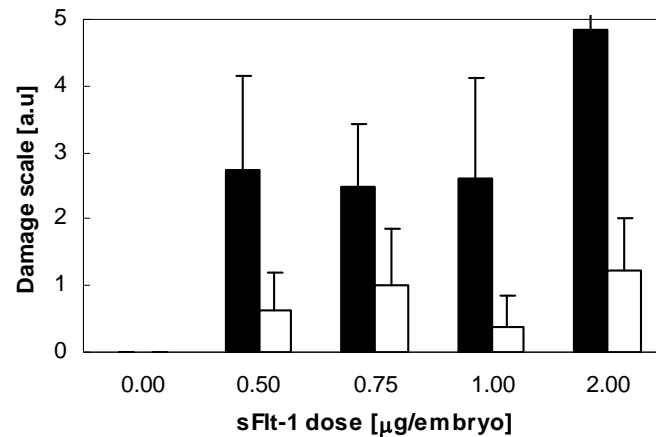
Figure 3. Vascular occlusion induced by sFlt-1. Vascular occlusion induced by sFlt-1 in the CAM as a function of anti-VEGF concentration 24 hours (■) and 48 hours (□) after topical application. Mean ± S.D. (n ≥ 5).

Increased damage was exhibited with increasing doses of sFlt-1. However, doses greater than 1 μg/embryo frequently led to changes of vascular architecture morphology and partial destruction of the CAM.

3.3. Synergies of photodynamic therapy and Anti-VEGF therapy

Results of PDT with BPM-DA in combination with increasing doses of sFlt-1 are summarized in Fig. 4. Fig. 4A clearly illustrates the differences between BPD-MA-PDT therapy (Fig 2II) and BPD-MA-PDT/sFlt-1 combined therapy (Fig 4A). Representative damage 24 hours after PDT was observed with BPD-MA (drug dose, 0.25 mg/embryo; light dose, 30 J/cm^2), followed by reperfusion of larger vessels and generation of new vessels 48 hours after PDT (Figs. 2IIC and 2.IID, respectively). However, vascular occlusion induced by the combined therapy (PDT, same conditions; sFlt-1: 1μg/embryo) 24 hours after PDT (Fig. 4a) was higher

than for PDT alone (Fig. 2IIC). Furthermore, after 48 h, combined treatment resulted in only minimal reperfusion in the PDT-treated area.
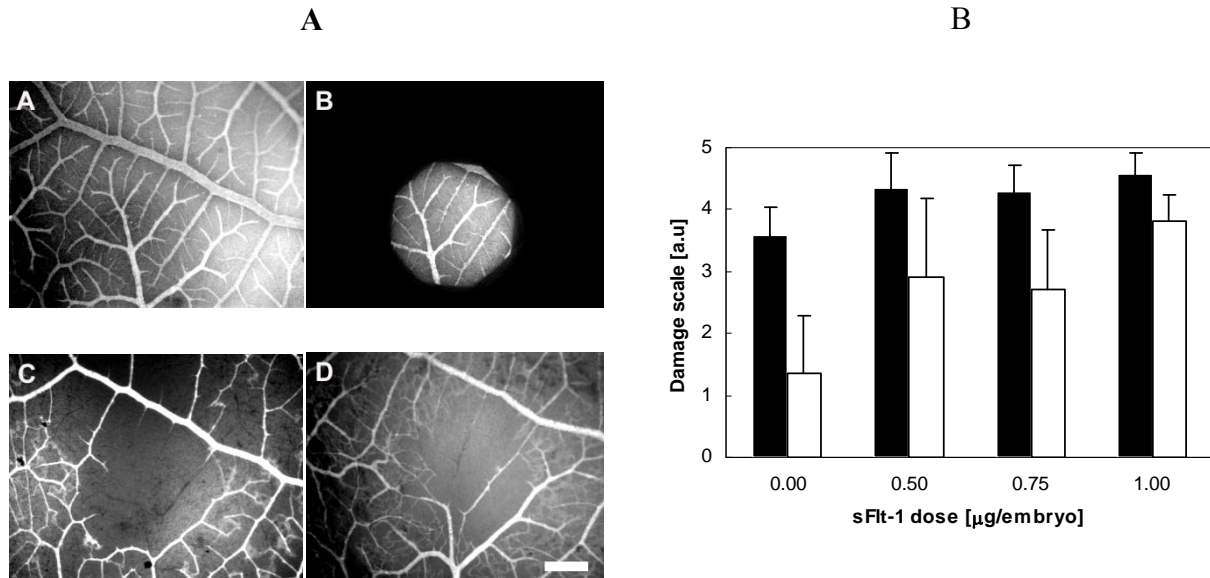
Figure 4. Synergistic effects from the combined use of photodynamic therapy and antiVEGF agents. (A) Sequence of fluorescence angiographies (see Fig. 2) with BPD-MA (0.25 mg/Kg embryo). PDT followed by anti-VEGF therapy using topically applied sFlt-1 (1µg/embryo) 6 hours after PDT. Damage score after 24 hours: BPD-MA-PDT/sFlt-1, 5. Damage score after 48 hours: BPD-MA-PDT/sFlt-1, 4. White bar: 500 µm. (B) Vascular damage induced by the sFlt-1 topically applied 6 hours after BPD-MA-PDT (0.25 mg/Kg; light dose, 30 J/cm^2) and 24 hours (■) and 48 hours (□) after PDT. The first concentration (0.00 µg/embryo) represents PDT alone.

A statistically significant increase ($P < 0.05$) of vascular occlusion was induced by the use of sFlt-1 in combination with PDT after 24 hours (Fig. 4B), from 3.4 U (PDT alone) to approximately 4.6 U (PDT/anti-VEGF). This increase represented the occlusion not only of capillaries and of vessel smaller than 70-µm diameter but also of vessels larger than 70-µm diameter. Furthermore, vascular reperfusion and neovascularization 48 hours after treatment was significantly reduced ($P<0.01$). Optimal results were obtained with the BPD-MA-PDT/sFlt-1 1 µg/embryo, leading to an average damage of 3.8 U after 48 hours. This resulted in more extensive vascular injury than that observed after PDT alone (1.4). Moreover, 48 hours after PDT, no statistically significant damage was observed compared with the effect observed after 24 hours (4.6) with the combined therapy was seen ($P>0.01$), indicating stabilization of the treatment outcome. Compared with sFlt-1 therapy alone, combined therapy

PDT/sFlt-1 resulted in a highly significant increase in vascular damage ($P<0.01$) at 48 hours, with a reduction of more than one third of the vascular reperfusion and neovascularization. No differences between PDT and s-Flt-1 as individual therapies could be established at 24 or 48 hours ($P > 0.01$; see Fig. 3).

4. Discussion

We have previously shown that the CAM model can be efficiently used to screen different parameters including photosensitizer, light dose, and dose-light interval, for optimized PDT of CNV [14,15]. In the present study, we have extended the potential use of this simple, yet effective, model to two additional aspects: the observation of angiogenic activity after PDT and the investigation of synergetic effect anti-VEGF treatment and PDT.

We have shown that liposomal BPD-MA or nanoencapsulated *m*-THPP, vascular reperfusion of previously occluded blood vessels, and formation of new blood vessels exclusively in the treated areas can be observed independently of the photosensitizer or formulation used. Therefore, this response is presumably intrinsic to this treatment modality.

It has been already shown that cytokines such as VEGF, tumor necrosis factor-α, and PEGF are expressed after PDT in patients with tumors [16-18] and in CNV associated with AMD [19,20]. Furthermore, it has been shown in tumor-bearing mice that the coadministration of antiangiogenic compounds after PDT is beneficial with respect to disease progression and survival [21].

Others have shown that the activation of neutrophils and macrophages induced by PDT can be beneficial with respect to the therapeutic outcome in patients with cancer [22,23]. However, because this scenario and the subsequent onset of inflammation is unfavorable with respect to the treatment of CNV, the administration of corticosteroidlike molecules after PDT is recommended for patients with AMD [13,24,25].

On a purely vascular level, PDT has been shown to induce damage, namely through alterations in endothelial cells and in the basement membrane. After the establishment of thrombogenic sites in the vascular space, platelet aggregation, release of vasoactive compounds, leukocyte adhesion, increased vascular permeability, and vessel obstruction have been observed in response to PDT. These effects lead to vascular obstruction and collapse,

resulting in a hypoxic environment. Results of the present study, however, revealed that the vascular obstruction was partially reversible 48 hours after PDT, in agreement with the characteristic hypofluorescence observed in the treated areas of patients 1 week after PDT fluorescence angiography, which resolves relatively rapidly. This rapid resolution indicates the reperfusion of most vascular lumina in those areas.

Tissue hypoxia induced by the occlusion of CNV or smaller choriocapillaries following PDT, however, triggers associated gene activation of the hypoxia-inducible factor 1α (HiF-1) transcription factor complex [26,27]. Under normoxic conditions HiF-1α is rapidly degraded, but oxygen deprivation results in the stabilization of the HiF-1α subunit of the heterodimeric HIF-1 active protein complex, leading to the activation of genes involved in the transcription of cytokines including VEGF-A, erythropoietin, and glucose transporter-1 [28].

The inmunohistopathologic examination of eyes of patients that underwent enucleation following PDT clearly revealed the elevated expression of VEGF-A. Furthermore, a correlation among the upregulation of VEGF-3, the staining for pigment epithelium-derived factor, and the area of treatment was found [29]. These findings, together with the results of the present study, might explain clinical observations following AMD-PDT, including hypofluorescence, continuous recurrence, vascular leakage, and progressive loss of visual acuity after multiple PDT sessions.

Conversely, the present study has clearly shown a benefit of the coadministration of compounds acting against VEGF-A because exposure of PDT-treated areas to sFlt-1 after PDT limited the formation of newly formed blood vessels in our model. This is more surprising if one considers that antiangiogenic support was useful even in such a purely neovascular model that did not include as much surrounding tissue, damage, and inflammation as found in patients with AMD.

VEGF-A exists in four major biological isoforms active in humans and containing 121, 165, 189, and 208 amino acids. Animal model data suggests that the 165-amino acid isoform (VEGF165) is primarily responsible for the pathogenesis in ocular neovascularization. [30,31] sFlt-1 has been reported to bind this isoform, preventing interaction with VEGFR-1 (Flt-1; fms-like tyrosine kinase and VEGFR-2 (KDR; kinase insert domain- containing region) [32,33]. Although human isoforms have been studied extensively, little is known about chick counterparts. It has been shown that exposure of the CAM to different angiogenic stimuli, including VEGF and bFGF resulted in increased angiogenic activity in this model [34]. In

these studies, VEGF was less potent in inducing angiogenesis than bFGF. It is also known that soluble Flt-1 binds chicken VEGF [35].

In our study, optimal dosing was not determined, and relatively high doses of sFlt-1 was applied to produce an observable effect and to show the benefits of using PDT in combination with clinically available drugs. Another factor that should be investigated more thoroughly is the optimal time point of administration of anti-VEGF agents. We have clearly revealed a synergetic effect with the combined use of both treatment options for CNV associated with AMD. However, if our data can be extrapolated to a clinical use of a combination therapy, care should be taken to optimize dosing to protect larger vessels from occlusion.

References

1. Kulkarni, A.D.; Kuppermann, B.D. Wet age-related macular degeneration. *Adv. Drug Deliv. Rev.*, **2005**, *57,* 1994.

2. Schmidt-Erfurth, U.; Hasan, T. Mechanisms of action of photodynamic therapy with verteporfin for the treatment of age-related macular degeneration. *Surv. Ophthalmol.*, **2000**, *45,* 195.

3. Treatment of age-related macular degeneration with photodynamic therapy (TAP) study group Acute severe visual acuity decrease after photodynamic therapy with verteporfin: case reports from randomized clinical trials--TAP and VIP report no. 3. *Am. J. Ophthalmol.*, **2004**, *137,* 683.

4. Treatment of age-related macular degeneration with photodynamic therapy (TAP) study group Verteporfin therapy of subfoveal choroidal neovascularization in age-related macular degeneration: two-year results of a randomized clinical trial including lesions with occult with no classic choroidal neovascularization--verteporfin in photodynamic therapy report 2. *Am. J. Ophthalmol.*, **2001**, *131,* 541.

5. Treatment of age-related macular degeneration with photodynamic therapy (TAP) study group Effect of lesion size, visual acuity, and lesion composition on visual acuity change with and without verteporfin therapy for choroidal neovascularization secondary to age-related macular degeneration: TAP and VIP report no. 1. *Am. J. Ophthalmol.*, **2003**, *136,* 407.

6. Japanese age-related macular degeneration trial: 1-year results of photodynamic therapy with verteporfin in Japanese patients with subfoveal choroidal neovascularization secondary to age-related macular degeneration. *Am. J. Ophthalmol.*, **2003**, *136,* 1049.

7. Schmidt-Erfurth, U.M.; Elsner, H.; Terai, N.; Benecke, A.; Dahmen, G.; Michels, S.M. Effects of verteporfin therapy on central visual field function. *Ophthalmology*, **2004**, *111,* 931.

8. Lopez P.F.; Sippy B.D.; Lambert H.M.; Tach A.B.; Hinton D.R. Transdifferentiated retinal pigment epithelial cells are immunoreactive for vascular endothelial growth factor in surgically excised age-related macular degeneration-related choroidal neovascular membranes. *Invest. Ophthalmol. Vis. Sci.*, **1996**, *37,* 855.

9.   Kvanta A.; Algvere P.V.; Berglin L.; Seregard S Subfoveal fibrovascular membranes in age-related macular degeneration express vascular endothelial growth factor. *Invest. Ophthalmol. Vis. Sci*, **1996**, *37,* 1929.

10. FranK, R.N.; Amin, R.H. Basic fibroblast growth factor and vascular endothelial growth factor are present in epiretinal and choroidal neovascular membranes. *Am. J. Ophthalmol.*, **1996**, *122,* 393.

11. Hera, R.; Keramidas, M.; Peoc'h, M.; Mouillon, M.; Romanet, J.P.; Feige, J.J. Expression of VEGF and angiopoietins in subfoveal membranes from patients with age-related macular degeneration. *Am. J. Ophthalmol.*, **2005**, *139,* 589.

12. Ng, E.W.M.; Adamis, A.P. Targeting angiogenesis, the underlying disorder in neovascular age-related macular degeneration. *J. Can. Ophthalmol.*, **2005**, *40,* 352.

13. Spaide, R.F.; Sorenson, J.; Maranan, L. Combined photodynamic therapy with verteporfin and intravitreal triamcinolone acetonide for choroidal neovascularization. *Ophthalmology*, **2003**, *110,* 1517.

14. Vargas, A.; Pegaz, B.; Debefve, E.; Konan-Kouakou, Y.; Lange, N.; Ballini, J.P.; van den, B.H.; Gurny, R.; Delie, F. Improved photodynamic activity of porphyrin loaded into nanoparticles: an in vivo evaluation using chick embryos. *Int. J. Pharm.*, **2004**, *286,* 131.

15. Lange, N.; Ballini, J.P.; Wagnieres, G.; van den Bergh, H. A new drug-screening procedure for photosensitizing agents used in photodynamic therapy for CNV. *Invest. Ophthalmol. Vis. Sci.*, **2001**, *42,* 38.

16. Osiecka, B.; Ziolkowski, P.; Gamiara E.; Lis-Nawara, A.; White, S.G.; Bonnett, R. Determination of vascular-endothelial growth factor levels in serum from tumor-bearing BALB/c mice treated with photodynamic therapy. *Med. Sci. Monitor*, **2003**, *9,* 110.

17. Zhang, X.; Jiang, F.; Zhang, Z.G.; Kalkanis, S.; Hong, X.; Decrvalho, A.C.; Chen J.; Yang, H.; Robin, A.M.; Chopp, M. Low-dose photodynamic therapy increases endothelial cell proliferation and VEGF expression in nude mice brain. *Lasers Med. Sci.*, **2005**, *20,* 74.

18. Uehara, M.; Inokuchi, T.; Sano, K.; ZuoLin, W. Expression of vascular endothelial growth factor in mouse tumours subjected to photodynamic therapy. *Eur. J. Cancer*, **2001**, *37,* 2111.

19. Gelisken, F.; Lafaut, B.; Inhoffen, W.; Voelker, M.; Grisanti, S.; Bartz-Schmidt, K.U. Clinicopathological findings of choroidal neovascularisation following verteporfin photodynamic therapy. *Br. J. Ophtalmol.*, **2004**, *88,* 207.

20. Rudolf, M.; Michels, S.; Schlötzer-Schrehardt, U.; Schmidt-Erfurth, U. Expression of Angiogenic Factors by Photodynamic Therapy. *Klinische Monatsblatter fur Augenheilkunde*, **2004**, *221,* 1026.

21. Zhou, Q.; Olivo, M.; Lye, K.; Yee, K.; Moore, S.; Sharma, A.; Chowbay, B. Enhancing the therapeutic responsiveness of photodynamic therapy with the antiangiogenic agents SU5416 and SU6668 in murine nasopharyngeal carcinoma models. *Cancer Chem. Pharmacol.*, **2005**, *56,* 569.

22. Korbelik, M.; Cecic, I. Contribution of myeloid and lymphoid host cells to the curative outcome of mouse sarcoma treatment by photodynamic therapy. *Cancer Letters*, **1999**, *137,* 91.

23. Cecic, I.; Parkins, C.S.; Korbelik, M. Induction of systemic neutrophil response in mice by photodynamic therapy of solid tumors. *Photochem. Photobiol.*, **2001**, *74,* 712.

24. Rechtman, E.; Danis, R.P.; Pratt, L.M.; Harris, A. Intravitreal triamcinolone with photodynamic therapy for subfoveal choroidal neovascularisation in age related macular degeneration. *Br. J. Ophtalmol.*, **2004**, *88,* 344.

25. Spaide, R.F.; Sorenson, J.; Maranan, L. Photodynamic therapy with verteporfin combined with intravitreal injection of triamcinolone acetonide for choroidal neovascularization. *Ophthalmology*, **2005**, *112,* 301.

26. Ratcliffe, P.J.; O'Rourke, J.F.; Maxwell, P.H.; Pugh, C.W. Oxygen sensing, hypoxia-inducible factor-1 and the regulation of mammalian gene expression. *J. Exp. Biol.*, **1998**, *201,* 1153.

27. Wang, G.L.; Semenza, G.L. General involvement of hypoxia-inducible factor 1 in transcriptional response to hypoxia. *Proc. Natl. Acad. Sci U. S. A.,* **1993**, *90,* 4304.

28. Forsythe, J.A.; Jiang, B.-H.; Iyer, N.V.; Agani, F.; Leung, S.W.; Koos, R.D.; Semenza, G.L. Activation of vascular endothelial growth factor gene transcription by hypoxia-inducible factor 1. *Mol. Cell. Biol.*, **1996**, *16,* 4604.

29. Schmidt-Erfurth Ursula; Schlotzer-Schrehard Ursula; Cursiefen Claus; Michels Stephan; Beckendorf Arne; Naumann Gottfried O H Influence of Photodynamic Therapy on Expression of Vascular Endothelial Growth Factor (VEGF), VEGF Receptor 3, and Pigment Epithelium-Derived Factor. *Invest. Ophthalmol. Vis. Sci.*, **2003**, *44,* 4473.

30. Ferrara, N.; Gerber, H.-P.; LeCouter, J. The biology of VEGF and its receptors. *Nature Medicine*, **2003**, *9,* 669.

31. Witmer, A.N.; Vrensen, G.F.J.M.; Van Noorden, C.J.F.; Schlingemann, R.O. Vascular endothelial growth factors and angiogenesis in eye disease. *Prog. Retin. Eye Res.*, **2003**, *22,* 1.

32. Kendall, R.L.; Thomas, K.A. Inhibition of vascular endothelial cell growth factor activity by an endogenously encoded soluble receptor. *Proc. Natl. Acad. Sci U. S. A.*, **1993**, *90,* 10705.

33. Joon-Hwa Lee; Canny, M.D.; De Erkenez, A.; Krilleke, D.; Ng, Y.S.; Shima, D.T.; Jucker, F. A therapeutic aptamer inhibits angiogenesis by specifically targeting the heparin binding domain of VEGF165. *Proc. Natl. Acad. Sci U. S. A.*, **2005**, *102,* 18902.

34. Flamme, I.; von Reutern, M.; Drexler, H.C.A.; Syed-Ali, S.; Risau, W. Overexpression of Vascular Endothelial Growth Factor in the Avian Embryo Induces Hypervascularization and Increased Vascular Permeability without Alterations of Embryonic Pattern Formation. *Dev. Biol.*, **1995**, *171,* 399.

35. Yamaguchi, S.; Iwata, K.; Shibuya, M. Soluble Flt-1 (Soluble VEGFR-1), a Potent Natural Antiangiogenic Molecule in Mammals, Is Phylogenetically Conserved in Avians. *Biochem. Biophys. Res. Commun.*, **2002**, *291,* 554.

PART B. TARGETED DRUG DELIVERY

Chapter 3. Urokinase-plasminogen-activator sensitive polymeric photosensitizer prodrugs:

Design, synthesis and in vitro evaluation

Doris Gabriel, Maria-Fernanda Zuluaga*, Maria-Noel Martinez, Marino A. Campo and

Norbert Lange

Department of Pharmaceutics and Biopharmaceutics, School of Pharmaceutical Sciences, University of Geneva, University of Lausanne, 30 Quai Ernest-Ansermet, 1211 Geneva 4, Switzerland
*The author partially contributed to this manuscript (fluorescence increase after urokinase digestion, cellular activation and phototoxicity test).

ABSTRACT. Polymeric photosensitizer prodrugs (PPPs) were developed that can be selectively activated by urokinase plasminogen activator (uPA). They are composed of uPA-cleavable photosensitizer-peptide-conjugates covalently attached to a poly-lysine backbone (25kDa). Phototoxicity of PPPs is efficiently reduced by energy transfer between closely positioned photosensitizers (PSs) on the polymeric backbone. Enzymatic cleavage by uPA, a serine protease that is up-regulated in certain types of cancer, leads to the release of PS-peptidyl-fragments and restoration of phototoxicity. In the current study, conjugates with different ε-lysine side chain modifications of the polymer-backbone were synthesised and characterised with respect to in vitro properties such as fluorescence and reactive oxygen species (ROS) quenching, as well as enzymatic cleavage by uPA. Based on those in vitro results and a cell screening experiment for photo- and dark toxicity, two compounds, PEG20-N-uPA-PPP and N-uPA-PPP, were selected as the most promising candidates for further evaluation in two uPA-expressing cell lines, DU-145 and PC-3. Here, the pegylated compound PEG20-N-uPA-PPP showed enhanced selective prodrug activation by uPA in comparison to N-uPA-PPP, pinpointing to the need for prolonged extracellular residence time of uPA-senstive prodrugs. In

preliminary PDT-experiments, a dose-dependent phototoxic effect of this compound was found in both tested cell lines. In conclusion, this study highlights the fact, that backbone substitution units may impact not only photochemical and physicochemical properties of the PPPs, but play an important role for cellular prodrug localisation and thus site selective enzymatic activation.

1. Introduction

Since the early proposition of macromolecular prodrugs in 1975 by Helmut Ringsdorf [1], polymer-drug-conjugates have found widespread application in drug delivery research [2,3]. They comprise three main components, namely a water-soluble polymer (usually of 10 000–100 000 Da), a biodegradable polymer–drug linker and a bioactive drug. Each of these components can be fine-tuned in order to obtain conjugates of well defined architecture and comparably small hydrodynamic size (2-10nm). Main impetus for research on polymer-drug conjugates arises from the opportunity to alter the pharmacokinetics of small drug molecules, with the potential to minimise drug toxicity and to improve passive tumour targeting via the enhanced permeability and retention effect (EPR) [4].

While the first macromolecular pro-drug entered clinical trials already in 1994 [5], it is only recently that this concept has been introduced to photodynamic therapy (PDT), an emerging therapeutic option for the treatment of cancer and other non-malignant diseases [6,7]. PDT combines the simultaneous use of a photosensitizer (PS), oxygen, and light to generate cytotoxic reactive oxygen species (ROS) in situ, causing the destruction of unwanted tissues. The selectivity in photodynamic therapy is dual and arises from the preferential localisation of the PS in target tissues and second, from the irradiation of a specified volume. Especially the latter proves to be challenging in certain clinical scenarios (e.g. cancer in pelvic, abdominal or thoracic cavities) and can lead to considerable secondary damage of healthy tissue structures within the irradiated area. Macromolecular photosensitizer prodrugs address this issue by controlling the PS action on three levels: Prodrug localisation, target selective activation of the prodrug and localised in situ generation of the cytotoxic effector molecules by light irradiation. Following this strategy and focussing on proteolytic enzymes as disease markers, we and others have previously reported the development of protease-sensitive polymeric photosensitizer prodrugs (PPPs) [8-10], that are activated through backbone cleavage by lysosomal enzymes such as cathepsin B. After these proof-of-principle studies, second generation PPPs were developed: Here, multiple PS units are covalently coupled to a polymeric backbone via protease cleavable peptide linkers. These initially non-photoactive compounds become fluorescent and phototoxic after specific enzymatic digestion of the peptide linkers and subsequent release of the photosensitizer-peptidyl moieties from the backbone [11] (see Fig. 1). These conjugates are distinctly different from those used in previous approaches [12], in the sense that the polymeric carrier, the PS, and its loading are deliberately adapted to favour intramolecular PS quenching and site selective activation by the target protease.
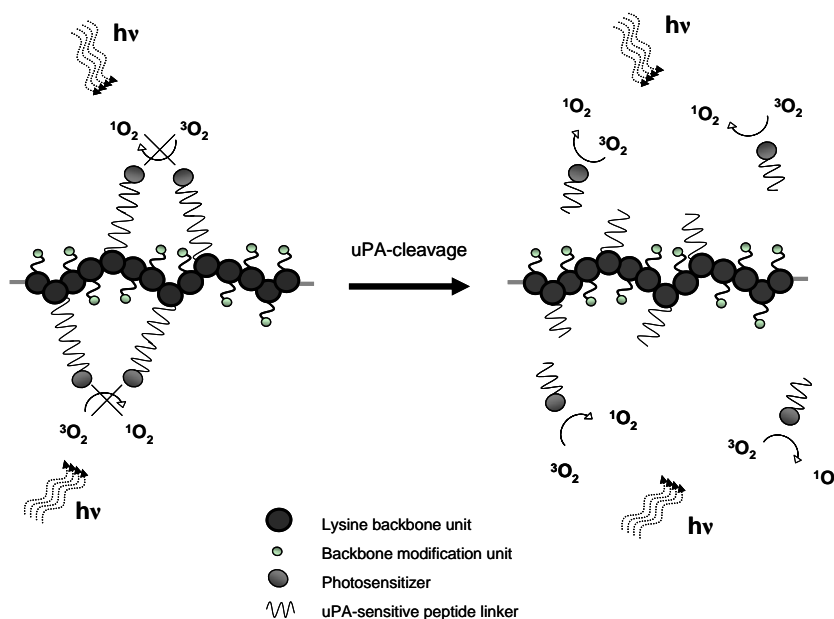
Figure 1. Principle of uPA-sensitive polymeric photosensitizer prodrugs: Intramolecular energy transfer between closely positioned photosensitizers efficiently depopulates irradiation-excited first and triplet states, resulting in reduced fluorescence and energy transfer to molecular triplet oxygen. Enzymatic cleavage of the prodrug leads to the release of photosensitizer-peptidyl fragments, which become fully photoactive again.

Proteolytic degradation of the extracellular matrix (ECM) is crucial for cancer development, invasion and metastasis, all of them associated with increased activities of several different protease families, such as metallo- serine- aspartyl- and cysteine- proteases [13,14]. Of particular interest in this context is the extracellular serine protease urokinase plasminogen activator (uPA), which generates plasmin from the extracellular zymogen plasminogen [15]. Besides facilitating cancer cell migration and invasion through the ECM by plasmin activation, uPA participates also in directed tissue remodelling processes like angiogenesis, stimulation of fibroblast proliferation or ECM protein synthesis. Overexpression of uPA has been found in a number of epithelial cancers including breast [16,17], colon [18], prostate [19], ovarian [20-22] or cervical carcinomas [23,24]. In this context, uPA as well as other proteases have raised interest not only as targets for small molecule inhibitors [25,26], but were also identified as candidates for controlled drug delivery in vivo, by exploiting their increased activity for the release of anticancer agents or cytotoxins from protease-sensitive prodrugs [27-38] or biomaterials [39,40].

In this study, we developed uPA-sensitive polymeric PS-prodrugs (Fig. 1) using an established minimal substrate *Ser-Gly-Arg-//Ser-Ala*, which is reported to be cleaved by uPA

approximately 1300 times faster than the *Cys-Pro-Gly-Arg//Val-Val-Gly-Gly* sequence within the physiological substrate plasminogen [41,42]. However, modification of the substrate by NH$_2$-terminal introduction of the relatively bulky photosensitizer pheophorbide *a* and covalent attachment to the polymeric backbone might influence the cleavage kinetics. Furthermore, protease-substrate affinity is not restricted to active site interactions – but net charge of the protease itself and also the PPP might influence overall affinity. Although this study focuses on uPA, the observed phenomena can also be translated to other extracellular or membrane bound proteases, since the presented chemistry can be easily adapted, to target endopeptidases involved in diverse diseases amenable to PDT. In vivo, most of the uPA activity arises mainly from uPA-receptor-bound enzyme at the cell surface and only a small part of the enzyme is secreted into the peri-cellular space, where it remains free or binds to soluble uPA-receptor. After passive accumulation, macromolecular constructs like PPPs will be taken up slowly by fluid phase endocytosis and degraded non-specifically in endolysosomes, a process which is not restricted to cancer cells. In the current research we investigated, if the selectivity of PPPs could be further enhanced by decreasing the affinity towards cellular membranes or by favouring endolysosomal escape. For this purpose, conjugates with different backbone substitution moieties and resulting net charges were obtained by simple modification of the epsilon-lysine side chains of the polymeric backbone. Cleavage kinetics and photosensitizer release of the corresponding conjugates were assessed, together with other in vitro characteristics such as fluorescence and ROS quenching. Furthermore, cytotoxicity and phototoxicity were screened on a HT-1080 fibrosarcoma cell line. The most promising candidates were then further evaluated with respect to mechanism of cellular uptake, intracellular fate, enzymatic activation and phototoxicity on uPA-expressing DU-145 and PC-3 cells of prostate cancer origin.

2. Materials and Methods

2.1. Chemicals

All commercial reagents were used as obtained. HGly-2-chlorotrityl resin, Boc-glycine, Fmoc-glycine, Fmoc-alanine, Fmoc-D-alanine, triphenylisopropysilane, *N*, *N*-diisopropylethylamine (DIPEA), piperidine, picrylsulfonic acid aqueous solution (1M), 2-sulfo-benzoic acid cyclic anhydride, sodium iodide, sodium hydroxide, amiloride HCl, p-aminobenzamidine and ethanol were purchased from Fluka (Buchs, Switzerland). The D- and

L- aminoacids Fmoc(tBu)-serine, Fmoc(Pbf)-arginine, as well as O-(7-azabenzotriazol-1-yl)-*N, N, N, N*-tetramethyluronium hexafluorophosphte (HATU) were obtained from Genscript (Piscataway, USA). Pheophorbide *a* was from Frontier Scientific (Logan, UT). Anhydrous forms of dichloromethane (DCM), dimethylformamide (DMF), dimethylsulfoxide (DMSO), acetonitrile (ACN) and trifluoroacetic acid (TFA) were purchased from Acros Organics (Geel, Belgium). Imidazole-4-acetic-acid sodium salt, fetal calf serum (FCS, heat inactivated), poly-L-lysine (PLL) 25kDa, poly-D-lysine (PDL) 25kDa, 3-(4, 5-Dimethylthiazol-2-yl)-2, 5-diphenyltetrazolium bromide (MTT) and 4', 6-diamidino-2-phenylindole (DAPI) were obtained from Sigma-Aldrich (Buchs, Switzerland). mPEG-NHS 20kDa and 5kDa were obtained from Nektar (San Carlos, USA). Urokinase (low molecular weight and mixture of low/high molecular weight), C64-me and E64-d were purchased from Calbiochem/VWR (Zug, Switzerland). DMEM/Glutamax-1, D-PBS, HBSS, TripleExpress®, Lysotracker Green and Penstrep (5000units resp. 5000µg/mL) were from Invitrogen (Basel, Switzerland). Poly-D-lysine coated glass bottom petri-dishes were provided by MatTek Cooperation (Ashland, USA).

2.2. Synthesis of photosensitizer-labelled peptides

2.2.1. Synthesis of G(L)SG(L)R(L)S(L)AG and G(D)SG(D)R(D)S(D)AG. A uPA-cleavable pheophorbide a-peptide and a D-configured control peptide were synthesised using an adapted minimal sequence of a reported urokinase substrate [41]. Briefly, the peptides were assembled manually on a HGly-2-chlorotrityl resin according to the standard FMOC protocol. Solid phase cleavage and side chain deprotection were done with a mixture of TFA/H_2O/Triphenylisopropylsilane (95:2.5:2.5). After RP-HPLC purification (Waters Delta 600 HPLC) on a C8 Nucleosil 300-10 column (Macherey-Nagel) using a 0.1%TFA water/acetonitrile gradient, molecular weight of peptides was analysed by ESI-MS, using a Finnigan MAT SSQ 7000 (Thermo Electron Co. Waltham, MA).

2.2.2. Synthesis of Pheo-G(L)SG(L)R(L)S(L)AG and Pheo-G(D)SG(D)R(D)S(D)AG.
Subsequent coupling of NHS-activated pheophorbide a to the NH_2-terminus of the peptides was performed as described previously [11] and yielded the corresponding pheophorbide -

peptides. Purification was done by RP-HPLC and molecular weight of the product was analysed by ESI-MS as described above.

2.3. Synthesis of final conjugates with different backbone substitution moieties

All conjugates were synthesized with a previously optimized pheophorbide-peptide loading of 25% per poly-lysine chain. The general synthetic route for the described conjugates involves in a first step the covalent attachment of the pheophorbide-peptide to the polymeric backbone.

Herefore, DIPEA (4.3 mg, 3.32moles, 3 equiv based on the number of $-NH_2$ functions of the polylysine), was added to a solution of the corresponding uPA-peptide (3.53mg, 2.76×10^{-6} moles), PLL (25 kDa, 2.31mg, 0.11×10^{-6}moles, 1.1×10^{-5}moles of $-NH_2$ functions), and HATU (1.37 mg, $3.6 \times 10\text{-}6$ moles, 1.3 equiv based on pheophorbide-peptide to be activated) in DMSO (0.65 mL). This mixture was stirred under argon and the reaction was allowed to proceed for four hours. Non-cleavable control conjugates were obtained in the same way, but using PDL (25kDa) and the peptide linker containing the corresponding D-aminoacids. Complete loading of the pheophorbide-peptides on the polylysine was confirmed by analytical RP-HPLC as described [11]. A next step involved the modification of the remaining epsilon-lysine residues with the corresponding moieties and is described below for each conjugate separately.

2.3.1. (1-Methyl-3-pyridinio)formate iodide substituted uPA-sensitive PPP, (N-uPA-PPP). Remaining free NH_2 functions of the polymeric backbone were reacted with N-succinimidyl (1-methyl-3-pyridinio)formate iodide (3.3 mg, 9.1×10^{-6} moles, 1.1 equiv, based on the number of free NH_2 functions remaining on the polylysine) in DMSO. After one hour, the reaction was quenched by adding a mixture of water, acetonitrile (70/30) and TFA to pH 3. The resulting solution was filtered and purified by size exclusion chromatography (SEC) using a Sephacryl S-100 (Amersham Biosciences, Otelfingen, Switzerland) column and a mixture of ACN/water/TFA (30/70/0.0025) as eluent. The resulting product was lyophilized and stored light-protected at -20°C.

2.3.2. Pegylated (20kDa), (1-Methyl-3-pyridinio)formate iodide substituted uPA-sensitive PPP (PEG20-N-uPA-PPP). mPEG-NHS (2.43 mg, 1.22 x 10^{-7}moles, 1.1 equiv, based of the number of free NH$_2$ functions remaining on the polylysine) was dissolved in 0.2 mL DMSO and added dropwise to the stirred, ice-cooled reaction mixture. The reaction was allowed to proceed overnight, while slowly reaching room-temperature. In a next step, N-succinimidyl (1-methyl-3-pyridinio)formate iodide (3.3 mg, 9.1 x 10^{-6}moles, 1.1 equiv, based on the number of free NH$_2$ functions remaining on the polylysine) in DMSO was added. After one hour, the conjugates were purified by size exclusion chromatography as described above and lyophilized.

2.3.3. Pegylated (5kDa) uPA-sensitive PPP, (PEG5-uPA-PPP). A solution of mPEG 5kD (45.5mg, 9.1 x 10^{-6}moles, 1.1 equivalents, based on the number of free NH$_2$ functions remaining on the polylysine) in DMSO was added dropwise to the reaction mixture. This mixture was stirred under argon and left to react overnight. Ph was then adjusted to 3 by addition of a water acetonitrile solution (70/30) containing 0.1% TFA. The resulting solution was filtered, purified by SEC and lyophilized as described above.

2.3.4. 2-Sulphobenzoic acid substituted uPA-sensitive PPP, (S-uPA-PPP). To acylate free NH$_2$ functions of the polymeric backbone 2-sulfobenzoic acid cyclic anhydride (1.68 mg, 9.1 x 10^{-6} moles, 1.1 equiv, based on the number of remaining free NH$_2$ functions on the polylysine) in DMSO was added dropwise under stirring and pH was kept at 8. After one hour, the reaction was stopped by adding a mixture of water, acetonitrile (70/30) and TFA to pH 3 and conjugate work up was done as described above.

2.3.5. Imidazole-substituted uPA-sensitive PPP, (I-uPA-PPP). Amidation of the non-functionalised epsilon-residues was done using HATU and DIPEA for *in situ* activation of the 4-imidazoleacetic acid carboxygroup, according to an adapted procedure [43]. 4-imidazole-acetic acid sodium salt (1.35mg, 9.1 x 10^{-6}moles, 1.1 equiv per non-functionalised lysine), HATU (4.5 mg, 1.2 x 10^{-5}moles, 1.3 equiv per 4-imidazoleacetic acids) and DIPEA (2.14 mg, 1.7 x 10^{-5}moles, 2 equiv per non-functionalised lysine units) in dry DMSO were added. The reaction tube was flashed with argon and left to react under stirring overnight. To separate

polymeric material from low-molecular weight components, the solution was filtered and subjected to SEC purification. The resulting product was lyophilized and stored light-protected at -20°C.

2.4. *In vitro* characterisation

2.4.1. Fluorescence quenching. The concentration of the different conjugates in aqueous solution was adjusted to 3.5 µM, based on pheophorbide a equivalents. The fluorescence intensity of each of these equimolar solutions was measured at 37 °C using a SPEX Fluoromax (Perkin Elmer, Wellesley, MA) setting the excitation at 400 nm and emission at 670nm. The fluorescence quenching factor (fold decrease of background substracted fluorescence at the 670 nm emission maximum) was calculated with respect to a non-quenched reference PPP loaded with 1% pheophorbide a. Results were obtained in triplicate and expressed as mean ± S.D.

2.4.2. ROS-quenching. Relative reactive oxygen species production was measured by monitoring I_3^- (286 nm absorbance band), generated by ROS oxidation of I^- in aqueous media, following a slightly modified procedure of Mosinger [44]. Aqueous D-PBS buffered solutions of all the uPA- PPPs were prepared by adjusting the PS-concentration to 3 µM pheophorbide a equivalents. To 0.6 mL of a given uPA-PPP in buffered solution, 0.2 mL of an aqueous NaI solution (2.5M) was added and the UV-VIS spectrum was recorded as background. This was repeated, after irradiation with white light for 2 min ($3.72J/cm^2$) in a 24 well cell culture plate. To obtain the actual increase in optical density, background absorbance at 286 nm was subtracted. Finally, the ROS quenching factor (fold decrease in optical densitiy at 286nm) was calculated with respect to a non-quenched reference PPP loaded with 1% pheophorbide a. All experiments were performed in triplicate using a Cintra 40 UV/VIS spectrometer (GBC, Dandenong, Australia) and results are expressed as mean ± S.D.

2.4.3. Fluorescence increase after urokinase digestion. PBS buffered solutions of the N-uPA-PPP, PEG20-N-uPA-PPP, PEG5-uPA-PPP, S-uPA-PPP and I-uPA-PPP at a concentration of 3 µM pheophorbide a equivalents, were incubated with urokinase (mixed

MW, 1000U) at 37°C in the dark. Aliquots of the digestion mixtures were sampled in DMSO (75%) after 5, 10, 20 and 30 minutes and fluorescence was measured as described in 2.4.1. Control experiments were performed under identical conditions for 30 minutes with a non-cleavable control N-uPA-PPP, or alternatively in the presence of the specific uPA-inhibitor Amiloride HCl (190μM). Sequence-specifity of urokinase cleavage was investigated by performing digestion experiments under identical experimental condition with PPPs designed for activation by two different serine proteases. The first conjugate targets thrombin with the aminoacid sequence G-(D)F-Pip-R-S-G-G-G-G-G and the second human kallikrein 2 with the sequence G-K-L-R-T-T-G in the peptide linker. Both conjugates (T-PPP and hK2-PPP) have a 25% loading of the corresponding pheophorbide-peptide and the polymeric backbone is substituted with (1-Methyl-3-pyridinio)formate iodide (the detailed synthesis and evaluation of these conjugates will be described elsewhere).

2.4.4. *In vitro* enzymatic cleavage of pheophorbide-uPA-peptides and uPA-sensitive PPPs. Release of the pheophorbide-peptidyl-fragment Pheo-Gly-Ser-Gly-Arg-OH after incubation with urokinase was monitored by RP-HPLC. Separation was done on a Nucleodur C18 gravity 3μ CC 125/4 column from Macherey-Nagel using a gradient method (water/acetonitrile/TFA (50/50/0.1) to (1/99/0.1) within 13 minutes). Fluorescence was detected on a Merck Hitachi FL detector L7480 at an emission wavelength of 670nm and an excitation wavelength of 405nm. Molecular weight of the cleaved fragment pheophorbide-GSGR was analysed by ESI-MS. All digestion experiments were done in D-PBS buffered solutions, with human urokinase (mixed MW, 1000U), for 60minutes, at 37° C in the dark.

2.5. Cellular evaluation

2.5.1. Cells and culture conditions. Human prostate cancer cell lines DU-145, PC-3, and human fibrosarcoma cell line HT1080 (ATCC-Catalogue no. HTB-81™ and CCL-121™) were grown as monolayers. The cells were routinely maintained in DMEM-Glutamax-1 medium supplemented with 10% fetal calf serum (FCS), 100μl/mL streptomycin and 100 IU/mL penicillin. Cells were cultivated at 37°C in 100% humidity and 5% CO_2 and seeded in new medium every 2-3 days.

2.5.2. Mechanism of uptake. Cellular uptake of the different uPA-PPPs was investigated under the following conditions: DU-145 cells grown in 96-well plates were incubated with the different conjugates (6 μM pheophorbide a equivalents) at either 37°C or 6°C for one hour. After subsequent washing with HBSS, they were immediately lysed with 100μl of a solution of 0.5% Triton in 1M NaOH and 100μl of ethanol was added. The fluorescence intensity of cell extracts was measured with a Saphire (Tecan, Switzerland) fluorescence microplate reader, using an excitation wavelength of 400nm and an emission wavelength of 680nm. Data were obtained from duplicate measurements of each experimental condition and are expressed as mean value ± S.D.

2.5.3. Cellular activation of N-uPA-PPP and PEG20-N-uPA-PPP on PC-3 and DU145 cells. 100μl of a cell suspension (PC-3 120000 cells/mL, DU-145 100000 cells/mL) were seeded into 96 well plates and allowed to attach overnight. The next day, they were rinsed with 200 μl HBSS and incubated with solutions of N-uPA-PPP, PEG20-N-uPA-PPP or the corresponding controls (1μM pheophorbide a equivalents) in a HBSS solution containing 10% FCS. In additional experiments, cells were separately co-incubated with the specific uPA-inhibitor amiloride (500nM), the broad spectrum serine protease-inhibitor p-aminobenzamidine (250μM), the specific Cathepsin B inhibitor CA-074me (10μM), or the broad spectrum inhibitor cysteinprotease inhibitor E-64d (50 μM). Immediately after incubation start, the fluorescence was read with a Saphire microplate reader (Tecan, Switzerland) using an excitation wavelength of 400nm and an emission wavelength of 675nm. Further measurements were performed 150, 480, 600 and 800 minutes later, without removal of the incubation medium. The increase in fluorescence emission was calculated by subtraction of the fluorescence intensity immediately after incubation start F_0, from the value F_x obtained at time x. Percentage inhibition was calculated with respect to the fluorescence values of cells treated with N-uPA-PPP or PEG20-N-uPA-PPP at the corresponding time point. All conditions were tested in sextuplicate and are expressed mean value ± S.D.

2.5.4. Dark- and Phototoxicity. Cell viability was measured using a mitochondrial MTT assay. Cells were seeded in 96-well-plates and grown for 12 to 18 hours. After incubation with different conjugates as described below, they were either irradiated or kept in the dark. All viability assays were performed 24h after PDT treatment. First, cells were washed once

with 200 μl HBSS and 50 μl of a solution of MTT (1mg/mL) in complete medium was added into each well. Three hours later, violet formazan crystals were dissolved by adding 200μl dimethylsulfoxide. After brief agitation on a microplate shaker, we measured the absorption at 525nm with a plate reader (Saphire, Tecan, Switzerland). Percentage cell survival was calculated with respect to control samples which were treated with either complete medium or a solution of Triton (0.1%) in NaOH 5M, as follows: [A (test-conc.) - A (100% dead) / A (100% viable) – A (100% dead)]*100. Mean values from six wells were determined and expressed as ± S.D.

2.5.4.1. Screening experiment of various uPA-PPPs on HT-1080 cells. Dark and phototoxicity of the different conjugates (N-uPA-PPP, PEG20-N-uPA-PPP, PEG5-uPA-PPP, S-uPA-PPP, I-uPA-PPP) were tested on HT-1080 fibrosarcoma cells at concentrations of 1.5, 3, 4.5, and 6 μM pheophorbide a equivalents. A cell suspension was inoculated into 96-well-plates (8 x 10⁵ cells/mL, 100μl) and allowed to grow overnight. After a washing step with HBSS 200μl, cells were incubated for 30 minutes with the corresponding test solution. This was followed by three washing steps with HBSS 200ul. After addition of complete medium, they were either irradiated (13.5 J/cm^2) or kept in the dark. Subsequently, cell viability was evaluated as described in 2.5.4.

2.5.4.2. Phototoxicity of PEG20-N-uPA-PPP on PC-3 and DU-145 cells. Phototoxicity of PEG20-N-uPA-PPP was tested on PC-3 and DU-145 prostate carcinoma cells. After seeding into 96-well plates (10000 and 9000 cells respectively, per well), the cells grew for approximately 12 hours. Incubations were done at concentrations of 0.5, 2.5, 5 and 7.5 μM pheophorbide a equivalents for 8 hours. After three washing steps with 200μl HBSS, cells were irradiated (13.5 J/cm^2) with white light. Cell viability was tested 24 hours post PDT as described in 2.6.4.

2.6. Intracellular fate of N-uPA-PPP

The intracellular localisation of N-uPA-PPP [1 μM pheophorbide a equivalents] was visualized using a confocal laser scanning microscope (LSM 510, Zeiss, Jena, Germany). PC-

3 cells were seeded into poly-D-lysine coated glass bottom dishes and left to attach overnight. Nuclei were stained with DAPI (10μg/mL) 30 minutes prior to imaging. Images were captured after different incubation intervals (1μM pheophorbide a equivalents) using fixed cells (4% paraformaldehyde in PBS for 15 minutes). Colocalisation studies with Lysotracker green® (50nM, 30 minutes incubation prior to imaging) were done on living PC-3 cells. A blue diode laser (405nm) was used for excitation of pheophorbide *a* and DAPI, and an argon laser (488nm) for Lysotracker green®. Emission wavelengths were collected at 420-480nm (DAPI), 505-530nm (Lysotracker green®) and above 620nm (pheophorbide *a*). Images were acquired at an 8-bit scale and processed with Zeiss software (Zeiss, Germany).

3. Results and Discussion

3.1. Synthesis of uPA-PPPs containing different backbone substitution moieties

Urokinase-sensitive polymeric photosensitizer prodrugs were obtained by adaptation of our previously established, facile three-step synthetic route [11]: First, a reported minimal substrate of uPA [41] was obtained using conventional FMOC-solid phase peptide synthesis.

The identity of the peptide and the control-peptide, containing the corresponding D-aminoacids, was confirmed by electrospray-mass spectrometry (ES-MS) analysis (591.6 [M+H] $^{+}$ = 591.3 calculated for $C_{21}H_{39}N_{10}O_{10}^{+}$) after purification of the resulting crudes by preparative RP-HPLC. Chemoselective coupling of *N*-hydroxysuccinimide pheophorbide *a* activated ester to the N-terminus of either of the two peptides yielded pheophorbide *a*-G-(L)S-G-(L)R-(L)S-(L)A-G and pheophorbide *a*-G-(D)S-G-(D)R-(D)S-(D)A-G. ESI-MS analysis after preparative RP-HPLC purification confirmed the identity of the obtained products (1165.8 ([M+H] $^{+}$ = 1165.6 calculated for $C_{57}H_{77}N_{14}O_{13}^{+}$) and 583.6 ([M+2H] $^{2+}$ = 1166.6 calculated for $C_{57}H_{78}N_{14}O_{13}^{+}$).Subsequently, uPA-PPPs with different backbone substitution moieties were assembled in a one-pot reaction, involving first covalent attachment of the photosensitizer-peptides to the poly-lysine backbone at a loading ratio of 25% units per polymer-chain and subsequent modification of the non-functionalized ε-residues. Importantly, PS-loading was carefully controlled during the synthesis of all conjugates, and quantitative reaction of pheophorbide-peptides was monitored by analytical HPLC during the synthesis of all conjugates. Fig. 2 summarizes the different substitution moieties tested in this study. All conjugates were designed to have a fully protected backbone (R^1+R^2 = 75%), in order to

assure protection from non-specific enzymatic degradation. The three conjugates I-uPA-PPP, S-uPA-PPP, N-uPA-PPP represent polymeric prodrugs with similar molecular weights [approximately 60-65kDa], but either non-charged at physiological pH, or having a negative or positive net-charge. The two pegylated compounds PEG20-N-uPA-PPP and PEG5-uPA-PPP were synthesised in order to investigate the influence of a single, high molecular weight PEG-substitution or in the second case of multiple PEGs. Calculated molecular weights are in both cases significantly higher (approximately 80-85kDa for PEG20-N-uPA-PPP or 400kDa for PEG5-uPA-PPP). This experimental setting allowed us in a first step to gather information, on how the substitution moiety influences intramolecular photosensitizer interactions, due to altered solubility or solution conformation.
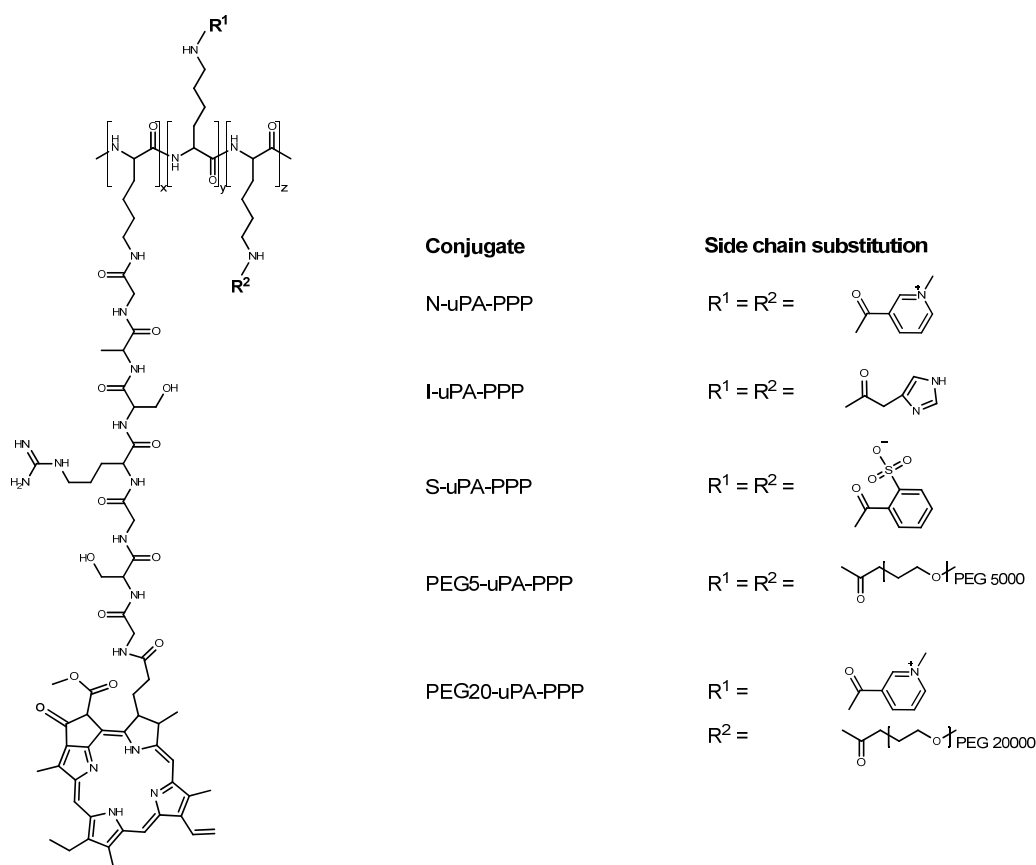

Figure 2. Schematic structure of uPA-PPPs. The loading of photosensitizer-peptide per polymer chain is 25 percent for all compounds (x = 25% of lysines per polymer chain). Non-functionalised ε-residues are modified with different substitution moieties (y =74% and z = 1% of lysines per polymer chain).

3.2. In vitro characterisation

3.2.1. Fluorescence- and ROS-quenching. Polymeric photosensitizer prodrugs require efficient energy transfer between closely positioned photosensitizers on the polymeric backbone, in order to depopulate irradiation-excited first and triplet states. This results in reduced fluorescence and energy transfer to molecular oxygen. In previous work, we and others [11,45,46] have demonstrated, that the fluorescence and ROS generation capacity of the lipophilic photosensitizer pheophorbide *a* can be efficiently quenched, if loaded at a sufficient amount on an appropriate delivery vehicle. The data provided in Table 1 show the impact of the backbone substitution moiety on PS-quenching.

Table 1. Comparison of fluorescence and ROS-quenching between 25% loaded uPA-sensitive PPPs with different backbone substitution moieties. Fluorescence quenching factors express the fold decrease in fluorescence emission or generation of reactive oxygen species of the corresponding conjugate, with respect to the non-quenched photosensitizer pheophorbide a.

Conjugate	Fluorescence quenching factor	ROS quenching factor	Water solubility* (mM)
N-uPA-PPP	187 ± 17	14.2 ± 0.8	0.08
PEG5-uPA-PPP	23 ± 2	5.6 ± 0.3	n.d.
S-uPA-PPP	196 ± 22	12.7 ± 0.7	0.11
I-uPA-PPP	239 ± 14	22.8 ± 3.3	0.11
PEG20-N-uPA-PPP	234 ± 23	14.4 ± 0.7	0.26

*Water solubility of the conjugates is expressed as pheophorbide a equivalents in mM.

All conjugates, except the PEG5-uPA-PPP, have fluorescence quenching factors in the same order of magnitude (190 to 240 times decreased in comparison to non-quenched pheophorbide *a*). This indicates that small molecule substituents of different charge do not significantly interfere with the PS-interactions. ROS quenching factors are very similar for N-uPA-PPP, S-uPA-PPP and PEG20-N-uPA-PP (between 13 and 14 times). In accordance with the highest fluorescence emission observed for PEG5-uPA-PPP, also ROS production was increased in comparison to the other conjugates. The higher ROS-quenching factor of approximately 23 times observed for I-uPA-PPP might be explained by the fact, that imidazole scavenges reactive oxygen species. Comparing the data of the N-uPA-PPP with a previously synthesized trypsin-sensitive prodrug (fluorescence quenching factor: 700x, ROS-quenching factor: 40x), that differs only in the aminoacid sequence [G-T-F-R-S-A-G] [11], nature and length of the

peptide linker appears to be relevant for PS-interactions, presumably due to alterations in secondary structure.

3.2.2. Enzymatic activation. Selective and efficient activation by the target enzyme is a crucial prerequisite for the successful development of PPPs. uPA belongs to the family of serine proteases and hydrolyses peptide bonds by means of the catalytic triad histidine 57, aspartate 102 and serine 195. The active site of uPA has three important binding clefts: A negatively charged S1-binding pocket similar to that of trypsin, a less accessible, hydrophobic S2-pocket and a more exposed S3-pocket, capable of accommodating a wide range of residues. uPA has only a small number of substrates. Amino-acids around the scissile bond of some physiological substrates such as fibronectin, uPAR or hepatocyte growth factor show specificity for a basic arginine at the P1 position, as well as a preference for small hydrophobic residues at the P1', P2' and P2 position [47]. The reported minimal substrate GSGRSAG, employed as peptide linker in this study, fulfils these requirements. Unfortunately, a direct comparison of the kinetic cleavage parameters (k_{cat}) between the peptide substrate and the photosensitizer-labelled substrate was not possible, due to the low solubility of the latter (data not shown). The observed differences in enzymatic activation of the different uPA-PPPs indicate that enzyme-substrate interactions are not restricted to the active site (Fig. 3A).
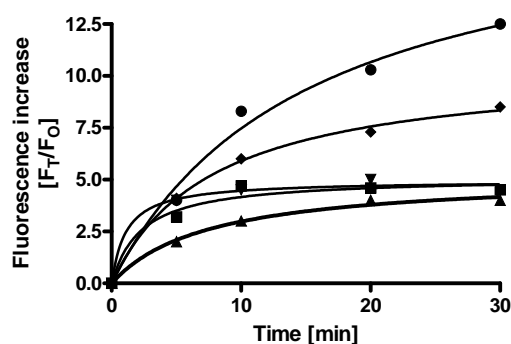
Figure 3. (A) Typical fluorescence-time profile after enzymatic cleavage of the different compounds by urokinase. The conjugates are represented by the following symbols: I-uPA-PPP (■), PEG5-uPA-PPP (▲), S-uPA-PPP (▼), PEG20-uPA-PPP (♦) and N-uPA-PPP (●). Fold fluorescence increase at time T is expressed as the ratio between the fluorescence emission after T minutes of digestion (F_T) and the fluorescence emission (F_O) before enzymatic digestion.

Cleavage occurred most efficiently for the positively charged N-uPA-PPP. Here, incubation with uPA for 30 minutes, led to an approximately 13-fold increase of fluorescence emission in comparison to the non-digested compound. Modification of N-uPA-PPP with a single high molecular weight PEG (20kDa), led to a slight reduction of activation. Activation of I-uPA-PPP, S-uPA-PPP and PEG-5-uPA-PPP were similar. These lower values might be explained by sterical hindrance of enzyme substrate interactions or by charge repulsion. Fig. 3B shows that uPA cleavage can be inhibited by amiloride, a specific uPA-inhibitor, representatively tested for N-uPA-PPP. No activation was observed, when a control conjugate bearing identical D-amino-acid linkers, was incubated with uPA.
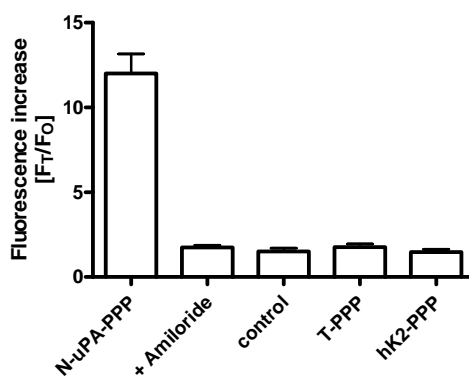

Figure 3. (B) Urokinase digestion of N-uPA-PPP leads to an approximately 13-fold fluorescence increase after 30 minutes of incubation. This cleavage can be inhibited by co-incubation with the specific uPA-inhibitor Amiloride. If a control conjugate with an identical sequence of D-amino-acids in the peptide linker (control-N-uPA-PPP) is incubated with the enzyme, no activation is observed. In a similar way, two alternative conjugates (T-PPP and hK2-PPP), which are activated by two different serine proteases (thrombin and human kallikrein 2) are not cleaved. Fold fluorescence increase after 30 minutes of digestion is expressed as the ratio between the fluorescence emission after 30 minutes of digestion (F_T) and the fluorescence emission (F_O) before enzymatic digestion.

In addition, two other conjugates, T-PPP and hK2-PPP, designed to be activated by the serine proteases thrombin and human kallikrein 2 respectively, were not cleaved by urokinase. Together, these data point to the fact that urokinase cleavage occurs in a sequence specific manner. However, in an in vivo scenario, macromolecular prodrugs will be exposed to various enzyme activities, particularly after passive accumulation to certain lymphatic organs and to the liver. Here, prodrugs will be degraded non-specifically, but due to the multiple selectivity of PDT, cytotoxicity is confined to sites of light irradiation.

The analytical HPLC traces shown in Fig. 3C demonstrate that fluorescence increase is due to cleavage of the peptide linker and release of the pheophorbide-peptidyl-fragment. Mass analysis of the fragment Pheo-G-S-G-R (950.7 ([M+H]$^+$ = 950.1 calculated for $C_{48}H_{61}N_{12}O_9^+$) confirmed cleavage at the expected site between the arginine and the serine residue.
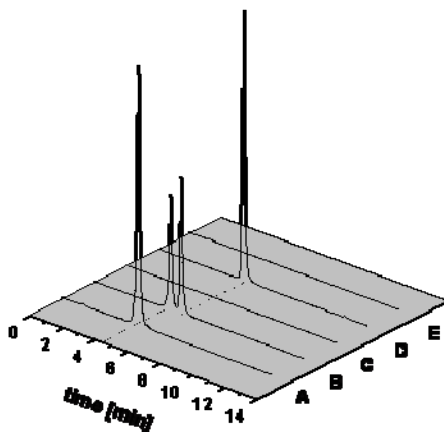

Figure 3. (C): A] Analytical HPLC trace of Pheo-G-S-G-R-S-A-G, with an RT of 4 minutes. B] After partial enzymatic digestion of the pheophorbide-peptide, a new peak appears at a RT of 5 minutes, corresponding to the more lipophilic pheophorbide-peptidyl-fragment. C] No fluorescence emission is detected for the quenched N-uPA-PPP. D] Enzymatic activation of the N- uPA-PPPs leads to release of the fluorescent Pheo-G-S-G-R fragment at a RT of 5 minutes. The mass of this fragment was found to be [M+H]$^+$ = 950.1 calculated for $C_{48}H_{61}N_{12}O_9^+$, confirming cleavage between the arginine and the serine residues. F] Under the given incubation conditions, the control N-uPA-PPP was not activated by uPA.

3.3 Cellular evaluation

3.3.1. Screening experiment for dark- and phototoxicity on HT-1080 fibrosarcoma cells.
In a first step, dark- and phototoxicity of all uPA-PPPs were evaluated in a screening experiment on HT-1080 cells. Photo- (A) and dark toxicity (B) of the different compounds is shown in Fig. 4. Based on these data, it is evident, that S-uPA-PPP is not suitable for PDT, as the compound is toxic by itself at low concentrations. Despite poor fluorescence and ROS quenching in vitro, PEG5-uPA-PPP is not phototoxic at the tested concentrations. Low cellular uptake under the given incubation conditions of the uncharged, high molecular weight compound, might be a potential reason for this observation. I-uPA-PPP and PEG20-uPA-PPP either irradiated or not, show no significant reduction in cell viability. A slight phototoxicity

at higher concentrations can be observed for N-uPA-PPP. With the exception of S-uPA-PPP, none of the conjugates shows dark toxicity under the given experimental conditions.
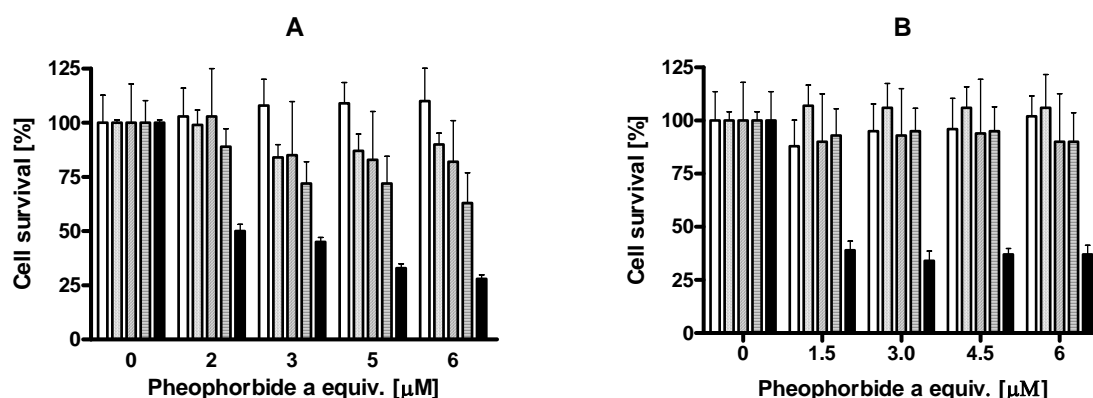

Figure 4. Phototoxicity (A) and dark toxicity (B) of uPA-PPPs with different backbone substitution moieties: ▢ PEG20-N-uPA-PPP, ▦ PEG5-uPA-PPP, ▨ I-uPA-PPP, ▤ N-uPA-PPP and ■ S-uPA-PPP, on HT-1080 fibrosarcoma cells. Cells were incubated for 0.5 hours with the corresponding conjugates and either immediately irradiated (13.5 J/cm^2) or kept in the dark. Cell viability was measured by an MTT-assay. All results were obtained in quadruplicate and are expressed as mean ± S.D.

Viability of cells receiving uPA-PPPs and light can be influenced by different parameters: Uptake kinetics, cleavage by cellular enzymes or ROS-quenching of the given compound. For instance N-uPA-PPP has a similar ROS quenching as PEG20-N-uPA-PPP, however the latter is less phototoxic on HT-1080 cells, especially at the highest tested concentration. In order to distinguish whether this is due to cellular activation or higher uptake of the first, additional experiments need to be performed.

3.3.2. Mechanism of cellular uptake. Mechanism of cellular uptake of the different compounds, with the exception of S-uPA-PPP exhibiting dark toxicity in the previous screening experiment, was investigated by incubation of DU-145 cells at conjugate concentrations of 6 μM pheophorbide *a* equivalents either at 37°C or at 6°C. The data in Fig. 5 shows that cellular entry of all conjugates is energy dependent and can be significantly reduced by incubation at a lower temperature (6 °C: black bars, 37 °C: white bars). Macromolecular prodrugs such as uPA-PPPs are expected to be taken up by cells via fluid phase endocytosis. However, certain cationic polymers are reported to form nano-holes within

the cell membranes and to subsequently diffuse passively into the cytoplasm [48]. It is well known that charge density plays an important role for such cytotoxic effects of certain positively charged polymers. In our positively charged conjugates, N-uPA-PPP and PEG20-uPA-PPP the backbone substitution moiety is N-methyl-nicotinic acid. Here, the charge is delocalised over the aromatic ring. Actual charge density might be reduced and detrimental interactions with cell membranes appear thus to be avoided. Furthermore, the high loading of the conjugates with the lipophilic pheophorbide *a* might alter the membrane active properties of the final conjugates. Although the experimental setting of the current study does not allow a direct correlation between cellular fluorescence and uptake efficiency, the data clearly indicate a decreased uptake of PEG5-uPA-PPP in comparison to the other tested conjugates. This in fact, can certainly be explained by the much higher molecular weight of this compound.
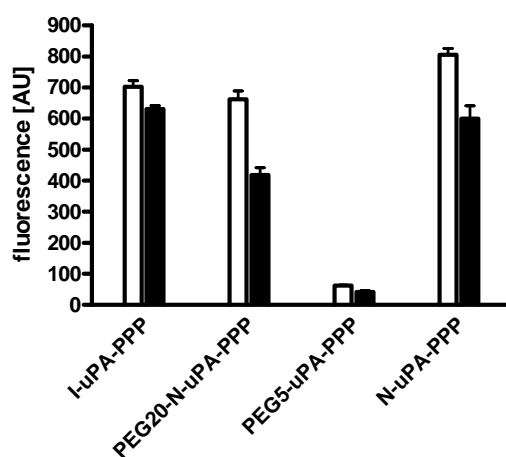
Figure 5. Uptake of all conjugates is energy dependent and cellular fluorescence is reduced by incubation at 6°C in comparison to 37°C. For each conjugate, white bars represent the fluorescence measured after incubation at 37° and black bars the corresponding values after incubation at 6°C. These findings point to fluid phase endocytosis as major route of cellular entry of the polymeric prodrugs. Results were obtained in duplicate and are expressed as mean ± S.D.

3.3.3. Cellular activation of N-uPA-PPP and PEG20-N-uPA-PPP by DU-145 and PC-3 cells.
Based on these results, N-uPA-PPP and PEG20-N-uPA-PPP were the candidate compounds for further evaluation in cell culture. Both conjugates showed a good fluorescence and ROS quenching, and were efficiently activated by uPA *in vitro*. In order to assess pro-drug activation by cellular enzymes, DU-145 and PC-3 cells, known for their expression of

uPA, were incubated with conjugate solutions corresponding to a concentration of 1μM pheohorbide a equivalents. Fig. 6 shows a time dependent fluorescence increase for DU-145 (A: N-uPA-PPP, B: PEG20-N-uPA-PPP) and for PC-3 cells (C; N-uPA-PPP and D: PEG20-N-uPA-PPP) which is significantly higher for the cleavable compounds (□) in comparison to the controls (●). Activation of both PPPs seems to be significantly higher in DU145 than in PC-3 cells. Furthermore, despite of its relatively poor activation by free uPA in vitro, PEG20-N-uPA shows higher fluorescence intensities than its non-pegylated counterpart. In all cases the control-conjugates show a slight fluorescence increase during the first 150 minutes. However, these values remain at the same level over the next couple of hours. The reasons for this observation are not yet understood, and might need further investigations, but changes in secondary structure due to membrane-PPP-interactions may account for this.
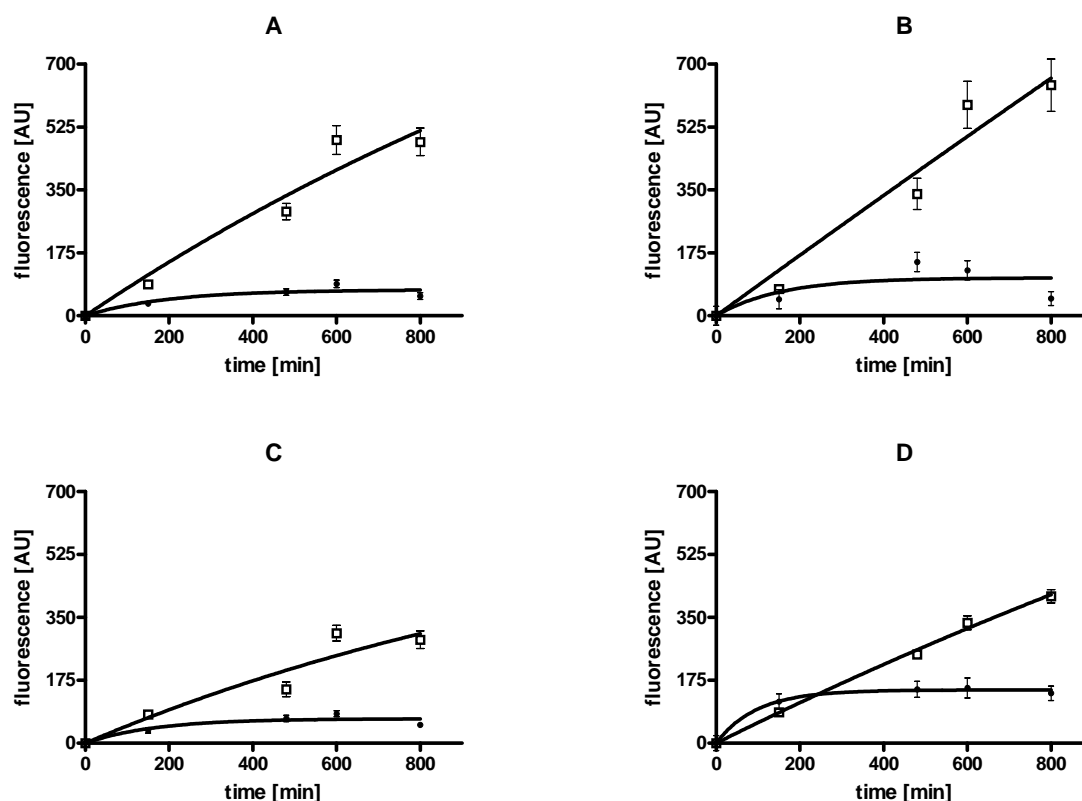

Figure 6. Time profile of cellular activation of N-uPA-PPP, PEG20-uPA-PPP on two uPA expressing cell lines. Graphs A (N-uPA-PPP) and B (PEG20-N-uPA-PPP) show the results obtained with the DU-145 prostate cancer cell line, graphs C (N-uPA-PPP and D (PEG20-N-uPA-PPP) the data of the PC-3 cell line. □ represents the cleavable compound and ● the non-cleavable control compound in all cases.

Although the two cell lines DU-145 and PC-3 were specifically chosen because of their reported high uPA-expression level, proteolytic activation in a more complex cellular environment involves the interaction and up-regulation of a whole cascade of proteases. Proteolytic activity is tightly controlled not only on the gene expression -, but also on the protein level. For instance, uPA is secreted as an inactive zymogen pro-uPA, which requires site-selective cleavage in order to become active. This activation is effected by different serine proteases such as kallikreins and plasmin, but also by the cystein proteases Cathepsin B and L [15]. To investigate the role of different cellular enzymes in prodrug activation, cells were co-incubated with the specific uPA-inhibitor amiloride, the broad spectrum serine protease inhibitor p-aminobenzamidine, the Cathepsin B inhibitor CA-064me and the broad spectrum cysteine protease inhibitor E-64d. The results in Fig. 7 show the percentage reduction of conjugate activation measured after 8 hours of coincubation with the different inhibitors on DU-145-cells and PC-3 cells. Amiloride (black bars) can inhibit up to approximately 40% of fluorescence increase.
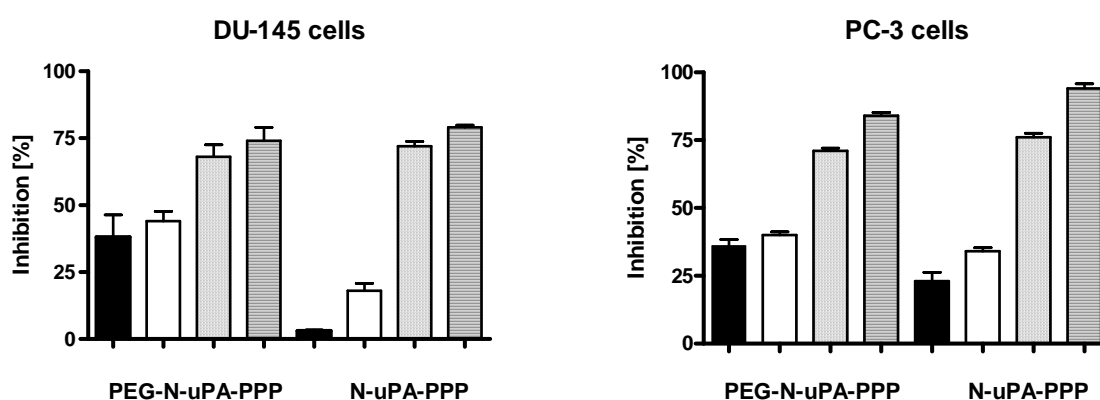
Figure 7. Percentage inhibition of cellular prodrug (PEG-N-uPA-PPP and N-uPA-PPP) activation by various protease inhibitors on two uPA-expressing cancer lines (DU-145 and PC-3) 480 minutes after incubation start.. Percentage inhibition of prodrug activation by coincubation with the different inhibitors is represented as the follows: ■ *Amiloride (500nM),* ▢ *p-aminobenzamidine (250μM),* ▨ *CA-064me (10 μM), and* ▤ *E-64d (50 μM). These results were obtained in sextuplicate at a PS concentration of 1μM pheophorbide a equivalents and are shown as mean ± S.D.*

This highlights the role of uPA in prodrug activation. The generally higher percentage of inhibition by the broad-spectrum serine protease inhibitor p-aminobenzamidine (white bars), pinpoints to the presence of additional serine proteases, such as plasmin or kallikreins, able to cleave the prodrugs. Once the conjugate has entered the cell, it is exposed to lysosomal enzymes such as cathepsin B or L, both expressed in the two cell lines used [49]. Thus both, CA-064me (dotted bars) and E-64d (striped bars) efficiently block prodrug activation, especially after longer incubation times, at which up to 100% of inhibition can be achieved (data not shown). However, it has to be considered, that they act not only on cystein proteases themselves, but prevent *de novo* activation of uPA, and hence inhibit indirectly uPA [50]. Interestingly, in both cell lines, PEG20-NuPA-PPP activation can be blocked to a higher extent by amiloride in comparison to N-uPA-PPP. This indicates that slower cellular uptake and longer extracellular residence time allow for a higher specific cleavage by uPA. In conclusion, this part of the present study shows that the backbone substitution moiety and molecular weight of the final compound have to be fine-tuned in order to co-localise pro-drug and target enzyme as much as possible.

3.3.4. Dark- and Phototoxicity of PEG20-uPA-PPP and DU-145 and PC-3 cells. To further investigate whether the cellular proteolytic activation of the compounds can be translated into a selective phototoxic effect, preliminary PDT experiments were performed on DU-145 and PC-3 cells. For this purpose, PEG20-N-uPA-PPP was chosen, based on the higher uPA-induced prodrug activation as observed above. After incubation with increasing conjugate concentrations for 8 hours, and thorough washing, cells were irradiated with white light (13.5 J/cm^2). Fig. 8 shows cell survival 24 hours after irradiation. The conjugate showed on both cell lines no phototoxicity up to a concentration of 2.5 μM (black bars: DU-145 cells, white bars: PC-3 cells). At a concentration of 5 μM a slight difference with respect to phototoxicity can be observed between the two cell lines. Despite the apparently higher activation in DU-145 cells, the PC-3 cell line seems to be more susceptible to PDT. However, this effect vanishes at higher concentrations. In a more complex in vivo scenario, uPA exists in a soluble form or bound to uPAR. However, the high affinity of uPA to uPAR confines enzyme activity to a great extent to membrane structures and protease activity in vivo is often confined to the immediate pericellular environment of the cells [51]. It is therefore expected that enzymatic cleavage of the prodrug occurs in a localised manner, mainly on the surface of uPA-binding cells and subsequent light irradiation leads to a selective phototoxic effect.
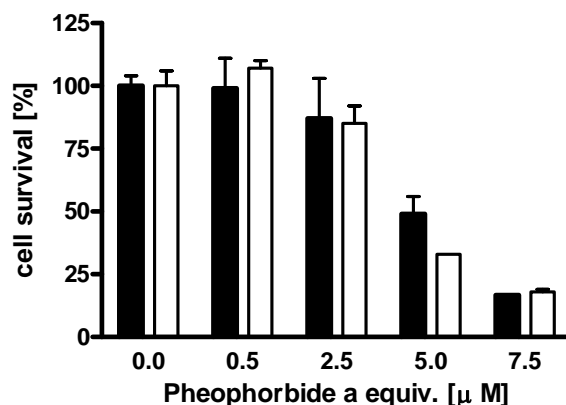
Figure 8. Phototoxicity of PEG20-N-uPA-PPP on DU-145 (black bars) and PC3 (white bars) cells after 8 hours of incubation and irradiation with white light (13.5 J/cm^2). Cell viability was obtained by MTT-tests. Experiments were performed in sextuplicate and are given as mean ± S.D.

3.3.5. Intracellular fate of N-uPA-PPP in PC-3 cells. Intracellular localisation and fate of the uPA-PPPs was representatively studied on PC-3 cells, using N-uPA-PPP. Based on the endocytotic cellular uptake mechanism, it was expected to find a vacuolar localisation of the compounds, corresponding to early endosomes or endo-lysosomes. Indeed, at later incubation times, a dotted distribution pattern can be found (Fig. 9A, 10 hours of incubation).
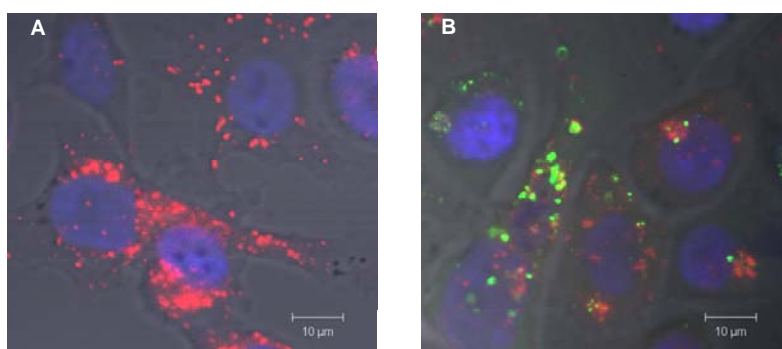
Figure 9. Intracellular localisation pattern of N-uPA-PPP (A) in PC-3 cells. Images were captured 10h after incubation start on fixed cells. DAPI stained nuclei are shown in blue, the photosensitizer in red. Photosensitizer fluorescence is mainly localised in vacuolar structures, but is to some extend also diffusely distributed in the cytoplasm. Using Lysotracker green® as a lysosomal marker (shown in green), 3 hours after incubation start, only modest localisation in lysosomes can be found in living cells (B).

However, there is also some diffuse cytoplasmic red PS fluorescence. In co-localisation studies with Lysotracker green®, a specific marker for lysosomes, only a modest overlap between red (PS) and green fluorescence (lysosomal staining) could be found after 3 hours of co-incubation (Figure 9B). Based on the cellular activation studies, conjugates are expected to be trafficked through the endolysosomal pathway and to be at least partly activated there.

The data indicate that 3 hours of incubation is potentially not long enough to reach a high proportion of lysosomally localised conjugate. An alternative explanation might be fast lysosomal escape and formation of larger vacuolar structures, transition into the cytoplasm or relocalisation to other organelles.

4. Conclusions

In the current work novel uPA-sensitive polymeric photosensitizer prodrugs have been designed and synthesized. Main purpose of the study was the investigation of the role of different backbone substitution units on basic photochemical, physicochemical and biological characteristics of the prodrugs. While the charge of the substitution moiety had no major impact on fluorescence and ROS quenching, substitution with high molecular polyethyleneglycol (5kD) reduced PS quenching. Enzymatic activation by urokinase was found to be the most efficient for the positively charged compounds, followed by I-uPA-PPP, S-uPA-PPP and finally PEG5-uPA-PPP. The capacity to specifically activate the designed uPA-sensitive prodrug, but not an hK2-sensitive or a thrombin-sensitive PPP reveals the sequence dependency of uPA cleavage. The cellular activation studies on the two uPA-expressing cell lines, DU-145 and PC-3, showed prodrug activation in a time dependent manner. Using a panel of protease inhibitors, the involvement of the different enzymes was elucidated. Amiloride inhibition of prodrug activation was more important after relatively short incubation times (up to eight hours), which is related to the mainly extra-cellular or membrane-bound localisation of uPA. Once the conjugates have entered the cell, they can be degraded by lysosomal enzymes such as cathepsin B or L. Both enzymes are expressed in the two cell lines, however upregulation is more important in DU-145 cells [49]. Interesting, especially from a drug delivery perspective, are the findings, that a single modification with a high molecular PEG could decrease cellular affinity and thus enhance the extracellular prodrug activation by uPA in both cell lines. It can be envisaged, that further increase of the molecular weight, or partial replacement of the positively charged N-methyl-nicotinic acid

moiety by a neutral backbone protection residue, might further prolong the extra-cellular residence time of the conjugates. In addition to slowing down cellular uptake, acceleration of extracellular prodrug activation is expected to enhance uPA selective prodrug activation. However, it extended the scope of this study to investigate further uPA-substrates as peptide linkers or the influence of additional spacers in a given substrate. Altogether, the current research demonstrates the requirement for careful prodrug design and highlights the crucial need for colocalisation of target enzyme and prodrug. With the compound PEG20-N-uPA-PPP a step towards this goal was accomplished. Preliminary PDT experiments demonstrated a dose dependent phototoxicity on both uPA-expressing cell lines. In spite of these promising results, it has to be kept in mind, that the full potential of polymeric prodrugs can be revealed only in an *in vivo* setting, where pharmacokinetic properties of the prodrug and site selective protease activation play together. In the current study a PLL with a molecular weight of 25kDa was chosen, which is well below the renal excretion limit. For the most promising conjugate PEG20-N-uPA-PPP, it can be envisaged, that the amide bond between the PEG and the PLL can be cleaved by various endo-proteases, followed by excretion via the renal or hepatic route. Although in some preliminary studies we have observed fluorescence in the urine of injected mice, the detailed evaluation of the in vivo pharmacokinetics and metabolism is currently under investigation.

References

1.   Ringsdorf, H. Structure and properties of pharmacologically active polymers. *J. Polym. Sci., Polym. Symp.*, **2004**, *51,* 135.

2.   Duncan, R. Polymer conjugates as anticancer nanomedicines. *Nat. Rev. Cancer*, **2006**, *6,* 688.

3.   Vicent, M.J.; Duncan, R. Polymer conjugates: nanosized medicines for treating cancer. *Trends Biotechnol.*, **2006**, *24,* 39.

4.   Maeda, H.; Wu, J.; Sawa, T.; Matsumura, Y.; Hori, K. Tumor vascular permeability and the EPR effect in macromolecular therapeutics: a review. *J. Control Release*, **2000**, *65,* 271.

5. Vasey, P.A.; Kaye, S.B.; Morrison, R.; Twelves, C.; Wilson, P.; Duncan, R.; Thomson, A.H.; Murray, L.S.; Hilditch, T.E.; Murray, T.; Burtles, S.; Fraier, D.; Frigerio, E.; Cassidy, J. Phase I clinical and pharmacokinetic study of PK1 [N-(2-hydroxypropyl)methacrylamide copolymer doxorubicin]: first member of a new class of chemotherapeutic agents-drug-polymer conjugates. Cancer Research Campaign Phase I/II Committee. *Clin. Cancer Res.*, **1999**, *5,* 83.

6. Dolmans, D.E.; Fukumura, D.; Jain, R.K. Photodynamic therapy for cancer. *Nat. Rev. Cancer*, **2003**, *3,* 380.

7. Hopper, C. Photodynamic therapy: a clinical reality in the treatment of cancer. *Lancet Oncol.*, **2000**, *1,* 212.

8. Campo, M.A.; Gabriel, D.; Kucera, P.; Gurny, R.; Lange, N. Polymeric photosensitizer prodrugs for photodynamic therapy. *Photochem. Photobiol.*, **2007**, *83,* 958.

9. Choi, Y.; Weissleder, R.; Tung, C.H. Selective antitumor effect of novel protease-mediated photodynamic agent. *Cancer Res.*, **2006**, *66,* 7225.

10. Choi, Y.; Weissleder, R.; Tung, C.H. Protease-mediated phototoxicity of a polylysine-chlorin(E6) conjugate. *Chem. Med. Chem.*, **2006**, *1,* 698.

11. Gabriel, D.; Campo, M.A.; Gurny, R.; Lange, N. Tailoring protease-sensitive photodynamic agents to specific disease-associated enzymes. *Bioconjug. Chem.*, **2007**, *18,* 1070.

12. Shiah, J.-G.; Konak, C.; Spikes, J.D.; Kopecek, J. Solution and Photoproperties of N-(2-Hydroxypropyl)methacrylamide Copolymer-Meso-chlorin e6 Conjugates. *J. Phys. Chem. B*, **2006**, *101,* 6803.

13. van Kempen, L.C.; de Visser, K.E.; Coussens, L.M. Inflammation, proteases and cancer. *Eur. J. Cancer*, **2006**, *42,* 728.

14. Berdowska, I. Cysteine proteases as disease markers. *Clin. Chim. Acta*, **2004**, *342,* 41.

15. Andreasen, P.A.; Kjoller, L.; Christensen, L.; Duffy, M.J. The urokinase-type plasminogen activator system in cancer metastasis: a review. *Int. J. Cancer*, **1997**, *72,* 1.

16. Han, B.; Nakamura, M.; Mori, I.; Nakamura, Y.; Kakudo, K. Urokinase-type plasminogen activator system and breast cancer (Review). *Oncol. Rep.*, **2005**, *14,* 105.

17. Harbeck, N.; Kates, R.E.; Gauger, K.; Willems, A.; Kiechle, M.; Magdolen, V.; Schmitt, M. Urokinase-type plasminogen activator (uPA) and its inhibitor PAI-I: novel tumor-derived factors with a high prognostic and predictive impact in breast cancer. *Thromb. Haemost.*, **2004**, *91,* 450.

18. Kim, T.D.; Song, K.S.; Li, G.; Choi, H.; Park, H.D.; Lim, K.; Hwang, B.D.; Yoon, W.H. Activity and expression of urokinase-type plasminogen activator and matrix metalloproteinases in human colorectal cancer. *B.M.C. Cancer*, **2006**, *6,* 211.

19. Cozzi, P.J.; Wang, J.; Delprado, W.; Madigan, M.C.; Fairy, S.; Russell, P.J.; Li, Y. Evaluation of urokinase plasminogen activator and its receptor in different grades of human prostate cancer. *Hum. Pathol.*, **2006**, *37,* 1442.

20. van der Burg, M.E.; Henzen-Logmans, S.C.; Berns, E.M.; van Putten, W.L.; Klijn, J.G.; Foekens, J.A. Expression of urokinase-type plasminogen activator (uPA) and its inhibitor PAI-1 in benign, borderline, malignant primary and metastatic ovarian tumors. *Int. J. Cancer*, **1996**, *69,* 475.

21.   Kuhn, W.; Schmalfeldt, B.; Reuning, U.; Pache, L.; Berger, U.; Ulm, K.; Harbeck, N.; Spathe, K.; Dettmar, P.; Hofler, H.; Janicke, F.; Schmitt, M.; Graeff, H. Prognostic significance of urokinase (uPA) and its inhibitor PAI-1 for survival in advanced ovarian carcinoma stage FIGO IIIc. *Br. J. Cancer*, **1999**, *79* 1746.

22.   Konecny, G.; Untch, M.; Pihan, A.; Kimmig, R.; Gropp, M.; Stieber, P.; Hepp, H.; Slamon, D.; Pegram, M. Association of urokinase-type plasminogen activator and its inhibitor with disease progression and prognosis in ovarian cancer. *Clin. Cancer Res.*, **2001**, *7,* 1743.

23.   Daneri-Navarro, A.; Macias-Lopez, G.; Oceguera-Villanueva, A.; Toro-Arreola, S.; Bravo-Cuellar, A.; Perez-Montfort, R.; Orbach-Arbouys, S. Urokinase-type plasminogen activator and plasminogen activator inhibitors (PAI-1 and PAI-2) in extracts of invasive cervical carcinoma and precursor lesions. *Eur. J. Cancer*, **1998**, *34,* 566.

24.   Daneri-Navarro, A.; Toro-Arreola, S.; Bravo-Cuellar, A.; Cabrera, N.; Orbach-Arbouys, S.; Perez-Montfort, R. Proteolytic activity in extracts of invasive cervical carcinoma and precursor lesions. *Biomed. Pharmacother.*, **1995**, *49,* 304.

25.   Stutchbury, T.K.; Al Ejeh, F.; Stillfried, G.E.; Croucher, D.R.; Andrews, J.; Irving, D.; Links, M.; Ranson, M. Preclinical evaluation of 213Bi-labeled plasminogen activator inhibitor type 2 in an orthotopic murine xenogenic model of human breast carcinoma. *Mol. Cancer Ther.*, **2007**, *6,* 203.

26.   Schweinitz, A.; Steinmetzer, T.; Banke, I.J.; Arlt, M.J.; Sturzebecher, A.; Schuster, O.; Geissler, A.; Giersiefen, H.; Zeslawska, E.; Jacob, U.; Kruger, A.; Sturzebecher, J. Design of novel and selective inhibitors of urokinase-type plasminogen activator with improved pharmacokinetic properties for use as antimetastatic agents. *J. Biol. Chem*, **2004**, *279,* 33613.

27.   Chung, D.E.; Kratz, F. Development of a novel albumin-binding prodrug that is cleaved by urokinase-type-plasminogen activator (uPA). *Bioorg. Med. Chem Lett.*, **2006**, *16,* 5157.

28.   Graeser, R.; Chung, D.E.; Esser, N.; Moor, S.; Schachtele, C.; Unger, C.; Kratz, F. Synthesis and biological evaluation of an albumin-binding prodrug of doxorubicin that is cleaved by prostate-specific antigen (PSA) in a PSA-positive orthotopic prostate carcinoma model (LNCaP). *Int. J. Cancer*, **2008**, *122,* 1145.

29.   Gerspach, J.; Nemeth, J.; Munkel, S.; Wajant, H.; Pfizenmaier, K. Target-selective activation of a TNF prodrug by urokinase-type plasminogen activator (uPA) mediated proteolytic processing at the cell surface. *Cancer Immunol. Immunother.*, **2006**, *55,* 1590.

30.   Abi-Habib, R.J.; Singh, R.; Liu, S.; Bugge, T.H.; Leppla, S.H.; Frankel, A.E. A urokinase-activated recombinant anthrax toxin is selectively cytotoxic to many human tumor cell types. *Mol. Cancer Ther.*, **2006**, *5,* 2556.

31.   Janssen, S.; Jakobsen, C.M.; Rosen, D.M.; Ricklis, R.M.; Reineke, U.; Christensen, S.B.; Lilja, H.; Denmeade, S.R. Screening a combinatorial peptide library to develop a human glandular kallikrein 2-activated prodrug as targeted therapy for prostate cancer. *Mol. Cancer Ther.*, **2004**, *3,* 1439.

32.   Janssen, S.; Rosen, D.M.; Ricklis, R.M.; Dionne, C.A.; Lilja, H.; Christensen, S.B.; Isaacs, J.T.; Denmeade, S.R. Pharmacokinetics, biodistribution, and antitumor efficacy of a human glandular kallikrein 2 (hK2)-activated thapsigargin prodrug. *Prostate*, **2006**, *66,* 358.

33.   Denmeade, S.R.; Jakobsen, C.M.; Janssen, S.; Khan, S.R.; Garrett, E.S.; Lilja, H.; Christensen, S.B.; Isaacs, J.T. Prostate-specific antigen-activated thapsigargin prodrug as targeted therapy for prostate cancer. *J. Natl. Cancer Inst.*, **2003**, *95,* 990.

34.   Chau, Y.; Tan, F.E.; Langer, R. Synthesis and characterization of dextran-peptide-methotrexate conjugates for tumor targeting via mediation by matrix metalloproteinase II and matrix metalloproteinase IX. *Bioconjug. Chem*, **2004**, *15,* 931.

35.   Chau, Y.; Padera, R.F.; Dang, N.M.; Langer, R. Antitumor efficacy of a novel polymer-peptide-drug conjugate in human tumor xenograft models. *Int. J. Cancer*, **2006**, *118,* 1519.

36.   Devy, L.; de Groot, F.M.; Blacher, S.; Hajitou, A.; Beusker, P.H.; Scheeren, H.W.; Foidart, J.M.; Noel, A. Plasmin-activated doxorubicin prodrugs containing a spacer reduce tumor growth and angiogenesis without systemic toxicity. *FASEB J.*, **2004**, *18,* 565.

37.   de Groot, F.M.; Broxterman, H.J.; Adams, H.P.; van Vliet, A.; Tesser, G.I.; Elderkamp, Y.W.; Schraa, A.J.; Kok, R.J.; Molema, G.; Pinedo, H.M.; Scheeren, H.W. Design, synthesis, and biological evaluation of a dual tumor-specific motive containing integrin-targeted plasmin-cleavable doxorubicin prodrug. *Mol. Cancer Ther.*, **2002**, *1,* 901.

38.   de Groot, F.M.; Busscher, G.F.; Aben, R.W.; Scheeren, H.W. Novel 20-carbonate linked prodrugs of camptothecin and 9-aminocamptothecin designed for activation by tumour-associated plasmin. *Bioorg. Med. Chem Lett.*, **2002**, *12,* 2371.

39.   Rizzi, S.C.; Hubbell, J.A. Recombinant protein-co-PEG networks as cell-adhesive and proteolytically degradable hydrogel matrixes. Part I: Development and physicochemical characteristics. *Biomacromolecules*, **2005**, *6,* 1226.

40.   Rizzi, S.C.; Ehrbar, M.; Halstenberg, S.; Raeber, G.P.; Schmoekel, H.G.; Hagenmuller, H.; Muller, R.; Weber, F.E.; Hubbell, J.A. Recombinant protein-co-PEG networks as cell-adhesive and proteolytically degradable hydrogel matrixes. Part II: biofunctional characteristics. *Biomacromolecules*, **2006**, *7,* 3019.

41.   Ke, S.H.; Coombs, G.S.; Tachias, K.; Navre, M.; Corey, D.R.; Madison, E.L. Distinguishing the specificities of closely related proteases. Role of P3 in substrate and inhibitor discrimination between tissue-type plasminogen activator and urokinase. *J. Biol. Chem.*, **1997**, *272,* 16603.

42.   Coombs, G.S.; Bergstrom, R.C.; Madison, E.L.; Corey, D.R. Directing sequence-specific proteolysis to new targets. The influence of loop size and target sequence on selective proteolysis by tissue-type plasminogen activator and urokinase-type plasminogen activator. *J. Biol. Chem*, **1998**, *273,* 4323.

43.   Putnam, D.; Gentry, C.A.; Pack, D.W.; Langer, R. Polymer-based gene delivery with low cytotoxicity by a unique balance of side-chain termini. *Proc. Natl. Acad. Sci. U. S. A*, **2001**, *98,* 1200.

44.   Mosinger, J.; Mosinger, B. Photodynamic sensitizers assay: rapid and sensitive iodometric measurement. *Experientia*, **1995**, *51,* 106.

45.   Hackbarth Steffen; Horneffer Verena; Hillenkamp Franz; Wiehe Arno; Roeder Beate Photophysical properties of pheophorbide-a-substituted diaminobutane poly-propylene-imine dendrimer. *Chem. Phys.*, **2001**, *269,* 339.

46.   Hackbarth, S.; Ermilov, E.A.; Roder, B. Interaction of Pheophorbide a molecules covalently linked to DAB dendrimers. *Opt. Commun.*, **2005**, *248,* 295.

47.   Spraggon, G.; Phillips, C.; Nowak, U.K.; Ponting, C.P.; Saunders, D.; Dobson, C.M.; Stuart, D.I.; Jones, E.Y. The crystal structure of the catalytic domain of human urokinase-type plasminogen activator. *Structure.*, **1995**, *3,* 681.

48.   Hong, S.; Leroueil, P.R.; Janus, E.K.; Peters, J.L.; Kober, M.M.; Islam, M.T.; Orr, B.G.; Baker, J.R., Jr.; Banaszak Holl, M.M. Interaction of polycationic polymers with supported lipid bilayers and cells: nanoscale hole formation and enhanced membrane permeability. *Bioconjug. Chem.*, **2006**, *17,* 728.

49.   Friedrich, B.; Jung, K.; Lein, M.; Turk, I.; Rudolph, B.; Hampel, G.; Schnorr, D.; Loening, S.A. Cathepsins B, H, L and cysteine protease inhibitors in malignant prostate cell lines, primary cultured prostatic cells and prostatic tissue. *Eur. J. Cancer*, **1999**, *35,* 138.

50.   Kobayashi, H.; Moniwa, N.; Sugimura, M.; Shinohara, H.; Ohi, H.; Terao, T. Effects of membrane-associated cathepsin B on the activation of receptor-bound prourokinase and subsequent invasion of reconstituted basement membranes. *Biochim. Biophys. Acta*, **1993**, *1178,* 55.

51.   Basbaum, C.B.; Werb, Z. Focalized proteolysis: spatial and temporal regulation of extracellular matrix degradation at the cell surface. *Curr. Opin. Cell Biol.*, **1996**, *8,* 731.

Chapter 4. Modulating Prostate Cancer Targeting of Protease Sensitive Photosensitizer Prodrugs by Side Chain Modifications of the Polymeric Carrier

Maria-Fernanda Zuluaga, Doris Gabriel and Norbert Lange

Department of Pharmaceutics and Biopharmaceutics, School of Pharmaceutical Sciences, University of Geneva, University of Lausanne, 30 Quai Ernest-Ansermet, 1211 Geneva 4, Switzerland

ABSTRACT. Prodrug designs combining macromolecular delivery systems with site-selective drug release represent a powerful strategy to increase selectivity of cancer treatments. We have employed this strategy to develop a novel polymeric photosensitizer prodrug (uPA-PPP) for photodynamic therapy of organ-confined prostate cancer. In uPA-PPPs multiple molecules of pheophorbide *a* are attached to a polymeric carrier via peptide linkers that can be cleaved by urokinase-plasminogen-activator, a protease overexpressed in prostate cancer. These prodrugs are non-phototoxic in their native state but become fluorescent and produce singlet oxygen after protease mediated activation. In the present work, we investigated the influence of side-chain modifications, molecular weight, and overall charge on the photoactivity and pharmacokinetics of uPA-PPPs. Although uPA-PPPs protected by small ethylene glycol oligomers were slightly less quenched and are less effectively activated *in vitro*, *in vivo*, these compounds are outperforming their positively charged counterparts. Systemic administration resulted in a selective accumulation and activation of the prodrug in luciferase transfected PC-3 xenografts, resulting in a four-fold increase in fluorescence emission over time. Irradiation of fluorescent tumors induced immediate tumor cell eradication as shown by whole animal bioluminescence imaging. PDT with uPA-PPP could therefore provide a more selective treatment of localized prostate cancer and reduce side effects associated with current radical treatments.

1. Introduction

Prostate cancer is the most frequent cancer in men and the second cause of cancer related death in men [1]. The past years, intensive research in this field has lead to remarkable changes in diagnosis and treatment [2]. At present, most patients are diagnosed at the early stage of disease onset with localized –non metastatic-disease [2]. Furthermore, the availability of new biomarkers [3,4] enables early detection of prostate cancer. Therefore, there is an overall tendency to treat prostate cancer radically at an early stage. While there is no curative therapy for metastatic disease so far, localized cancers can be treated by definitive local therapy (locally confined therapy). Current treatments for localized prostate cancer such as radical prostatectomy and external beam radiation therapy, show a strong survival benefit for men with high risk disease (up to 32%) [5]. However, these radical treatments are associated with substantial morbidity and decreased quality of life [6]. Patient's continence (urinary and intestinal) and sexual function are particularly affected. In principle, these adverse effects might be reduced by increasing the selectivity of the treatment and limiting damage to structures that surround the prostate (including the rhabdosphincter, neurovascular bundles, rectum and ejaculatory apparatus). In the case of whole-gland treatment, a sufficient drug dose needs to be delivered to the entire gland while in the case of focal therapy an accurate identification of tumor tissue within the gland and accurate treatment of the identified target is needed [6].

Photodynamic therapy (PDT), a current option for cancer and other non-malignant diseases [7] has the potential to fill some of the gaps in current treatment. PDT combines the simultaneous use of a photosensitizer (PS), oxygen and light to locally generate cytotoxic reactive oxygen species (ROS) causing the destruction of unwanted tissues. PDT was first used clinically for superficial conditions, nevertheless, nowadays, the combination of lasers with appropriate application systems, makes it possible to apply it to hollow and parenchymatous organs [8]. The first report of the use of PDT for prostate cancer was published in 1990 by Windhal et al. [9]. Since then, an increasing number of studies investigating PDT for prostate cancer has been reported [10-19]. Besides light penetration depth and tissue oxygenation, a current limitation of PDT for prostate cancer is the heterogeneity of response (which may be related to heterogeneity of PS uptake itself) [6]. Moreover, prolonged skin sensitivity [9-11] and less often extraprostatic treatment effects [18] have been reported as major disadvantages in clinical PDT of prostate cancer. The development of strategies that circumvent the unfavorable biodistribution and limited tumor

selectivity of most PS has been one of the major occupations of researchers in this field. One of these strategies exploits characteristics changes in the vasculature of solid tumors to improve drug delivery via enhanced permeability and retention effect [20]. Beside altered vascular architecture, many tumors show to have elevated levels of proteases presumably in adaptation to rapid cell cycling; repression of important regulatory proteins; and sustained invasion, metastasis, and angiogenesis [21]. Because these proteolytic enzymes are present at high levels in tumors, they represent an attractive target for tumor imaging and prodrug activation. We and others have translated these concepts into PDT by the development of macromolecular protease-sensitive photosensitizer prodrugs (PPPs) [22,23], in which inactivation of photoactivity is achieved by intramolecular interactions between closely positioned PS units. The delivery vehicle should passively guide high payloads of inactive PS to the target site via EPR effect. Activation of prodrug is then triggered in response to protease-mediated release of PS moieties and leads to the restoration of its fluorescent and photodynamic activity.

We tailored PPPs sensitive to urokinase plasminogen activator (uPA), a protease over-expressed in prostate cancer. uPA plays a very important role in prostate cancer development and metastasis [24]. uPA-PPPs have the dual functionality, to lighten up lesions in response to uPA activity and to exert a selective cytotoxic effect upon irradiation with light. The present study is dedicated to the optimization of uPA-PPPs in order to enhance selectivity for tumor tissue. Synthesis, characterization, and activation of different uPA-PPPs based on a poly-L-lysine (PL) backbone with different side chain modifications are described. Fluorescence imaging allowed establishing tumor homing in a prostate cancer xenograft-model. Furthermore, preliminary PDT studies in the same model are also reported.

2. Materials and Methods

2.1. Chemicals

Anhydrous forms of dichloromethane (DCM), dimethylformamide (DMF), dimethylsulfoxide (DMSO), acetonitrile (ACN), diethylether and trifluoroacetic acid (TFA) were purchased from Acros Organics (Geel, Belgium). HGly-2-chlorotrityl resin (1.1mmol/g), Boc-glycine, Fmoc-glycine, Fmoc-alanine, triphenylisopropylsilane, Boc-D-glycine, Fmoc-D-alanin, *N,N*-diisopropylethylamine (DIPEA), piperidine, picrylsulfonic acid aqueous solution (1 M),

sodium iodide and ethanol were obtained from Fluka (Buchs, Switzerland). The D- and L-aminoacids Fmoc(tBu)-serine, Fmoc(Pbf)-arginine, as well as O-(7-azabenzotriazol-1-yl)-*N,N,N,N*-tetramethyluronium hexafluorophosphate (HATU) were purchased from Genscript (Piscataway, USA). Poly-L-lysine HBr (PL; 18 kDa and 45KDa), poly-D-lysine (20 kDa), were provided by Sigma-Aldrich (Buchs, Switzerland). Urokinase (high molecular weight, human urine) was obtained from Calbiochem/VWR (Zug, Switzerland). Pheophorbide *a* (Pb*a*) was purchased from Frontier Scientific (Carnforth, UK). mPEG-NHS (20 kDa) was purchased from Nektar (San Carlos, USA). HBSS, D-PBS, TripleExpress®, were purchased from Invitrogen (Basel, Switzerland). mPEO$_4$-NHS and mPEO$_8$-NHS, as well as MEM/EBSS, Sodium pyruvate 100mM solution, MEM vitamin solution, L-glutamine 200mM solution, MEM non-essential aminoacids solution and defined Fetal Bovine Serum were provided by ThermoFisher Scientific (Erembodegem, Belgium). D-Luciferin Firefly, potassium salt was purchased from Biosynth AG (Staad, Switzerland).

2.2. Synthesis

uPA-PPPs were synthesized in three steps as described in detail elsewhere [25]. Briefly, the peptide G(L)SG(L)R(L)S(L)AG containing the reported urokinase minimal substrate [26] and a corresponding D-configured control peptide were synthesized manually on solid phase according to the standard FMOC protocol. NHS-activated Pb*a* was subsequently coupled to the N-terminus of the peptides and the corresponding Pb*a*-peptides conjugates were purified by preparative RP-HPLC (Waters Delta 600 HPLC) on a C8, Nucleosil 300-10 column (Macherey–Nagel) using a 0.1%TFA/water/acetonitrile gradient and molecular weight was analysed by ESI-MS, with a Finnigan MAT SSQ 7000 (Thermo Electron Co. Waltham, MA). Final uPA-PPPs were prepared with a previously optimized Pb*a*-peptide loading of 25 units per 100 free epsilon-NH$_2$ groups of the PL. For this propose, DIPEA (3.7 mg, 3.3×10^{-5}mol, 3 equivalents of free -NH$_2$ functions of PL), was added to a solution of the corresponding Pb*a*-peptide (3.06 mg, 3.1×10^{-6}mol), PL 18KDa or 45KDa (2.00 mg, 0.11×10^{-6}mol, 1.1×10^{-5}mol of –NH$_2$ functions), and HATU (1.36 mg, 4.03×10^{-6}mol, 1.3 equivalents based on Pb*a*-peptides to be activated) in DMSO (0.65 mL). The solution was kept in the dark under argon for 4h at room temperature. Complete loading of the Pb*a*-peptides on PL was confirmed by analytical RP-HPLC as described in [25]. The polymeric carrier was further modified by the covalent coupling of one or two high molecular weight mPEG chains. For

this propose, mPEG-NHS 20KDa (1.91/3.83 mg, 9.56/19.1 $\times 10^{-8}$mol 1.1 equivalents based on the number of -NH$_2$ of PL) previously dissolved in 0.2 mL DMSO was added to the stirred, ice-cooled reaction mixture. The reaction was kept in the dark and allowed to proceed overnight at room temperature. Final modifications of conjugates were achieved by capping the remaining epsilon-lysine residues with the corresponding moieties. Therefore, *N*-succinimidyl (1-methyl-3-pyridinio)formate iodide (NICO) (2.56mg, 7.01 $\times 10^{-6}$mol, 1.1 equivalents of the remaining -NH$_2$-lysine residues), mPEO$_4$-NHS (2.36mg, 7.01 x $\times 10^{-6}$mol) or mPEO$_8$-NHS (3.61mg, 7.01 x $\times 10^{-6}$mol) dissolved in 0.1 mL of DMSO were added to different previous reaction mixtures. Reactions were kept in the dark for 24h at room temperature and subsequently, final conjugates were purified by size exclusion chromatography using a sephacryl™ S-100 (Amersham Biosciences, Otelfingen, Switzerland) column and a mixture of acetonitrile/water/TFA (30:70:0.00025) as eluent. The resulting product was lyophilized and stored light-protected at $-20\,°C$ until use. The corresponding D-amino acids containing control conjugates were obtained in the same way, using as final modification either NICO or mPEO$_8$. Table 1 summarized the composition and calculated molecular weight of synthesized uPA-PPPs.

Table 1. Composition (units per 100 lys ε-residues) and calculated molecular weight of uPA-PPPs

uPA-PPP	Pb*a*-peptide	mPEG20	NICO	mPEO$_{8/4}$	~MW (KDa)
N-PEG-*	25	1	74	-	80
N-2PEG-	25	2	73	-	100
PEO$_4$-PEG-	25	1	-	74	80
PEO$_8$-PEG-*	25	1	-	74	90
45PL-N-2PEG-	25	2	73	-	220

*A homologous D-control conjugate was also synthesized

PEG, Methyl polyethylene glycol 20KDa;N, (1-methyl-3-pyridinio) formate iodide; PEO$_8$,[N-methyl] octa-ethylene oxide; PEO$_4$, [N-methyl] tetra-ethylene oxide;45PL, Poly-L-lysine 45KDa

2.3. Fluorescence and ROS quenching

Fluorescence and ROS quenching factors were determined for all conjugates as follows: the fluorescence intensity of equimolar solutions of conjugates (3 μM Pb*a* equivalents) was measured at 37 °C using a SPEX Fluoromax [excitation:emission = 400:670nm] (Perkin

Elmer, Wellesley, MA, USA). The fluorescence quenching factor (*x*-fold decrease of background subtracted fluorescence at the 670 nm emission maximum) was calculated with respect to the non-quenched reference conjugate loaded with 1% Pb*a*. The relative photo-induced ROS production was indirectly determined by measuring the oxidation of I^- to I_3^- (286 nm absorbance band) in aqueous solution [25]. To 0.6 mL of D-PBS buffered solutions of uPA-PPPs (3 μM Pb*a* equivalents), 0.2 mL of an aqueous NaI solution (2.5 M) was added and the UV–VIS spectrum was recorded before and after irradiation (3.7 J/cm^2). The ROS quenching factor (*x*-fold decrease in optical density at 286 nm) was calculated with respect to the non-quenched reference conjugate. All measurements were performed with a Cintra 40 UV/Vis spectrometer (GBC, Dandenong, Australia). Results were obtained in triplicate and sextuplicate, respectively, and expressed as mean ± SD.

2.4. Enzymatic activation

To test the enzymatic activation of the prodrug by urokinase, D-PBS buffered solutions of uPA-PPPs (3 μM Pb*a* equivalents) were incubated with the enzyme (100 U) at 37 °C in the dark. Aliquots of the digestion mixture were sampled in DMSO (75%) after 5, 10, 20, 30, 60 and 120 min, and fluorescence was measured with a FluoroMax spectrofluorimeter as described above. Further control experiments were performed under identical conditions with the non-cleavable D-conjugate. Moreover, the release of the Pb*a*-peptidyl-fragment Pb*a*-GSGR after urokinase digestion (100 U, 60 min, 37 ° C, in the dark) was monitored by analytical RP-HPLC. Separation was performed on a Nucleodur C18 gravity 3 μm CC 125/4 column (Macherey–Nagel) using a gradient method (water/acetonitrile/TFA from 50/50/0.1 to 1/99/0.1 within 13 min). Fluorescence was detected on a Merck Hitachi FL detector L7480 [exitation:emission = 400:670nm] (Tokyo, Japan). The molecular weight of the cleaved fragment Pb*a*-GSGR was analyzed by ESI-MS with a Finnigan MAT SSQ 7000 (Thermo Electron Co. Waltham, MA, USA).

2.5. Cell culture

The luciferase transfected PC-3M-luc-C6 cell line of prostate cancer origin was a generous gift from Caliper LifeSciences (Alameda, CA, USA). Cells were cultured in MEM/EMBSS supplemented with 10% fetal bovine serum, non-essential amino acids, L-glutamine, sodium

pyruvate and MEM vitamin solution, and maintained at 37 °C in a humidified incubator containing 5% CO_2. The cells were maintained as a monolayer and, for experiments, were harvested using TrypLE Express® and resuspended in fresh complete medium.

Cellular activation of conjugates on PC-3M-luc-C6 was evaluated as follows: 100μl of a cell suspension (1.2 x 10^5 cells/mL) were seeded into 96 well plates and allowed to attach overnight. The next day, they were rinsed with 200 μl HBSS and incubated with solutions of the corresponding uPA-PPP (1μM Pb*a* equivalents) in a HBSS solution containing 10% FCS. Immediately after incubation start, the fluorescence was measured with a Saphire microplate reader (Tecan, Switzerland) [excitation:emission = 400:675nm]. Further measurements were performed 3, 6, 12 and 24 h later, without removal of the incubation medium. The increase in fluorescence emission was calculated by subtraction of the fluorescence intensity immediately after incubation start F_0, from the value F_x obtained at time x. Results were obtained in sextuplicate and expressed as mean ± SD.

2.6. In vivo fluorescence and bioluminescence imaging

Female swiss Nu/Nu mice (5–6 weeks, 17–22 g) were supplied by Charles River Laboratories (L'arbresle, France). The mice were maintained with *ad libitum* access to sterile food and acidified water in a light cycled room acclimatized at 22 ± 2 °C and under specific pathogen free status. All experimental procedures on animals were performed in compliance with the Swiss Federal Law on the Protection of the Animals, according to a protocol approved by the local veterinary authorities.

To induce xenografts, 1.5 x 10^5 cells were injected subcutaneously into the dorsal region of mice. Tumors of 100-150 mm^3 in size were formed within 3 weeks after inoculation. An IVIS 200 small-animal imaging system (Caliper Life Sciences Inc., Massachusetts) was used to quantify the PS-fluorescence in tumors. All fluorescent images were acquired with a cooled CCD camera system, using a Cy5.5 filter set (excitation: 615–665 nm, emission: 695–770 nm), a field of view (FOV) of 12.8 cm, an exposure time of 10 s, and a lens aperture of $f/2$. Data were analyzed with Living Image 3.0 software (Caliper Life Sciences Inc., California) and the fluorescence intensity of regions of interests (ROIs) was expressed as fluorescence efficiency (emitted photons normalized to the incident excitation intensity per cm^2). Prior to prodrug administration, "prescan" images were acquired for each animal to

record tumor autofluorescence. This "background" fluorescence was subsequently subtracted from all further images. Mice (n=3/conjugate) were injected retro-orbitally with conjugates (100 µl, 2.5mg/kg Pba equivalents in 5% ethanol, 65% deionised water and 30% PEG 400) and imaged 3, 6, 12 and 24 h post-injection under 1–2% isoflurane inhalation. Bioluminescence *in vivo* imaging was also carried out in order to colocalize the bioluminescence produced by transfected tumor cells with the fluorescence signal in tumors. Ten to fifteen minutes prior to *in vivo* imaging at 2 and 24h time after injection of the conjugates, animals received the substrate D-luciferin at 150mg/kg in DPBS by intraperitoneal injection and bioluminescent images were obtained together with the fluorescent images using the same camera with an exposure time of 2s.

2.7.   PDT on prostate cancer xenografts

Preliminary PDT studies were preformed in three PC-3M-luc-C6 xenografts bearing mice. The animals were injected retro-orbitally with the PEO$_8$-PEG-uPA-PPP conjugate at three different doses corresponding to 2.5, 5.0 and 10.0 mg/Kg Pba equivalents, respectively. Sixteen hours after conjugate administration, tumors were given a light dose of 100 J/cm2 at 665 ± 5 nm (Ceralas I 670, Biolitec; Jena, Germany) while maintaining the animals under 1–2% isoflurane inhalation. PDT effects were followed for 5 days by bioluminescence imaging of animals as mentioned elsewhere.

3.   Results

3.1.   Synthesis

Three steps were involved in the synthesis of uPA-sensitive polymeric photosensitizer prodrugs. A minimal peptide substrate of uPA and a control peptide, consisting of the corresponding D-amino acids, were synthesized by conventional FMOC-solid phase peptide synthesis. ESI-MS analysis after preparative RP-HPLC of the crudes, confirmed the identity of the two peptides (591.6 [M+H]$^+$ = 591.3 calculated for $C_{21}H_{39}N_{10}O_{10}^+$). Chemoselective coupling of Pba to the N-terminus of the two peptides yielded the corresponding Pba-peptide conjugates. Their identity was confirmed by ESI-MS analysis (1165.8 ([M+H]$^+$ = 1165.6 calculated for $C_{57}H_{77}N_{14}O_{13}^+$) and 583.6 ([M+2H]$^{2+}$ = 1166.6 calculated for $C_{57}H_{78}N_{14}O_{13}^+$).

Subsequently, uPA-PPPs with different backbone substitutions were assembled in a one-pot reaction. First, the photosensitizer-peptides were attached to the PLL backbone at a loading ratio of 25%. Then, the non-functionalized ε-residues were subsequently modified. The substitution ratio (number of Pb*a* attached to each polymeric chain) was quantitatively monitored by analytical HPLC. The structures of all uPA-PPPs are graphically depicted in Fig. 1. All conjugates were designed to have a fully protected backbone ($R^1+R^2 = 75\%$), to prevent non-specific enzymatic degradation and at least one 20KDa mPEG chain to increase water solubility, to prevent rapid renal elimination and to circumvent the immune system by stealth properties.

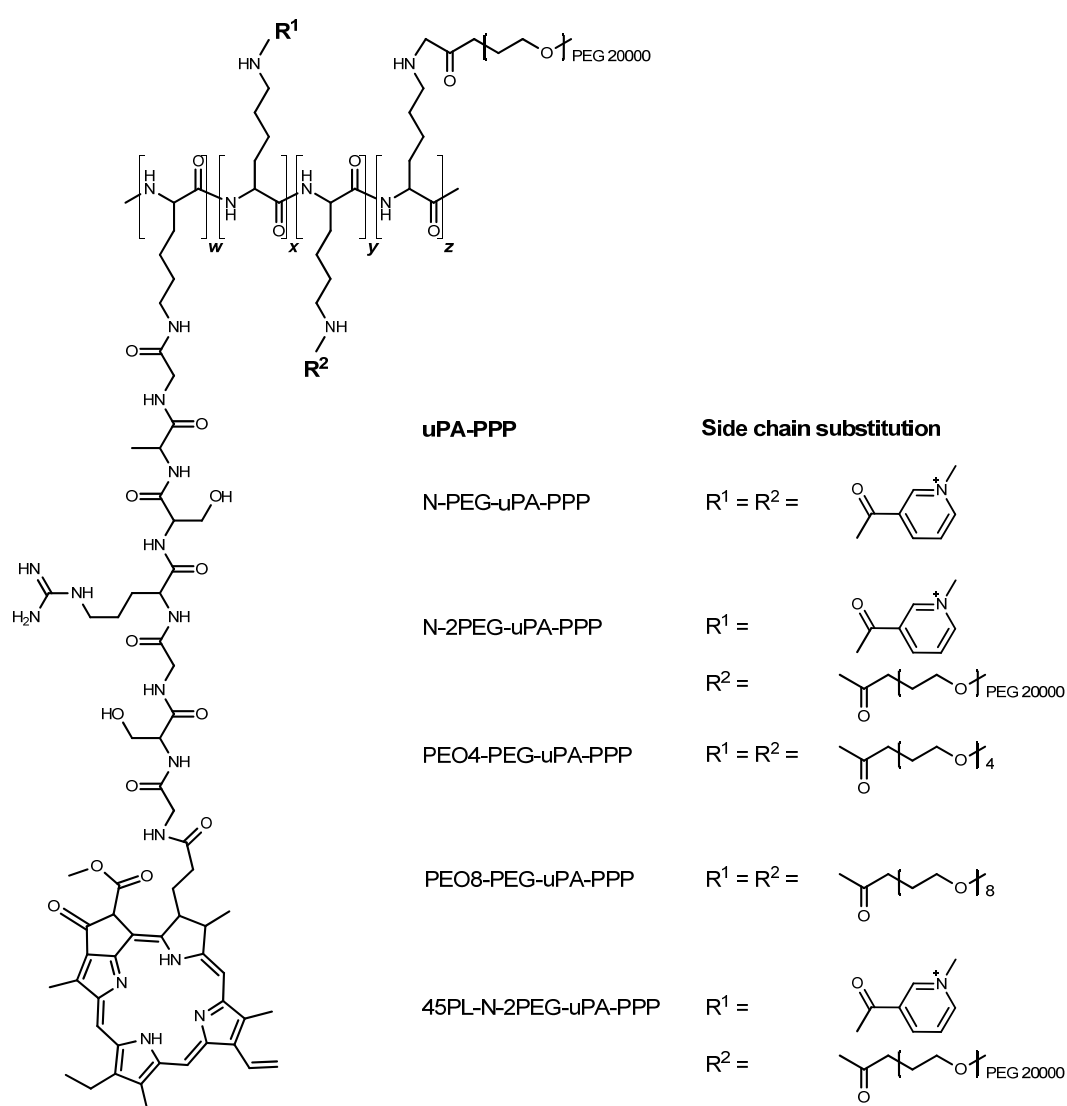| uPA-PPP	Side chain substitution
N-PEG-uPA-PPP	$R^1 = R^2 =$
N-2PEG-uPA-PPP	$R^1 =$
	$R^2 =$
PEO4-PEG-uPA-PPP	$R^1 = R^2 =$
PEO8-PEG-uPA-PPP	$R^1 = R^2 =$
45PL-N-2PEG-uPA-PPP	$R^1 =$
	$R^2 =$

Figure 1. Schematic structure of uPA-PPPs. The loading of Pba-peptide per polymer chain is 25 percent for all compounds (w = 25% of lysines per polymer chain). Non-functionalised ε-residues are modified with different moieties (x =73%, y=1% and z = 1% of lysines per polymer chain).

The three conjugates N-PEG-, PEO$_4$-PEG- and PEO$_8$-PEG-uPA-PPP represent polymeric prodrugs with similar molecular weight [approximately 80-90kDa], but are either non-charged or have a positive net-charge at physiological pH. Negatively charged analogues were not included in the study due to their intrinsic *in vitro* toxicity [27]. N-2PEG-uPA-PPP and 45PL-N-2PEG-uPA-PPP were synthesized in order to investigate the influence of the molecular weight increase by an additional high molecular weight mPEG-substitution and/or the use of a higher molecular weight PL as polymeric backbone. Estimated molecular weights are in both cases significantly higher (approximately 100 and 220kDa, respectively).

3.2. Fluorescence and ROS quenching

Data for quenching of fluorescence emission and ROS generation of fully assembled conjugates is summarized in Table 2.

Table 2. Quenching Factors of uPA-PPPs calculated with respect to the non-quenched Pba $\pm SD$.

uPA-PPP	Fluorescence Quenching Factor	ROS Quenching Factor
N-PEG-	83 ± 6	15.4 ± 0.6
N-2PEG-	84 ± 3	9.0 ± 0.2
PEO$_4$-PEG-	48 ± 2	10.5 ± 0.2
PEO$_8$-PEG-	61 ± 3	8.6 ± 0.2
45PL-N-2PEG-	172 ± 6	10.3 ± 0.3

All conjugates display fluorescence quenching factors in the same order of magnitude, except the 45PL-N-2PEG-uPA-PPP, which was two times higher. This corroborates our previous studies on a homologous series of uPA-PPPs with increasing PL size chain, showing a significantly decrease in fluorescence emission with increasing molecular weight (data not shown). Although these studies also showed decreasing ROS production with increasing backbone size, here the 45PL conjugate shows a similar value compared to the other

conjugates. This implies that the reduction in ROS could not be simply attributed to molecular size, since the N-PEG-uPA-PPP with low MW was most efficiently quenched with respect to ROS production presumably due to a particular configuration of this compound where strong interactions between PS occur. We have already observed that although small molecular substituents of different charge do not significantly interfere with PS interactions, high degree of substitution with polyethylene glycol groups strongly increases ROS production. This is coherent with lower ROS quenching factors calculated for the neutral PEO_4- and PEO_8- and the two positively charged N-2PEG- substituted PPPs.

3.3. Enzymatic activation

Activation of fully assembled uPA-PPPs was tested by fluorescence spectroscopy. Incubation of conjugates with uPA resulted in an increase in fluorescence over time and reached plateau within 2h (Fig. 2A).
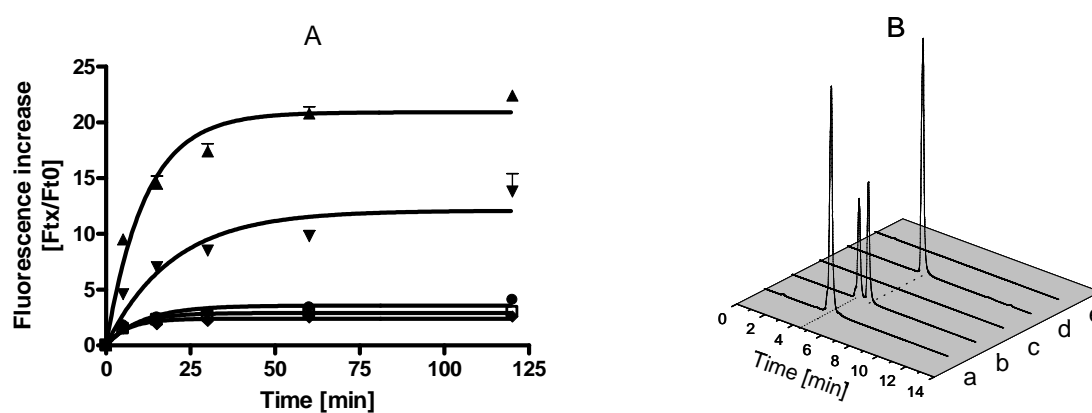

Figure 2. (A) Fluorescence-time-profile after enzymatic cleavage of uPA-PPPs by urokinase. N-PEG- (▲), N-2PEG- (▼), PEO_4-PEG- (●), PEO_8-PEG- (♦), 45PL-N-2PEG-uPA-PPP (□). Fold fluorescence increase at time t is expressed as the ratio between the fluorescence emission after t minutes of digestion (F_t) and the fluorescence emission (F_0) before enzymatic digestion. All measurements were preformed in sixtuplicate and are expressed as mean values ± S.D. B) (a) Analytical HPLC trace of Pba-GSGRSAG (RT: 4 minutes). (b) After partial enzymatic digestion of Pba-GSGRSAG a new peak appears (RT: 5 minutes), corresponding to the more lipophilic Pba-GSGR. (c) No fluorescence emission is detected for the quenched N-PEG-uPA-PPPs. (d) Enzymatic activation of the N-PEG-uPA-PPPs leads to release of the fluorescent Pba-GSGR (RT of 5 minutes. (e) Under the same conditions, the D-control N-PEG-uPA-PPP was not activated by uPA.

The positively charged conjugates N-PEG- and N-2PEG-uPA-PPP showed an overall fluorescence change of 22 and 14 times, respectively. The fluorescence increase found for the pegylated positively charged conjugates also significantly exceeds that of the neutral compounds PEO$_4$-PEG- (4 %) and PEO$_8$-PEG-uPA-PPP (3 %) as well as that of the 45PL conjugate (3 %).

The analytical HPLC traces shown in Fig. 2B demonstrate that uPA-induced fluorescence increase of the conjugate is due to cleavage of the peptide linker and release of the Pb*a*-peptidyl-fragment. After cleavage of the Pb*a*-peptide (A, retention time (RT) 4min), a peak of the more lipophilic Pb*a*-peptidyl-fragment appears at a RT of 5 min (B). If the intact prodrug is injected, no fluorescence is visible (C). After enzyme incubation, a peak with a RT of 5 minutes appears (D). Furthermore, the corresponding control PPP was not activated by uPA (E). Mass analysis of the fragment Pb*a*-G-S-G-R (950.7, $[M+H]^+ = 950.1$ calculated for $C_{48}H_{61}N_{12}O_9^+$) confirmed cleavage at the expected site between the arginine and the serine residue.

3.4. Activation *in vitro*

PPP activation by proteases expressed by PC-3M-LUC-C6 was confirmed for all conjugates by a time-dependent fluorescence increase after incubation with the respective 1µM solutions (Fig. 3).

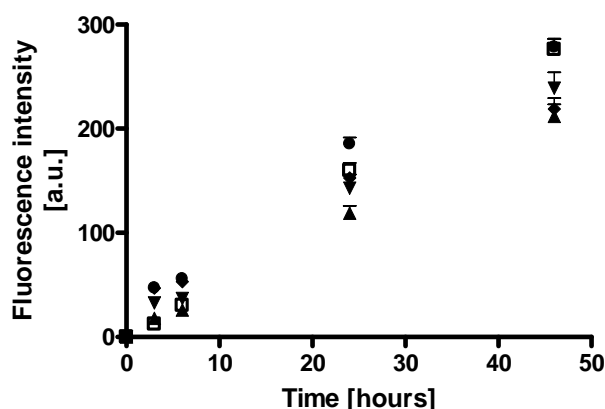
Figure 3. Fluorescence-time-profile of cellular activation of N-PEG- (▲), N-2PEG- (▼), PEO$_4$-PEG- (●), PEO$_8$-PEG- (♦), 45PL-N-2PEG- (□) on PC-3M-luc-C6. All measurements were preformed in sixtuplicate and are expressed as mean values ± S.D.

Incubation of cells with conjugates showed that after six hour of incubation the neutral conjufates (PEO$_4$-PEG- and PEO$_8$-PEG-uPA-PPP) were more efficiently activated than the cationic conjugates (N-PEG-, N-2PEG- and 45PL-N-2PEG-uPA-PPP). This is in contrast to the results obtained after incubation of prodrugs with uPA where the positively charged conjugates were better cleaved.

3.5. *In vivo* fluorescence and bioluminescence imaging

In order to monitor non-invasively prodrug accumulation and activation in nude mice, conjugates were administered systemically (2mg/kg Pb*a* equivalents) via retro-orbital injection and fluorescence and bioluminescence images were taken. As an example, Fig. 4A-B shows an imaging sequence for PEO$_8$-PEG-uPA-PPP. The image on the left corresponds to the bioluminescence produced by PC-3M-LUC-C6 cancer cells after administration of luciferin allowing for the localization of tumor grafts. The other images show the fluorescence increase after injection of the conjugate as a function of time. 6h post injection, the conjugate is largely accumulated in tumors and the liver, with a fluorescence increase of up to 5 times inside tumors compared to the fluorescence immediately after injection. 24h-post injection the fluorescence remains mainly confined to the tumors. After this time point, the fluorescence signal is 3 times higher in the tumor compared to the adjacent tissue.
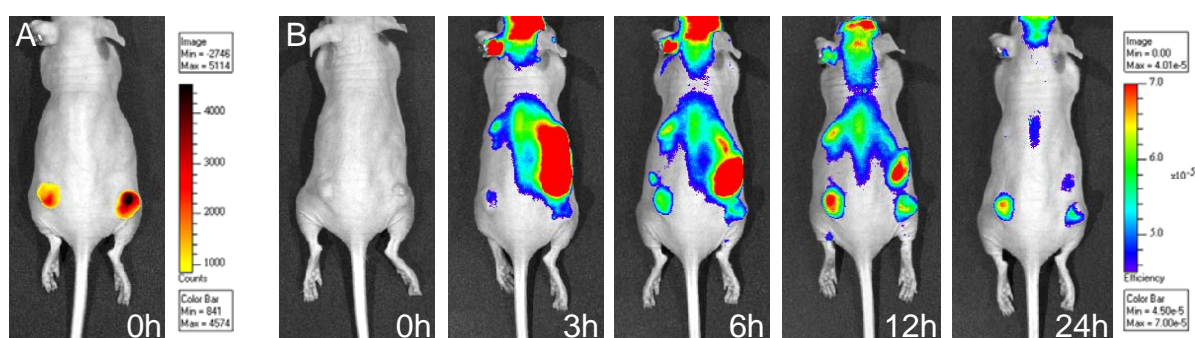

Figure 4. (A) Bioluminescence of luciferase-expressing PC-3M-luc-C6 tumor after D-luciferin peritoneal injection. (B) Tumoral fluorescence intensity following retro-orbital administration of 2 mg/Kg of PEO$_8$-PEG-uPA-PPP (as Pba equivalents).

Quantitative values of the different conjugates for the tumor fluorescence over time are depicted in Fig. 4C. All conjugates show enhancement of fluorescence emission during the first 6 hours post administration, followed by a plateau. In contrast to the *in vitro* results, positively charged conjugates N-PEG-, N-2PEG- and 45PL-2PEG-uPA-PPP showed the lower fluorescence intensities while the neutral conjugates PEO$_4$- and PEO$_8$-PEG-uPA-PPP accumulated well in tumors. No significant difference was observed between N-PEG- and N-2PEG-uPA-PPP. Furthermore, analysis of fluorescence *in vivo* images suggests also a rapid clearance of the positively charged conjugates compared to the neutrally charged (data not shown). Fig. 4D compares the profiles obtained after administration of PEO$_8$-PEG-uPA-PPP and its homologous D-control. After PEO$_8$-PEG-uPA-PPP administration, activation by endogenous uPA, led to increased fluorescence, whereas fluorescence of the D- control conjugate remained close to the baseline level.
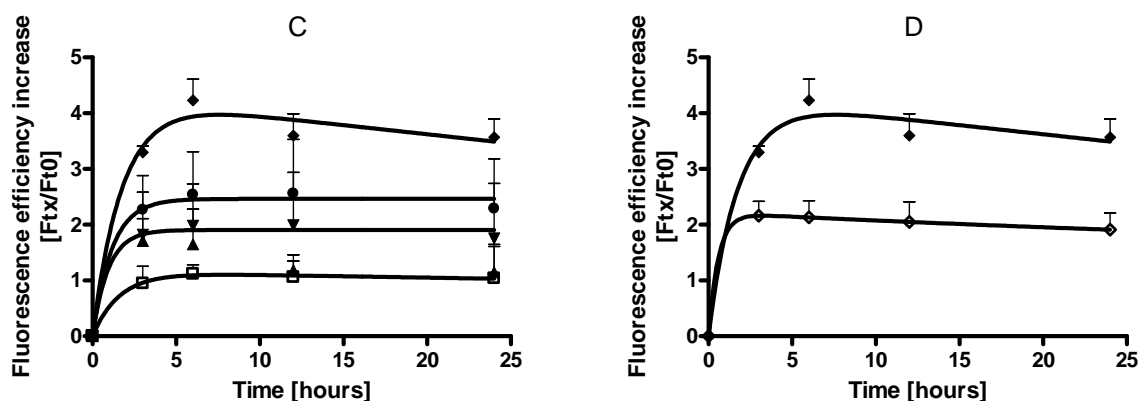
Figure 4. (C) Time-dependent fluorescence increase after retro-orbital injection of 2.5mg/kg Pba equivalents of N-PEG- (▲), N-2PEG- (▼), PEO$_4$-PEG- (●), PEO$_8$-PEG- (♦), 45PL-N-2PEG- (□) and of (D) PEO$_8$- PEG- (♦), D-control (◊). Values are expressed as the mean ratio (F$_t$/F$_0$ ± SEM) between the fluorescence emission at time t (F$_t$) and the autofluorescence (F$_0$) in the respective tumour. (n=3).

3.6. PDT on prostate cancer xenografts

Bioluminescence *in vivo* imaging was used to assess the photodynamic effect on tumors after administration of PEO$_8$-PEG-uPA-PPP *in vivo*. Right tumors of mice injected systemically with 2.5, 5.0 and 10.0 mg of Pb*a* equivalents, were irradiated 16 hours after administration of conjugates with 100J/cm2 at 665nm. Left tumors were not irradiated and served as controls. Bioluminescence images were taken –after previous injection of D-luciferin- before

irradiation as well as 24, 72, 120 and 168 hours after PDT. Strong reductions of bioluminescence signal were observed in mice treated with 5 and 10 mg doses of the conjugate. Bioluminescent images after 24h (see Fig. 5) suggest a vast destruction of tumor cells in the irradiated tumor (right) as no bioluminescent signal is observed while non-irradiated tumors are not affected. PDT related effects such edema and necrosis were also visible 24 hours post irradiation in the treated areas. 120 hours after PDT a slight bioluminescent signal was observed in the periphery of the treated area indicating the re-growth of tumor cells.
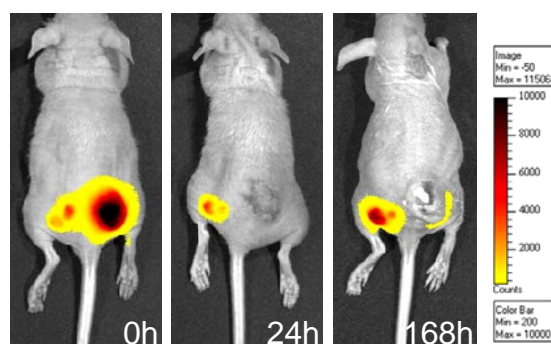

Figure 5. Bioluminescence in vivo imaging post PDT performed 16h after retro-orbital administration of 5 mg/Kg of PEO$_8$-PEG-uPA-PPP (as Pba equivalents). 15 min. prior imaging D-luciferin was administered peritoneally.

4. Discussion

Altered proteolytic activity in neoplastic and other degenerative diseases makes proteases attractive targets for disease imaging strategies and therapeutic approaches [28-30]. More recently this concept has also been translated into PDT, with the major goal of enhancing selectivity. We and others have tailored several protease-sensitive photodynamic agents to specific disease-associated proteases [22,23]. We have recently successfully applied this strategy for the selective delivery of the photosensitizer to inflammatory lesions in an *in vivo* rheumatoid arthritis model [31]. In the present study, we successfully designed a urokinase-plasminogen-activator-sensitive agent uPA-PPP for the simultaneous detection and treatment of prostate cancer. In our previous studies we found that a positively charged uPA-PPP was a good compromise with respect to fluorescence quenching, ROS quenching and solubility [27]. This conjugate in combination with light proved to be efficient in killing prostate cancer cells

overexpressing uPA *in vitro*. However, in a prostate cancer murine model this compound showed suboptimal biodistribution.

The key of our PPP approach is based not only on its accumulation in the target tissue but also on its selective proteolytic activation. Instead of the typical elimination phase in the pharmacokinetic profiles, a plateau was observed for all conjugates suggesting that they were not only accumulated but activated inside tumors. Intratumoral injection of the positively charged N-PEG-uPA-PPP, which was poorly accumulated in tumors after systemic administration, resulted in an 8.5-fold fluorescence intensity increase compared to the fluorescence immediately after injection (data not shown). This underlines that the low fluorescent signal of tumors after systemic injection is primarily due to its suboptimal biodistribution and not due to a poor activation.

Therefore, we modified the polymeric backbone of the positively charged uPA-PPP in order to optimize the pharmacokinetics, particularly the biodistribution without significant loss of quenching capacity and solubility. These modifications induced changes in the molecular size and also in the net charge of the conjugates. Basically, all uPA-PPPs consisted of a polymeric backbone of poly-lysine, either 18 or 45 KDa, with a previously optimized Pb*a*-peptide loading of 25% per PL chain. One or two units of mPEG 20 KDa were in addition coupled to the polymeric chain. The remaining ε-lysine residues were capped with either the positively charged N-succinimidyl (1-methyl-3-pyridinio) formate iodide or the neutral PEGs, $mPEO_4$ and $mPEO_8$, respectively.

PPPs require efficient energy transfer between closely positioned photosensitizers on the polymeric backbone, in order to depopulate irradiation-excited first and triplet states. This results in reduced fluorescence and energy transfer to molecular oxygen. It has been demonstrated that the fluorescence and ROS generation capacity of the lipophilic photosensitizer Pb*a* can be efficiently quenched, if loaded at a sufficient amount on an appropriate polymeric backbone [25,32,33]. In the present study, all backbone designs showed a reasonable quenching of fluorescence and ROS production. However, differences between conjugates evidence that the increase in molecular size reduces their fluorescence while the degree of pegylation mainly alters the ROS production.

Activation of protease-sensitive prodrugs occurs via specific disease-related trigger which should ultimately result in higher selectivity. Therefore, another fundamental requirement for the appropriate performance of uPA-PPPs is the selective and efficient activation by uPA, the

target protease. Using the reported minimal substrate GSGRSAG, prodrug activation occurred for all conjugates efficiently by cleavage between the arginine-serine residues as confirmed by RP-HPLC and mass analysis of the released Pb*a*-GSGR fragment. However, the *in vitro* activation by uPA was markedly reduced as the molecular size and/or degree of pegylation increased. This is in agreement with previous studies where the attachment of a single chain of 20kDA PEG or several of 5KDa PEG to the polymeric backbone negatively affected enzymatic activation [27]. Differences in enzymatic activation between various conjugates suggest that enzyme-substrate interactions are not restricted to the active site and therefore, prodrug activation may be explained also in terms of inter- and intra-molecular interactions that result in steric hindrance from the reactive site. Activation of prodrugs by uPa in the test tube and by PCa cells showed contrasting results. The exogenous protease activated more efficiently the cationic conjugates than their neutral counterparts whereas incubation of prodrugs with cells resulted in the opposite: the neutrally charged conjugates were more efficiently activated than the positively charged conjugates. In the cell assay, uPA is secreted into the medium or cell surface bound. Due to the higher intracellular uptake of positively charge conjugates [34] these are less colocalized with the enzyme and activation is lower as compared to the neutral conjugates.

Following systemic administration, N-PEG-, N-2PEG- and 45PL- N-2PEG-uPA-PPP were only slightly accumulated in tumors, as evidenced by the low fluorescence increase. In comparison, PEO_4- and PEO_8-PEG-uPA-PPP showed higher fluorescence intensities. Moreover, a rapid clearance of the positively charged conjugates was observed. Although we expected a higher tumor accumulation in xenografts through increasing molecular weight, no significant effect was observed when the 45 KDa PL was used instead of the 18 KDa PL or when the single substitution of mPEG20KDa was changed for a double substitution. In contrast, changing the charge of the substituents from positive to neutral significantly increased the accumulation in the tumor tissue. In fact, an earlier report by Hamblin et al. concludes that pegylation improved the ability of polymer-PS conjugates to target cancer both *in vitro* and *in vivo* [35,36].

The higher selectivity of PEO_8-PEG-uPA-PPP fluorescence for tumoral tissue after 24 hours may be consequently attributed to a passive accumulation and an active release of the fluorescent PS-peptidyl-fragment. A further proof for the contribution of the proteolytic activation of this prodrug is given by the higher fluorescence increase measured for the PEO_8-

PEG-uPA-PPP in comparison to its homologous D-control after systemic administration due to the relative resistance to proteolytic cleavage of the latter.

The design of PPPs implies that these prodrugs label lesions characterized by enhanced proteolytic activity and also induce selective cell death following local irradiation. The protease-mediated phototoxicity of polymeric photosensitizer agents have been demonstrated *in vitro* [34,22,23] and *in vivo* [37]. The latter constitutes a proof-of-principle that tumor-associated proteases can activate polymeric compounds by cleavage of the polymeric backbone sufficiently to mediate phototoxicity. In contrast to these agents, in our design a protease-sensitive peptide linker is introduced between the PS and the polymeric backbone in order to increase the specificity of the prodrug by the target protease. Here, we have optimized a uPA-sensitive agent, PEO_8-PEG-uPA-PPP. Preliminary studies in nude mice demonstrated the feasibility of this agent to eradicate prostate cancer cells *in vivo*, as evidenced by complete disappearance of the tumor bioluminescence 24 hours after irradiation. Altogether these results suggest that PEO_8-PEG-uPA-PPP is an excellent candidate for further PDT studies for prostate cancer treatment.

5. Conclusions

We developed a uPA sensitive agent that fluoresces and decimates prostate cancer *in vivo* after localized light irradiation. This prodrug is capable to accumulate substantially in a murine xenograft model for prostate cancer. It is locally activated by up-regulated uPA, selectively releasing the photosensitizer Pb*a* in tumor tissue. Finally, it induces eradication of cancer cells after irradiation of fluorescent tumors. Unfavorable PS biodistribution and insufficient selectivity toward pathological tissue are recognized as major limitations of PDT of prostate cancer, frequently causing skin photosensitization and extraprostatic treatment effects. Our strategy combining passive targeting of tumors due to the EPR effect and site-selective PS release, localized light irradiation and phototoxicity, could increase selectivity of PDT for the treatment of prostate cancer.

Acknowledgements

References

1. Jemal, A.; Siegel, R.; Ward, E.; Hao, Y. P.; Xu, J. Q.; Murray, T.; Thun, M. J. Cancer statistics, 2008. *CA Cancer J. Clin.*, **2008**, *58,* 71.

2. Denmeade, S. R.; Isaacs, J. T. A history of prostate cancer treatment. *Nat. Rev. Cancer*, **2002**, *2,* 389.

3. Makarov, D. V.; Loeb, S.; Getzenberg, R. H.; Partin, A. W. Biomarkers for Prostate Cancer. *Annu. Rev. Med.*, **2009**, *60,* 139.

4. Pavlou, M.; Diamandis, E. P. The Search for New Prostate Cancer Biomarkers Continues. *Clin. Chem.*, **2009**, *55,* 1277.

5. Parker, C.; Muston, D.; Melia, J.; Moss, S.; Dearnaley, D. A model of the natural history of screen-detected prostate cancer, and the effect of radical treatment on overall survival. *Br. J. Cancer*, **2006**, *94,* 1361.

6. Moore, C. M.; Pendse, D.; Emberton, M. Photodynamic therapy for prostate cancer-a review of current status and future promise. *Nat. Clin. Pract. Urol.*, **2009**, *6,* 18.

7. Dolmans, D. E. J. G.; Fukumura, D.; Jain, R. K. Photodynamic therapy for cancer. *Nat. Rev. Cancer*, **2003**, *3,* 380.

8. Muschter, R. Photodynamic therapy: A new approach to prostate cancer. *Curr. Urol. Rep.*, **2003**, *4,* 221.

9. Windahl, T.; Andersson, S. O.; Lofgren, L. Photodynamic therapy of localised prostatic cancer. *Lancet*, **1990**, *336,* 1139.

10. Nathan, T. R.; Whitelaw, D. E.; Chang, S. C.; Lees, W. R.; Ripley, P. M.; Payne, H.; Jones, L.; Parkinson, M. C.; Emberton, M.; Gillams, A. R.; Mundy, A. R.; Bown, S. G. Photodynamic therapy for prostate cancer recurrence after radiotherapy: A phase I study. *J. Urol.*, **2002**, *168,* 1427.

11. Moore, C. M.; Nathan, T. R.; Lees, W. R.; Mosse, C. A.; Freeman, A.; Emberton, M.; Bown, S. G. Photodynamic therapy using meso tetra hydroxy phenyl chlorin (mTHPC) in early prostate cancer. *Laser Surg. Med.*, **2006**, *38,* 356.

12. Zaak, D.; Sroka, R.; Khoder, W.; Adam, C.; Tritschler, S.; Karl, A.; Reich, O.; Knuechel, R.; Baumgartner, R.; Tilki, D.; Popken, G.; Hofstetter, A.; Stief, C. G. Photodynamic diagnosis of prostate cancer using 5-aminolevulinic acid - First clinical experiences. *Urology*, **2008**, *72,* 345.

13. Pinthus, J. H.; Bogaards, A.; Weersink, R.; Wilson, B. C.; Trachtenberg, J. Photodynamic therapy for urological malignancies: Past to current approaches. *J. Urol.*, **2006**, *175,* 1201.

14. Verigos, K.; Stripp, D. C. H.; Mick, R.; Zhu, T. C.; Whittington, R.; Smith, D.; Dimofte, A.; Finlay, J.; Busch, T. M.; Tochner, Z. A.; Malkowicz, S. B.; Glatstein, E.; Hahn, S. M. Updated results of a phase I trial of motexafin lutetium-mediated interstitial photodynamic therapy in patients with locally recurrent prostate cancer. *J. Environ. Pathol. Toxicol. Oncol.*, **2006**, *25,* 373.

15. Patel, H.; Mick, R.; Finlay, J.; Zhu, T. C.; Rickter, E.; Cengel, K. A.; Malkowicz, S. B.; Hahn, S. M.; Busch, T. M. Motexafin lutetium-photodynamic therapy of prostate cancer: Short- and long-term effects on prostate-specific antigen. *Clin. Cancer Res.*, **2008**, *14,* 4869.

16. Weersink, R. A.; Bogaards, A.; Gertner, M.; Davidson, S. R. H.; Zhang, K.; Netchev, G.; Trachtenberg, J.; Wilson, B. C. Techniques for delivery and monitoring of TOOKAD® (WST09)-mediated photodynamic therapy of the prostate: Clinical experience and practicalities. *J. Photochem. Photobiol. B-Biol.*, **2005**, *79,* 211.

17. Trachtenberg, J.; Bogaards, A.; Weersink, R. A.; Haider, M. A.; Evans, A.; McCluskey, S. A.; Scherz, A.; Gertner, M. R.; Yue, C.; Appu, S.; Aprikian, A.; Savard, J.; Wilson, B. C.; Elhilali, M. Vascular targeted photodynamic therapy with palladium-bacteriopheophorbide photosensitizer for recurrent prostate cancer following definitive radiation therapy: Assessment of safety and treatment response. *J. Urol.*, **2007**, *178,* 1974.

18. Trachtenberg, J.; Weersink, R. A.; Davidson, S. R. H.; Haider, M. A.; Bogaards, A.; Gertner, M. R.; Evans, A.; Scherz, A.; Savard, J.; Chin, J. L.; Wilson, B. C.; Elhilali, M. Vascular-targeted photodynamic therapy (padoporfin, WST09) for recurrent prostate cancer after failure of external beam radiotherapy: a study of escalating light doses. *Bju International*, **2008**, *102,* 556.

19. Haider, M. A.; Davidson, S. R. H.; Kale, A. V.; Weersink, R. A.; Evans, A. J.; Toi, A.; Gertner, M. R.; Bogaards, A.; Wilson, B. C.; Chin, J. L.; Elhilali, M.; Trachtenberg, J. Prostate gland: MR imaging appearance after vascular targeted photodynamic therapy with palladium-bacteriopheophorbide. *Radiology*, **2007**, *244,* 196.

20. Maeda, H.; Wu, J.; Sawa, T.; Matsumura, Y.; Hori, K. Tumor vascular permeability and the EPR effect in macromolecular therapeutics: a review. *J. Controlled Release*, **2000**, *65,* 271.

21. Weissleder, R.; Tung, C. H.; Mahmood, U.; Bogdanov, A. In vivo imaging of tumors with protease-activated near-infrared fluorescent probes. *Nature Biotech.*, **1999**, *17,* 375.

22. Choi, Y.; Weissleder, R.; Tung, C. H. Protease-mediated phototoxicity of a polylysine-chlorin(e6) conjugate. *Chem. Med. Chem.*, **2006**, *1,* 698-+.

23. Campo, M. A.; Gabriel, D.; Kucera, P.; Gurny, R.; Lange, N. Polymeric photosensitizer prodrugs for photodynamic therapy. *Photochem. Photobiol.*, **2007**, *83,* 958.

24. Cozzi, P. J.; Wang, J.; Delprado, W.; Madigan, M. C.; Fairy, S.; Russell, P. J.; Li, Y. Evaluation of urokinase plasminogen activator and its receptor in different grades of human prostate cancer. *Human Pathol.*, **2006**, *37,* 1442.

25. Gabriel, D.; Campo, M. A.; Gurny, R.; Lange, N. Tailoring protease-sensitive photodynamic agents to specific disease-associated enzymes. *Bioconjugate Chem.*, **2007**, *18,* 1070.

26. Ke, S. H.; Coombs, G. S.; Tachias, K.; Navre, M.; Corey, D. R.; Madison, E. L. Distinguishing the specificities of closely related proteases - Role of P3 in substrate and inhibitor discrimination between tissue-type plasminogen activator and urokinase. *J. Biol. Chem.*, **1997**, *272,* 16603.

27. Gabriel, D.; Zuluaga, M. F.; Martinez, M. N.; Campo, M. A.; Lange, N. Urokinase-plasminogen-activator sensitive polymeric photosensitizer prodrugs: design, synthesis and in vitro evaluation. *J. Drug Deliv. Sci. Technol.*, **2009**, *19,* 15.

28. Weissleder, R.; Cheng, H. C.; Marecos, E.; Kwong, K.; Bogdanov, A. Non-invasive in vivo mapping of tumour vascular and interstitial volume fractions. *Eur. J. Cancer*, **1998**, *34,* 1448.

29. Tung, C. H.; Mahmood, U.; Bredow, S.; Weissleder, R. In vivo imaging of proteolytic enzyme activity using a novel molecular reporter. *Cancer Res.*, **2000**, *60,* 4953.

30. Law, B.; Curino, A.; Bugge, T. H.; Weissleder, R.; Tung, C. H. Design, synthesis, and characterization of urokinase plasminogen-activator-sensitive near-infrared reporter. *Chem. Biol.*, **2004**, *11,* 99.

31. Gabriel, D.; Busso, N.; So, A.; van den Bergh, H.; Gurny, R.; Lange, N. Thrombin-sensitive photodynamic agents: A novel strategy for selective synovectomy in rheumatoid arthritis. *J. Controlled Release*, **2009**, *138,* 225.

32. Hackbarth, S.; Horneffer, V.; Wiehe, A.; Hillenkamp, F.; Roder, B. Photophysical properties of pheophorbide-a-substituted diaminobutane poly-propylene-imine dendrimer. *Chem. Phys.*, **2001**, *269,* 339.

33. Hackbarth, S.; Ermilov, E. A.; Roder, B. Interaction of Pheophorbide *a* molecules covalently linked to DAB dendrimers. *Optics Commun.*, **2005**, *248,* 295.

34. Soukos, N. S.; Hamblin, M. R.; Hasan, T. The effect of charge on cellular uptake and phototoxicity of polylysine chlorin(e6) conjugates. *Photochem. Photobiol.*, **1997**, *65,* 723.

35. Hamblin, M. R.; Miller, J. L.; Rizvi, I.; Ortel, B.; Maytin, E. V.; Hasan, T. Pegylation of a chlorin(e6) polymer conjugate increases tumor targeting of photosensitizer. *Cancer Res.*, **2001**, *61,* 7155.

36. Hamblin, M. R.; Miller, J. L.; Rizvi, I.; Loew, H. G.; Hasan, T. Pegylation of charged polymer-photosensitiser conjugates: effects on photodynamic efficacy. *Br. J. Cancer*, **2003**, *89,* 937.

37. Choi, Y.; Weissleder, R.; Tung, C. H. Selective antitumor effect of novel protease-mediated photodynamic agent. *Cancer Res.*, **2006**, *66,* 7225.

Chapter 5. Selective Photodynamic Therapy for the Treatment of Prostate Cancer through Targeting of Proteolytic Activity

Maria-Fernanda Zuluaga, Nawal Sekkat and Norbert Lange

Department of Pharmaceutics and Biopharmaceutics, School of Pharmaceutical Sciences, University of Geneva, University of Lausanne, 30 Quai Ernest-Ansermet, 1211 Geneva 4, Switzerland

ABSTRACT. Interstitial photodynamic therapy shows potential for the treatment of localized prostate cancer. Current limitations include lack of selective accumulation of photosensitizer in tumors or incomplete ablation. We have developed a photosensitizer prodrug (uPA-PPP) capable to accumulate sufficiently in tumors, to be selectively activated by overexpressed urokinase, and to exert a strong photoxic effect upon irradiation. The prodrug alone (8 μM as pheorphide *a* equivalents) was not toxic to PC cells but reduced cell viability *in vitro* by 90 % in combination with light (10 J/cm^2). A single dose of PDT (7.5 mg as pheophorbide *a* equivalents /kg + 150 J/cm^2) was able to completely eradicate prostate cancer in a xenograft-model. The amount of activated prodrug found in tumors was much higher that that found in neighboring skin. No activated prodrug was detected in muscle. These results altogether reinforce our hypothesis of an improved outcome and selectivity of PDT with the uPA-sensitive prodrug for the treatment of localized prostate cancer.

Keywords: Polymeric prodrugs; protease-sensitive prodrugs; photodynamic therapy; urokinase-like plasminogen-activator; prostate cancer.

1. Introduction

Prostate cancer (PC) is the most prevalent male cancer [1]. Gold standard for the treatment of localized disease is radical prostatectomy or radiation therapy. A minority of low risk patients is under active surveillance only, but this often only delays definitive treatment [2]. The excellent results of radical treatment are hampered by the high frequency of side effects (e.g. sexual or urinary dysfunction) and their long-lasting impact on quality of life. Novel mapping techniques (e.g. mapping biopsies) lay the foundation for local therapies, which might be associated with lesser side effects.

Todays physician's toolbox for this purpose include cryotherapy, high intensity focused ultrasound, laser ablation, and photodynamic therapy (PDT) [2].

PDT requires three main elements: a photosensitizer (PS), light and oxygen [3]. After administration, the PS accumulates in target tissues and subsequently can be selectively activated by light to produce reactive oxygen species. Although originally employed for the treatment of superficial cancer, recent progress in light delivery and dosimetry have allowed PDT to be entered in the treatment of cancers in the hollow-organs and solid tumors including PC [4,5].

Studies in animal models for PC have revealed the large potential of PDT in this indication [6]. Moreover, clinical studies have shown the effectiveness of PDT for treatment of both localized disease and salvage therapy after failed external radiation therapy [5,7,8]. Photofrin®-like compounds were the first PSs assessed in clinical trials [9]. Subsequently, small prospective clinical trials using Foscan® [10] and 5-aminolevulinic acid [11], have been reported. Despite promising PDT responses, observed prolonged skin sensitization along with extra-prostatic tissue injury fostered further research efforts aiming at improving PDT selectivity and reducing side effects. In this context, alternative PDT agents including LuTex® and Tookad® specifically targeting the tumor vasculature were evaluated [12]. Trials for the treatment of recurrent PC escaping radiation therapy and primary PC using these agents showed good efficacy but still considerable adverse effects [13-16]. The latest results of a more recent trial with an improved soluble form of Tookad® were still disappointing with respect to response and collateral damage [Emerton, IPA congress, Innsbruck, 2011].

In this context, selective accumulation of the PS in tumor tissues has been a long standing goal in order to avoid collateral damage of the urethra, rectum and urinary sphincter [7]. To

address this issue, we have developed polymeric protease-sensitive photosensitizer prodrugs. These water-soluble therapeutic agents consist of several PS molecules attached to a pegylated polylysine backbone through a cleavable peptide linker. Selective delivery and uptake of the PS into tumor tissue is promoted by the polymeric carrier through the enhanced permeation and retention effect [17]. The photoactivity of PS outside target tissue is impeded by the efficient quenching between very close positioned PS molecules on the polymeric carrier. Finally, the PS's activity is reestablished only in target tissues through proteolytic activation. This is a consequence of selective cleavage of the peptide linker by urokinase plasminogen-activator, a protease over-expressed by prostate cancer cells. In other words, our prodrug strategy aims to achieve a selective phototoxic effect in the target tissue, while minimizing effects to surrounding tissues and the skin.

Our previous studies show that our prodrug displays a dual functionality: it allows visualization of lesions in response to uPA activity and to exert a selective cytotoxic effect upon irradiation with light (submitted manuscript). This report describes its phototoxic effect in vitro in PC-3 cancer cells and luciferase-transfected PC-3M-luc-C6 as well as in vivo PDT using the PC xenograft-model.

2. Materials and Methods

2.1. Materials

Dichloromethane, dimethylformamide, dimethylsulfoxide (DMSO), acetonitrile, diethylether, trifluoroacetic acid (Acros Organics, Geel, Belgium); HGly-2-chlorotrityl resin (1.1mmol/g), boc-glycine, fmoc-glycine, fmoc-alanine, triphenylisopropylsilane, *N,N*-diisopropyl-ethylamine (DIPEA), piperidine, picrylsulfonic acid aqueous solution (1 M), sodium iodide, ethanol were provided by Fluka (Buchs, Switzerland). L-aminoacids, Fmoc(tBu)-serine, fmoc(Pbf)-arginine, O-(7-azabenzotriazol-1-yl)-*N,N,N,N*-tetramethyluronium hexafluoro-phosphate (HATU) were obtained from Genscript (Piscataway, NJ); Poly-L-lysine HBr (PL; 18 kDa) were from Sigma-Aldrich (Buchs, Switzerland) urokinase high molecular weight, human urine from Calbiochem/VWR (Zug, Switzerland); pheophorbide *a* (Pb*a*) from Frontier Scientific (Carnforth, UK). Nektar (San Carlos, CA) delivered the mPEG-SPA 20 kDa. F-12 growth media, HBSS, D-PBS, TrypL Express were provided from Invitrogen (Basel, Switzerland). mPEO$_8$-NHS, defined fetal bovine serum (FBS), MEM/EBSS, sodium pyruvate 100mM, MEM vitamin solution, L-glutamine 200mM, and MEM non-essential aminoacids

solution were obtained from ThermoFisher Scientific (Erembodegem, Belgium). D-luciferin firefly potassium salt was purchased from Biosynth AG (Staad, Switzerland). All chemicals were of analytical grade and used without further purification.

2.2. **Synthesis of prodrug**

uPA-PPP is a urokinase plasminogen activator polymeric photosensitizer prodrug in which 25% of available ε-NH2 of the polylysine (PL) were capped with pheophorbide *a* (Pb*a*)– peptide conjugate. It was synthesized in three steps, as described in detail elsewhere [18]. Briefly, the peptide G(L)SG(L)R(L)S(L)AG containing the reported minimal urokinase plasminogen activator minimal substrate [19] was synthesized manually on solid phase according to the standard FMOC protocol. Subsequently, NHS-activated Pb*a* was coupled to the N-terminus of the peptide. The Pb*a*-peptide conjugate was purified by preparative RP-HPLC (Waters Delta 600 HPLC, Mildford, MA) on a C8 column (Nucleosil 300-10; Macherey–Nagel, Düren, Germany) and molecular weight analyzed by ESI-MS (Finnigan MAT SSQ 7000; Thermo Electron Co., Waltham, MA). Pb*a*-peptide was then loaded on PL (25 units per 100 free epsilon-NH$_2$ groups of the PL). DIPEA (3.7 mg, 3.3×10^{-5} mol) was added to a solution containing Pb*a*-peptide (3.1 mg, 3.1×10^{-6} mol), PL 18KDa (2.0 mg, 0.11×10^{-6} mol), and HATU (1.4 mg, 4.03×10^{-6} mol) in DMSO (0.65 mL). The reaction was stirred in the dark under argon atmosphere for 4 hours at room temperature. Complete loading was confirmed by analytical RP-HPLC, as described in Ref [18]. Further modifications were performed by capping the remaining epsilon-lysine residues with 1 mPEG 20kDa chain and multiple mPEO$_8$ chains. For this purpose, mPEG-SPA 20kDa (1.9 mg, 9.56×10^{-8} mol in DMSO (0.2 mL) was added to the reaction under stirring at 10 °C. The reaction was stirred in the dark and allowed to warm-up overnight to room temperature. Then, mPEO$_8$-NHS (3.6 mg, $7.01 \text{ x} \times 10^{-6}$ mol) was added in the same manner. The final conjugate was purified by size exclusion chromatography using a Sephacryl^{TM} column (S-100; Amersham Biosciences, Otelfingen, Switzerland), lyophilized, and stored protected from light at -20 °C.

2.3.   **Cell culture**

Human prostate cancer PC-3 cells (ATCC, Manassas, VA) were cultured in F-12 growth medium supplemented with 10% FBS. Luciferase-transfected PC-3M-luc-C6 cells, a kind gift of Caliper LifeSciences (Alameda, CA), were maintained in MEM/EMBSS with 10% FBS, non-essential amino acids, L-glutamine, sodium pyruvate, and MEM vitamin solution. Both

cell lines were grown as monolayers at 37°C in a humidified incubator containing 5% CO_2. The cells were harvested using TrypLE Express, and passaged every 4 to 5 days.

2.4.   Prostate cancer model

Female swiss Nu/Nu mice (5 to 6 weeks, 17 to 22 g) were supplied by Charles River Laboratories (L'arbresle, France). The mice were maintained with *ad libitum* access to sterile food and acidified water in a light cycled room acclimatized at 22±2 °C under pathogen free conditions. All experimental procedures on animals were performed in compliance with the Swiss Federal Law on the Protection of the Animals, according to a protocol approved by the local veterinary authorities. To induce xenografts, 1.5 x 10^5 cells were injected subcutaneously into the dorsal region of mice. Tumors of approximately 200 mm^3 in size were formed within 3 weeks after inoculation.

2.5.   In vitro PDT

Phototoxicity was tested on PC-3 and luciferase-transfected PC-3M-luc-C6 cells. Aliquots of 1.2 x 10^4 and 1.0 x10^4 cells, respectively, in 100 μL complete medium were seeded in 96-well plates and cultured for 12 hours until 70% confluence. Cells were given fresh complete medium containing uPA-PPP at final concentrations of 0.5, 1.0, 2.0, 4.0 and 8.0 μM Pb*a* equivalents for 6 hours. Cells were washed twice with sterile HBSS and fresh medium was added. Plates were either exposed to blue light (Narwa, LT 18W/O18) from bellow at light doses of 2.5, 5.0 and 10 J/cm^2 or kept in the dark. After irradiation, cells were incubated in fresh medium for 24 hours. Cell viability was measured using a mitochondrial MTT assay. First, cells were washed once with 200 μl HBSS and 50 μl MTT (1mg/mL) in complete medium was added into each well. After 3 hours, DMSO (200μl) was added to dissolve formed violet formazan crystals. After brief agitation on a microplate shaker, the absorption at 525 nm was measured with a plate reader (Saphire, Tecan, Switzerland). Positive and negative controls were treated with complete medium or 0.1% Triton in NaOH 5M, respectively. Percentage cell survival was calculated with respect to control samples, as follows: [A (test-conc.) - A (100% dead)] / [A (100% viable) − A (100% dead)]*100. All conditions were tested in sextuplicates.

2.6.   In vivo PDT

PC-3M-luc-C6 xenograft bearing mice (n=7) were injected retroorbitally with uPA-PPP (7.5 mg Pb*a* equivalents /kg) when tumors had an estimated volume of 200 mm^3 (3-4 weeks after

inoculation). Tumors were irradiated with a light dose of 150 J/cm^2 at 665 ± 5 nm (Ceralas I 670, Biolitec; Jena, Germany) 16 hours after conjugate administration. Animals were maintained under 1–2% isoflurane inhalation and body temperature at 37°C during irradiation. Two other groups of animals received drug alone (n=4) and light alone (n=4). PDT effects were followed 90 days by bioluminescence imaging of animals using an IVIS 200 small-animal imaging system (Caliper Life Sciences Inc., Hopkinton, MA). 10 to 15 minutes before *in vivo* imaging, animals were injected interperitoneally with the D-luciferin (150 mg/kg in DPBS). Mice were sacrificed when tumors reached volumes bigger than 1000 mm^3 or at the end of the study (90 days after treatment). Data were analyzed with Living Image 3.0 software (Caliper Life Sciences Inc.).

2.7. Preliminary analysis of prodrug cleavage products

Cleavage products were qualitatively analyzed in tumor, skin and muscle homogenates of a prostate cancer-xenografted mouse, sacrificed 24 hours after retroorbital injection of uPA-PPP (7.5 mg Pb*a* equivalents /kg). Briefly, frozen tissues were weighed and homogenized with a solution containing a protease-inhibitor cocktail (5 μl per 100 mg tissue) and acetonitrile:water (1:1; 1 mL per 100 mg tissue) by means of a tissue homogenizer (Eurostar digital IKA; Werke, Staufen, DE). The suspension was sonicated (15 min at 14 kHz) and centrifuged (15 min at 1450 rpm). The supernatant was collected and extraction was repeated twice as described. Collected supernatants were lyophilized and subsequently reconstituted in acetonitril:water (1:1; 1 mL /100 mg tissue). Samples were sonicated (5 min, 14 kHz), filtered and subjected to RP-HPLC analysis. Separation was performed on a C18 column (Nucleodur gravity 3μ CC 125/4; Macherey-Nagel).

2.8. Statistical analysis

Mean ± SD values were used for expression of data. Statistical analyses of data were done using Student's t test. Differences of *P* < 0.05 were considered statistically significant.

3. Results

The phototoxic effect induced by uPA-PPP was investigated in PC -3 and PC-3M-luc-C6 cells. The latter is a luciferase-transfected cell type employed to quantitatively monitor the *in vivo* PDT studies in our experimental animal model of PC. The effect of PDT on cells treated

with prodrug (0.5, 1.0, 2.0, 4.0 and 8.0 µM Pb*a* equivalents), either irradiated with a light dose of 2.5, 5.0 and 10 J/cm^2 or kept in the dark is summarized in Fig. 1.
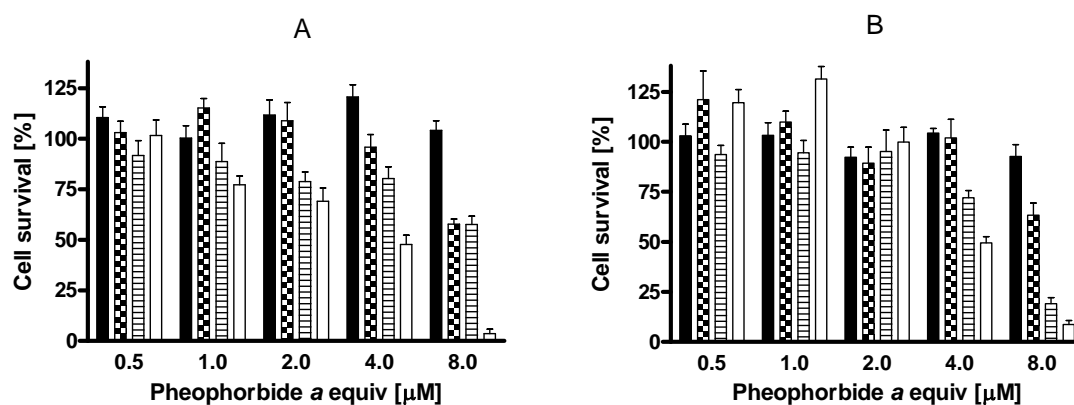

Figure 1. Light and drug dose-dependent phototoxicity mediated by uPA-PPP in (A) PC-3 and (B) PC-3M-luc-C6 cells. After incubation with the conjugate for 6 h, cells were kept in the (■) dark or irradiated with blue light at (▪▫) 2.5 J/cm^2, (≡) 5 J/cm^2 or (▫) 10 J/cm^2. Cell viability determined by means of MTT-tests.

Both cell lines display a light and drug dose-dependent cell survival. uPA-PPP alone presented little to no toxic effect as shown by cell survival percentages around 100% for all prodrug concentrations. Phototoxic effects were particularly evident at 4.0 µM or higher, where all light doses reduced cell survival rate. In PC-3 cells at 8 µM of Pb*a* equivalents approximately 50% of cells survived irradiation with 2.5 or 5 J/cm^2 of light, while at a dose of 10 J/cm^2 of light only 5 % of cells remained viable. In PC3-3M-luc-C6 cells similar dose-response curves were observed, although these cells were slightly less sensitive to PDT.

Although slightly less sensitive, we have used PC-3M-luc-C6 as basis for our experimental animal model for PC, since they allow non-invasively following tumor growth through bioluminescence in a quantitative manner [20]. In this study, bioluminescence was used to assess the photodynamic effect of uPA-PPP on tumors. Adequate drug and light dose and drug-light interval were established according to previous work. Colocalization of fluorescence (rainbow-color scale) and bioluminescence (yellowhot-color scale) 16 hours after administration of the prodrug, is shown in Fig. 2.
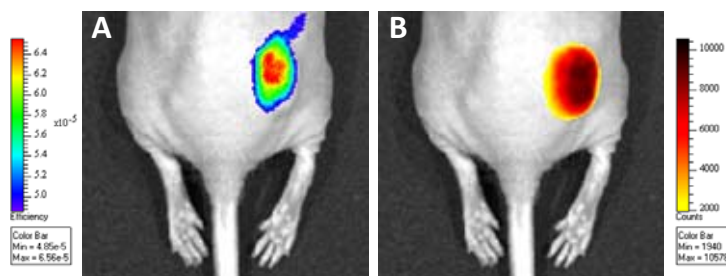
Figure 2. (A) Tumoral fluorescence intensity 16 hours after retro-orbital administration of 2 mg/Kg of PEO$_8$-PEG-uPA-PPP (as Pba equivalents) and (B) Bioluminescence of luciferase-expressing PC-3M-luc-C6 tumor 15 minutes after D-luciferin peritoneal injection.

For PDT, 7.5 mg Pb*a* equivalents /kg of the prodrug was given to mice via retroorbital injection and 16 hours later, tumors were irradiated with 150 J/cm^2 at 665 ± 5 nm. Animals receiving the drug alone or irradiated with light were used as controls. Fig. 3A shows a sequence of images taken of one mouse completely responding to PDT before and after treatment. Bioluminescent images taken 15 minutes after administration of luciferin were used to quantify PC cells. The tumor is visualized on a yellowhot-color scale. On average a tumor volume of 200 mm^3 tumor volume corresponds to 2.5 x 10^7 photon s^{-1}. Macroscopically one day after treatment a local inflammatory response was visible. Inflammation developed into necrosis that appeared as a dark crust on the skin by day 3 and succeeded by healing and culminated in complete elimination of the tumor. The absence of bioluminescence, which persisted over 90 days, also indicated complete destruction of the tumor associate cells. Fig. 3*B* summarizes the ROI analysis of sequences of images obtained for the three treatment regimes (PDT, drug alone and light alone) until day 15 after treatment. Mice receiving both light and drug showed a three log reduction of tumor bioluminescence the day after treatment. In this group the mean bioluminescent signal remained below the initial value for at least 30 days (data not shown). In contrast to PDT, light alone showed a slight reduction on tumor bioluminescence and no reduction in bioluminescence was observed for animals receiving prodrug alone. In both control groups, we observed a 4-fold increase in tumor bioluminescence until day 15 after treatment, day at which the animals were euthanized. PDT was significantly different from light and prodrug alone ($P = 0.002$ and $P = 0.001$, respectively) whereas no significant difference between the two latter could be established ($P = 0.6$).
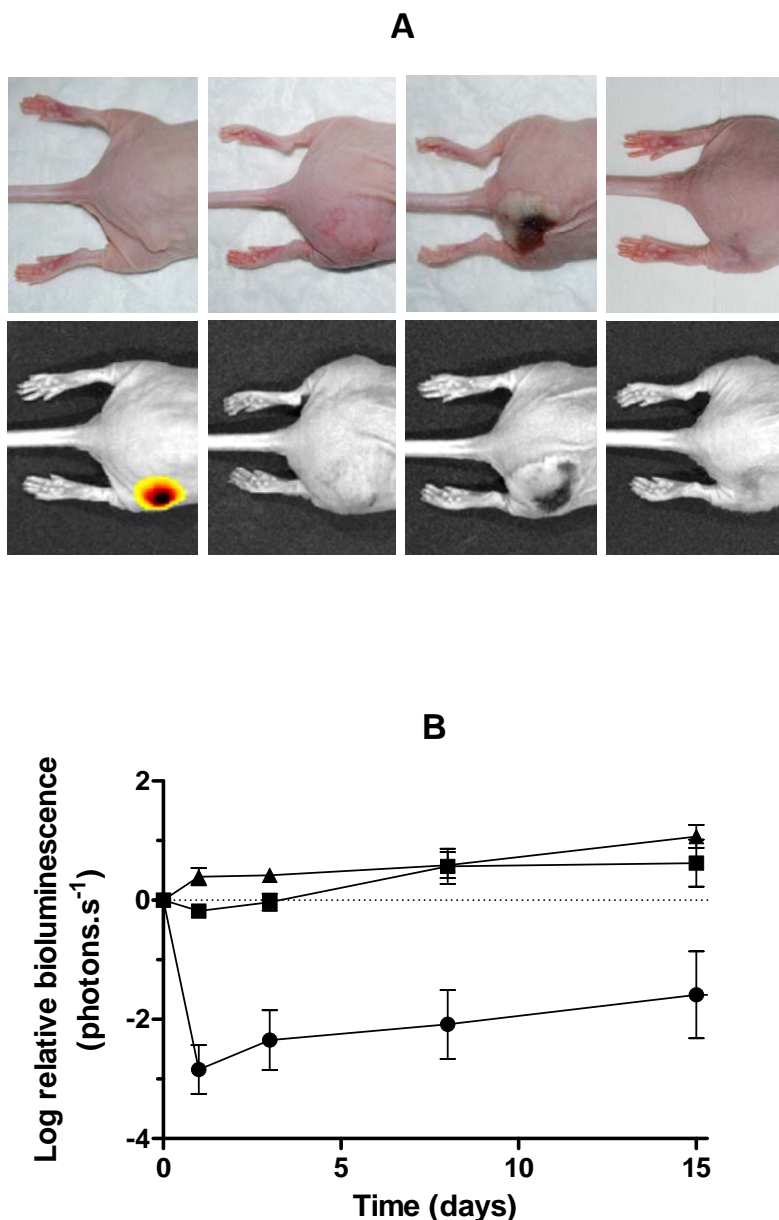
A

B

Figure 3. Treatment response was evaluated in terms of tumor growth. (A) In vivo imaging of a PC-3M-luc-C6 tumor bearing mouse receiving PDT. D-luciferin was administered peritoneally 15 minutes before imaging. Intensity of the signal is correlated to cell density. Sequence on the top corresponds to white-light images, from left to right: before, day 1, 3 and 90 after PDT. Sequence on the bottom corresponds to bioluminescent images, which confirmed total eradication of tumor cells. (B) Relative bioluminescence after treatment. Animals bearing subcutaneous prostate tumors were administered with 7.5 mg/kg of uPA-PPP as Pba equivalents and 16 hours after injection, tumors were irradiated with 150 J/cm^2 at 665 ± 5 nm (●; n=8). Control animals were administered with the drug alone (▲; n=4) or light alone (■; n=4). Tumor growth was monitored weekly by in vivo bioluminescence imaging. Images were taken 15 min after peritoneal injection of D-luciferin. Since control mice had to be sacrificed 15 days post PDT comparison was done only for this period.

Complete remission to PDT treatment was observed in 3 mice (see Table 1). Only partial remission was detected in the remaining animals from this group which, in part, explains the relatively big error bars in the bioluminescence analysis from this group. However, all mice from this group survived until day 30. All animals in the control groups survived over a period of 15 days.

Table 1. Treatment responses

Treatment	Complete remission	Partial remission	No response
PDT	3	4	
Prodrug	0	0	4
Light	0	0	4

Survival of mice treated with PDT, prodrug alone, and light alone is presented in Fig. 4A. All animals treated with prodrug alone and with light alone were sacrificed before or on day 15 after treatment. PDT survival curve was significantly different from these two groups ($P = 0.001$). Four animals which presented partial response to PDT were sacrificed on day 30 or 45 after treatment (57% survival). The three remaining mice which completely responded to PDT were sacrificed at the end of the study (43% survival).

A
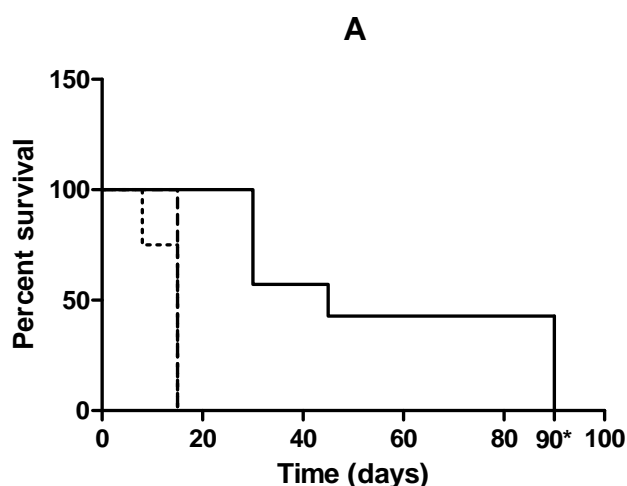
Figure 4. (A) Survival curves after administration of (—) PDT; 7.5 mg/kg of uPA-PPP (as Pba equivalents) were injected retroorbitally. 16 hours after injection, tumors were irradiated with a light dose of 150 J/cm² at 665 ± 5 nm. (– –) light alone; tumors were irradiated with a light dose of 150 J/cm² at 665 ± 5 nm. And (---) drug alone; 7.5 mg/kg of uPA-PPP (as Pba equivalents) were injected retroorbitally. * The study concluded after 90 days.

HPLC analysis of tissue extracts confirmed the presence of the expected photoactive Pba-GSGR fragment inside tumors (see Fig. 4B). Concentration of this compound in tumor was much higher than in the skin. Some smaller fragments with longer retention times presumably due to further proteolytic processing were also found in the tumor and to a much smaller extend in the skin. In contrast, no photoactive fragments were found in muscle.
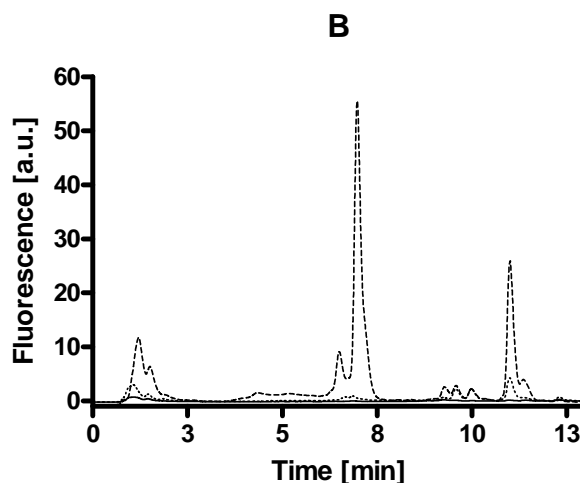
B

Figure 4 (B) Analytical HPLC analysis of (---) tumor, (—) skin, and (—) muscle extracts. In tumor a major peak was found at 7.5 minutes, corresponding to the cleaved Pba-peptidyl-fragment. The small peaks at 6.3 and 10 minutes are other minor cleavage Pba peptidyl-fragments. The same compounds were detected in skin in trace amounts. In muscle, no cleavage products were detected. Chromatograms show representative traces of mouse tissues 16 hours after retroorbital injection of uPA-PPP (7.5 mg Pba equivalents /kg).

4. Discussion

We and others have developed protease-sensitive photosensitizer prodrugs for selective PDT cancer and in other degenerative diseases [21,22]. We have recently optimized PPPs that are sensitive to urokinase-like plasmin activator, known for its overexpression in PC, with respect to their pharmacokinetics and biodistribution (submitted manuscript). These conjugates target diseased tissue through multiple mechanisms. Before the essential activation through proteolytic cleavage, the macromolecular prodrug accumulates preferentially in tumors through the EPR effect. The low water solubility of the released Pb*a*-peptidyl fragments and thus reduced clearance as compared to the intact prodrug further increases the tumor to normal tissue ration. In PC, our results show that selective targeting can be achieved through

urokinase-sensitive polymeric photosensitizer prodrugs allowing detection and treatment of the disease. Here we have adapted the light dose, drug dose and the drug light interval.

Because we have mostly used the wild type prostate cancer cell line PC-3 for *in vitro* optimization but wanted to monitor PDT effects *in vivo,* we first investigated prodrug phototoxicity with a luciferase transfected counterpart, PC-3M-luc-C6. *In vitro* PDT resulted in light and prodrug dose-dependent phototoxicity for both cell lines. However, the PC-3M-luc-C6 cells were slightly less susceptible to PDT. Furthermore, no dark toxicity was observed with the uPA-PPP in both cell lines. In a previous work prodrug activation was confirmed for both wild and transfected PC-3 cells suggesting that the activated prodrug was responsible for the observed PDT effects.

In vivo, uPA-PPP produced a strong photodynamic effect after irradiation of fluorescent PC-3M-luc-C6 tumors. Bioluminescence images show a drastic reduction of tumor cells in all animals included in the PDT group. 3 animals were completely cured from PC after PDT (43% cure rate). Few PC cells remained after treatment in 4 animals. However, tumor growth was delayed and tumors reached original volumes only 30 days after treatment or later. The phototoxic effect induced by prodrug alone and by light alone was negligible.

Similar results were reported for a vascular-targeted PDT study including Tookad[®] [23], so far, one of the most studied photosensitizer in the treatment of PC and currently under clinical investigation for recurrent PC [16]. In comparison to the present study, a lower dose of Tookad[®] (4 mg/kg) was injected to PC-xenografted nude mice and tumors were immediately irradiated with a light dose of 360 J/cm^2. We use a higher PS dose because the prodrug is not entirely processed and a longer drug-light interval, based on optimal tumor to normal tissue ratios, to prevent collateral damage.

HPLC analysis of tissue extracts revealed a major peak corresponding to Pb*a*-GSGR fragment in the tumors which confirmed the activation of the prodrug by PC cells. Neighboring skin contained insignificant amounts of Pb*a*-GSGR fragments. PS content in skin and tissues in close proximity to the prostate including nerve, rectum, and lymph node has been found to be similar in orthotopic models [24]. Conversely, comparison of orthotopic and subcutaneous tumors has evidenced significant differences in PS distribution and PDT outcome [25]. Thus, direct evaluation of our prodrug in orthotopic models will be necessary to study selectivity.

In contrast to both control groups, all mice that have been irradiated with 150J/cm2 at 665nm subsequent to administration of uPA-PPP survived until day 30 after PDT. Bioluminescence imaging helped to evaluate the tumor progression non-invasively. Furthermore, the ratio between the photon counts before PDT and 1 day after was an indicative for the therapeutic outcome. This is in accordance with Fleshker et al. [26] who evaluated bioluminescence imaging in the treatment of breast cancer with WST11 after vascular targeted PDT. In the present study a reduction of more than 3-log values was necessary to cure the animals. Thus, bioluminescence imaging can help to improve the cure rate and adapt photodynamic treatment regimes.

Here only a single treatment was evaluated; however, repeated treatments could be envisaged when partial response to PDT is observed. Multiple treatments using different drug-light intervals intended to cause both vascular and tissue PDT effects has shown to improve therapeutic outcomes [27]. Alternatively, combination treatments might help to improve PDT efficacy. It is now widely accepted that stress induced through photodynamic insult in certain cases initiates signaling pathways, leading to VEGF increase in PC cells [28], which in turn contribute to tumor survival and regrowth. In this context, PDT in combination with antiangiogenic agents for PC might result in increased anticancer response.

5. Conclusions

We developed a uPA-sensitive prodrug that is not toxic to PC cells but combined with light efficiently inactivates cells *in vitro*. *In vivo* PDT can completely destroy tumor PC xenografts as demonstrated by bioluminescence imaging. Activation of the prodrug was only modest in adjacent tissues. More research in orthotropic PC models is envisioned to confirm the potential advantages of our strategy over other current PDT approaches.

References

1. Jemal, A. *et al.* Global cancer statistics. *CA Cancer J. Clin.*, **2011**, *61*, 69.

2. Ahmed, H. U. *et al.* Will focal therapy become a standard of care for men with localized prostate cancer? *Nat. Clin. Pract. Oncol.*, **2007**, *4*, 632.

3. Dolmans, D. E.;Fukumura, D.;Jain, R. K. Photodynamic therapy for cancer. *Nat. Rev. Cancer*, **2003**, *3*, 380.

4. Pinthus, J. H.;Bogaards, A.;Weersink, R.;Wilson, B. C.;Trachtenberg, J. Photodynamic therapy for urological malignancies: past to current approaches. *J. Urol.*, **2006**, *175*, 1201.

5. Moore, C. M.;Hoh, I. M.;Bown, S. G.;Emberton, M. Does photodynamic therapy have the necessary attributes to become a future treatment for organ-confined prostate cancer? *B.J.U. Int.*, **2005**, *96*, 754.

6. Muschter, R. Photodynamic therapy: a new approach to prostate cancer. *Curr. Urol. Rep.*, **2003**, *4*, 221.

7. Arumainayagam, N.;Moore, C. M.;Ahmed, H. U.;Emberton, M. Photodynamic therapy for focal ablation of the prostate. *World J. Urol.*, **2010**, *28*, 571.

8. Martin, N. E.;Hahn, S. M. Interstitial photodynamic therapy for prostate cancer: a developing modality. *Photodiagn. Photodyn.*, **2004**, *1*, 123.

9. Windahl, T.;Andersson, S. O.;Lofgren, L. Photodynamic therapy of localised prostatic cancer. *Lancet*, **1990**, *336*, 1139.

10. Moore, C. M. *et al.* Photodynamic therapy using meso tetra hydroxy phenyl chlorin (mTHPC) in early prostate cancer. *Lasers Surg. Med.*, **2006**, *38*, 356.

11. Zaak, D. *et al.* Photodynamic Therapy by Means of 5-ALA Induced PPIX in Human Prostate Cancer - Preliminary Results. *Med. Laser Appl.*, **2003**, *18*, 91.

12. Lepor, H. Vascular targeted photodynamic therapy for localized prostate cancer. *Rev. Urol.*, **2008**, *10*, 254.

13. Verigos, K. *et al.* Updated Results of a Phase I Trial of Motexafin Lutetium-Mediated Interstitial Photodynamic Therapy in Patients with Locally Recurrent Prostate Cancer. **2006**, *25*, 373.

14. Patel, H. *et al.* Motexafin lutetium-photodynamic therapy of prostate cancer: short- and long-term effects on prostate-specific antigen. *Clin. Cancer Res.*, **2008**, *14*, 4869.

15. Trachtenberg, J. *et al.* Vascular targeted photodynamic therapy with palladium-bacteriopheophorbide photosensitizer for recurrent prostate cancer following definitive radiation therapy: assessment of safety and treatment response. *J. Urol.*, **2007**, *178*, 1974.

16. Trachtenberg, J. *et al.* Vascular-targeted photodynamic therapy (padoporfin, WST09) for recurrent prostate cancer after failure of external beam radiotherapy: a study of escalating light doses. *B.J.U. Int.*, **2008**, *102*, 556.

17. Maeda, H.;Wu, J.;Sawa, T.;Matsumura, Y.;Hori, K. Tumor vascular permeability and the EPR effect in macromolecular therapeutics: a review. *J.Control. Release*, **2000**, *65*, 271.

18. Gabriel, D.;Campo, M. A.;Gurny, R.;Lange, N. Tailoring protease-sensitive photodynamic agents to specific disease-associated enzymes. *Bioconjug. Chem.*, **2007**, *18*, 1070.

19. Ke, S. H. *et al.* Distinguishing the specificities of closely related proteases. Role of P3 in substrate and inhibitor discrimination between tissue-type plasminogen activator and urokinase. *J. Biol. Chem.*, **1997**, *272*, 16603.

20. Jenkins, D. E.;Yu, S. F.;Hornig, Y. S.;Purchio, T.;Contag, P. R. In vivo monitoring of tumor relapse and metastasis using bioluminescent PC-3M-luc-C6 cells in murine models of human prostate cancer. *Clin. Exp. Metastasis*, **2003**, *20*, 745.

21. Choi, Y.;Weissleder, R.;Tung, C. H. Selective antitumor effect of novel protease-mediated photodynamic agent. *Cancer Res.*, **2006**, *66*, 7225.

22. Gabriel, D. *et al.* Thrombin-sensitive photodynamic agents: a novel strategy for selective synovectomy in rheumatoid arthritis. *J. Control. Release*, **2009**, *138*, 225.

23. Koudinova, N. V. *et al.* Photodynamic therapy with Pd-Bacteriopheophorbide (TOOKAD): successful in vivo treatment of human prostatic small cell carcinoma xenografts. *Int. J. Cancer*, **2003**, *104*, 782.

24. Momma, T.;Hamblin, M. R.;Wu, H. C.;Hasan, T. Photodynamic therapy of orthotopic prostate cancer with benzoporphyrin derivative: local control and distant metastasis. *Cancer Res.*, **1998**, *58*, 5425.

25. Chen, B. *et al.* Effect of tumor host microenvironment on photodynamic therapy in a rat prostate tumor model. *Clin Cancer Res*, **2005**, *11*, 720.

26. Fleshker, S.;Preise, D.;Kalchenko, V.;Scherz, A.;Salomon, Y. Prompt assessment of WST11-VTP outcome using luciferase transfected tumors enables second treatment and increase in overall therapeutic rate. *Photochem. Photobiol.*, **2008**, *84*, 1231.

27. Chen, B.;Pogue, B. W.;Hoopes, P. J.;Hasan, T. Combining vascular and cellular targeting regimens enhances the efficacy of photodynamic therapy. *Int. J. Radiat. Oncol. Biol. Phys.*, **2005**, *61*, 1216.

28. Solban, N.;Selbo, P. K.;Sinha, A. K.;Chang, S. K.;Hasan, T. Mechanistic investigation and implications of photodynamic therapy induction of vascular endothelial growth factor in prostate cancer. *Cancer Res.*, **2006**, *66*, 5633.

Summary and Conclusions

The full success of PDT for the treatment of cancer and degenerative diseases has so far been restricted among others by two main limitations: incomplete ablation and unwanted side effects due to low PS selectivity to target tissue. In this thesis project, combination therapy and targeted drug delivery were investigated as strategies to overcome these drawbacks.

PART A. COMBINATION THERAPY

Chapter 1. Combination of Photodynamic Therapy with Anti-Cancer Agents

Combination therapies have often been recently accepted as a better treatment option for adequate cancer control and cure. This is not surprising since the disease is usually genetically instable and may also involve multiple pathological pathways. In addition, current chemotherapy presents in many cases the inconvenience of dose-limiting toxicity and resistance presumably enhanced by the fact that most anticancer agents react only through one mechanism of action. Other therapies such as immunotherapy may be insufficient as single treatment modality. PDT can kill cells directly, induce microvascular shutdown and trigger an immune response. This multiple mechanism has made of PDT an interesting modality, also in combination therapies in the treatment of diseases. *In vitro* and precilinical research on PDT combined with chemotherapeutics has clearly demonstrated improved outcomes as compared to those displayed by single therapies. On the other hand, PDT triggers the expression of angiogenic and cell survival factors, which may partially explain the incomplete response and tumor regrowth observed after PDT. The use of angiogenesis inhibitors after PDT has resulted in enhanced response and improved long term cancer control. Some advantages have been also observed for combinations of PDT and immunological therapy. Altogether, these studies give evidence for the large potential of PDT in combination with other therapies in the fight against cancer. Unfortunately, despite convincing data, this research has not yet overcome the barrier and been transferred into formal clinical studies.

Chapter 2. Synergies of VEGF Inhibition and Photodynamic Therapy in the Treatment of Age-related Macular Degeneration

Good control of CNV associated to age-related macular degeneration is currently achieved by PDT. Because inflammation and expression of cytokines such as VEGF are observed after PDT, repeated treatments and/or subsequent use of anti-VEGF and corticoid-like molecules are recommended. We were able to mimic the revascularization observed in patients after PDT treatment in the chick CAM model. Combination of PDT with angiogenesis inhibitors was studied in this model. A clear benefit of the combination was observed after exposure of PDT treated areas to the soluble receptor of VEGF, sFlt-1. The combination was more effective when the inhibitor was applied subsequently to PDT, 6 hours after, than before PDT. Extrapolation of this research suggests the combined use of PDT and agents targeting angiogenic cytokines as a synergistically improved therapy for patients with CNV secondary to AMD or cancer.

PART B. DRUG DELIVERY

Chapter 3. Urokinase-plasminogen-activator sensitive polymeric photosensitizer prodrugs: Design, synthesis and in vitro evaluation

Our second approach to improve PDT outcome corresponds to the design of drug delivery systems that increase the selectivity of PS to tumor tissue. We designed a urokinase-like plasminogen activator-sensitive agent that consisted of a poly-lysine backbone to which multiple copies of uPA cleavable PS peptide conjugates were attached. 25 units per 100 NH_2 were found to be optimal with respect to quenching and reactivation. As most of uPA activity is exerted at the membrane surface, different ε-lysine side chain modifications were performed in order to assure colocalization of the prodrug with the protease. These modifications also protect the backbone from unspecific cleavage and increase solubility of conjugates in pharmaceutically acceptable formulations. Quenching of fluorescence and ROS production was not significantly affected by the charge of these moieties whereas pegylation slightly decreased the observed quenching efficacy. Enzymatic activation was favored by positively charged side chain modifications representing a good compromise between fluorescence and ROS capacity, solubility and photodynamic inactivation in prostate cancer

cells *in vitro*. Attaching a single, high molecular weight mPEG to the polymeric cancer increased the selectivity for uPA-selective activation and might be beneficial with respect to the pharmacokinetic properties and passive accumulation in tumors.

Chapter 4. Modulating prostate cancer targeting of protease sensitive photosensitizer prodrugs by side chain modifications of the polymeric carrier

Whereas the positively charged conjugates targeting thrombin associated with rheumatoid arthritis have already shown selective accumulation in experimental animal models for this disease, similar conjugates optimized for uPA in the previous chapter have been further exploited in *in vivo* studies. However, after injection into PC-xenografted mice, this compound exhibited somewhat suboptimal accumulation in tumors. Therefore, additional efforts focused on modifications of the polymeric backbone to improve pharmacokinetic and biodistribution of the PS delivery system. Increased molecular weight further improved fluorescence and ROS quenching but did not result in better accumulation in tumors *in vivo*. Alternatively, new neutral poly-ethylene moieties, PEO_4 and PEO_8, were introduced instead of the previous positively charge N-methyl-nicotinic acid. Changes in the overall charge of conjugates from positive to neutral resulted in reduced but still appropriate PS quenching and solubility. Although *in vitro* activation was slightly decreased this modification significantly improved *in vivo* accumulation in PC tumors.

In particular, the conjugate with single PEG 20KDa and multiple PEO_8 modifications displayed high selectivity for tumor after 24 hours. Differences in fluorescence increase of this conjugate and its homologous non-cleavable D-control indicate passive accumulation of the cleavable conjugate and its site specific activation Moreover, a single irradiation of fluorescent tumors induced a strong reduction in cancer cell population which suggests that this compound is a good candidate for further PDT studies.

Chapter 5. Selective Photodynamic Therapy for the Treatment of Prostate Cancer through Targeting of Proteolytic Activity

Before further *in vivo* PDT studies, the photoxicity of the optimized prodrug, uPA-PPP, was investigated in a luciferase transfected prostate cancer cell line, PC-3M-luc-C6 and in the

corresponding wild type line. In both cell lines PDT led to a light and prodrug dose-dependent phototoxicity. However, PC-3M-luc-C6 cells were slightly more resistant to PDT than the wild type.

In vivo, uPA-PPP produced a strong photodynamic effect after irradiation of fluorescent tumors. Administration of the prodrug alone or light alone resulted in no or minimal effect on tumor growth, respectively. 3/4 animals in the PDT group completely responded to the treatment as no bioluminescence or tumor volume recovery was observed after treatment, until the end of the study. A reduction of more than 3-log values in the bioluminescence of tumors was necessary to cure the animals. The remaining animals of this group presented a tumor growth delayed by 15 days compared to the tumor growth of animals in the control groups.

The presence of the PS-peptidyl fragment, Pb*a*-GSGR, was confirmed in tumors using HPLC of tumor tissue extracts. This indicates that the prodrug was certainly activated in tumors. Negligible amounts of this fragment were found in neighboring skin. No activated prodrug was detected in muscle. Although activated prodrug was primary found in tumor tissue, selectivity of PDT with uPA-PPP for localized PC tumors and reduced side effect in neighboring tissue can only be confirmed in future studies in orthotropic models.

                                              ***

Despite the acceptance of PDT as efficient treatment for some selected indications, there is still place for improvement. In the present work we have followed two different strategies to (i) improve the therapeutic outcome of PDT using a combination approach and (ii) increase the selectivity of this treatment through targeting a physiological trigger that is intrinsic to cancer progression and proliferation.

Using the chick chorioallantoic membrane model we were able to demonstrate that the administration of anti-angiogenic agents subsequent to PDT treatment results in a synergetic effect and maintains the vascular occlusion over a longer period of time. Because PDT and angiogenesis inhibitors are both approved treatments for age-related macular degeneration, the association of both therapies could potentially improve to the current outcome of individual therapies with respect to vision gain and recurrence. Although we have focused preliminarily on the treatment of AMD in our studies, similar prinicles can be applied to the

treatment of cancer where the use of antiangiogenic agents is becoming more frequent. Therefore, such combination therapy may also be of benefit with respect to disease progression and survival in cancer.

We developed and optimized a PS prodrug sensitive to uPA. The current studies clearly demonstrate that although substrate selectivity plays a crucial role in the activation of our prodrugs, care must be taken with respect to the polymeric carrier to achieve selective activation *in vivo*. The optimized prodrug was (i) activated by uPA *in vitro* and PC cells expressing uPA; (ii) not toxic to PC cells in the dark but lethal in combination with light; (iii) able to be actived and to accumulate sufficiently in PC tumors *in vivo*; and (iv) in certain cases "cured" xenografted mice after appropriate dosage and irradiation. Activation of the prodrug was observed to be slight in adjacent tissue. However, selectivity and prevention of unwanted side effects in PC treatment should further be studied in orthotopic models.

Our previous studies have shown that the peptide linker may crucially influence the quenching efficiency. Therefore, alternative substrates targeting uPA may be exploited to achieve improved quenching and selectivity. As not all animals were cured in our single treatment PDT studies and bioluminescence gave a good indication of the possible therapeutic outcomes, a second dose of PDT should be envisaged in future studies. Alternatively, PDT may be administered at two different periods to induce vacular and cellular effects.

This research is a proof-of principle that demonstrates the feasibility of using combination therapy and targeted drug delivery as two different strategies that improve PDT in two specific applications. The first strategy applied to age-related macular degeneration, an already approved field of PDT; and the second, to a new promising PDT application which is the treatment of localized prostate cancer. However, the concept of combination therapy and protease sensitive prodrugs can be applied and adjusted to a wide spectrum of diseases. Furthermore, the use of both strategies together could be envisaged for more powerful and selective PDT treatments. As mentioned previously, alternative peptide substrates or spacer units between the polymeric carrier and the peptide substrate may further improve the accessibility to the peptide substrate. In our studies we have preliminarily used pheophorbide *a* as PS but alternative PS and/or the addition of supplementary dark quenchers can also be exploited. Finally, one has to take into account that further improvement should focus on the development of suitable carriers for clinical research. The used polymeric scaffold in these studies shows a relatively large size distribution. In principle it should be possible in the

future to prepare poly-L-lysine carriers of defined molecular weight with defined attachment point for the high molecular weight mPEG. However, due to the current chemical approach, the PS-peptide conjugates will be randomly distributed over the polymer. Therefore, more emphasis should be placed on the development of alternative scaffolds with defined molecular weight and attachment points. Today's diversity of orthogonal synthetic strategies might well solve this problem.

***

French Summary

La thérapie photodynamique (PDT pour photodynamic therapy) est actuellement considérée comme une alternative aux traitements actuels du cancer et des maladies dégénératives. La PDT consiste en l'administration systémique ou topique d'un photosensibilisateur (PS), suivie, après un intervalle de temps permettant une meilleure répartition de ce dernier entre tissu sain et malade, de son activation par irradiation du tissu cible à l'aide de lumière à une longueur d'onde appropriée. Le PS activé est ainsi capable d'interagir avec les biomolécules environnantes ou l'oxygène et produire des radicaux libres capables d'induire la mort cellulaire.

Néanmoins, dans le traitement de ces maladies, la PDT n'a pas obtenu un succès total à cause de deux principales raisons : une ablation incomplète du tissu malade et des effets indésirables liés à une faible sélectivité du PS vis-à-vis du tissu malade par rapport aux tissus sains.

Dans le cadre de ma thèse, deux stratégies différentes ont été retenues pour pallier à ces limitations, à savoir l'utilisation d'une thérapie combinée de la PDT avec d'autres modalités établies de traitement ainsi que l'augmentation de la sélectivité du traitement par ciblage de phénomènes physiologiques spécifiques à la progression et la prolifération du cancer.

Tout d'abord, au vue de la complexité physiopathologique du cancer, la thérapie combinée présente de nos jours de sérieux avantages par son action multiple comparée aux monothérapies. Par exemple, la sélectivité de la chimiothérapie est suboptimale et non spécifique et les cellules cancéreuses peuvent acquérir une certaine résistance au traitement.

La PDT quant à elle, peut selon les cas, détruire spécifiquement et directement des cellules tumorales, déstabiliser les vaisseaux sanguins irriguant la tumeur et d'activer une réponse immunitaire. Sa multiplicité d'actions en fait par conséquent une approche prometteuse dans le cadre d'une thérapie combinée.

Il faut toutefois tempérer ces avantages puisque la PDT peut également induire la surexpression de facteurs angiogéniques et de survie cellulaire. Ce qui est peut être la raison

pour laquelle, d'une part, certains patients atteints de cancer ne guérissent pas totalement et que des tumeurs peuvent parfois réapparaître. Et d'autre part, être à l'origine de l'inflammation et de la surrexpression de cytokines observées après le traitement par PDT dans le cas de la dégénérescence maculaire liée à l'âge (AMD pour age-related macular degeneration).

La PDT et l'utilisation d'inhibiteurs de l'angiogenèse sont deux monothérapies approuvées pour le traitement de l'AMD. A l'aide du modèle de membrane chorioallantoïque, nous avons pu démontrer un effet synergique du traitement par administration d'agents anti-angiogèniques après celui de PDT. En effet, contrairement à l'un ou l'autre des traitements seuls, la combinaison des deux permet d'observer le maintien de l'occlusion vasculaire pendant une période plus longue et donc une meilleure efficacité sur la déstructuration des vaisseaux sanguins. Leur association pourrait ainsi s'avérer bénéfique pour améliorer la vision de patients atteints d'AMD et de diminuer leurs récidives. Bien que nous ayons concentré nos efforts sur l'AMD, cette combinaison de traitement peut également être envisagée pour lutter contre le cancer.

Ensuite, notre seconde approche, toujours dans le but d'améliorer l'effet thérapeutique de la PDT, a consisté en l'élaboration d'un système de libération contrôlée du PS afin d'augmenter sa sélectivité vis-à-vis du tissu tumoral. Nous avons réussi à concevoir un agent spécifiquement reconnu par l'activateur du plasminogène du type urokinase (uPA pour urokinase-like plasminogen-activator). Il s'agit d'un polymère de poly-L-lysine sur lequel sont attachées, de manière covalente, de multiples copies du PS lui-même couplé à un peptide clivable par l'uPA. De plus, il a été précédemment déterminé qu'un couplage de 25 unités de PS-peptide pour 100 résidus NH_2 est un ratio optimal permettant d'atteindre un *quenching* du PS réversible et adéquat pour l'activation enzymatique. Comme la plupart de l'activité de l'uPA se situe au niveau de la surface membranaire, différentes modifications des chaînes latérales de lysine ont été effectuées afin d'assurer la co-localisation de l'agent et de la protéase. Des conjugués positivement chargés comportant des groups d'acide N-méthylnicotinique représentent un bon compromis d'un point de vue du quenching du PS, de la solubilité du conjugué ainsi que de son activation. Cependant, après leur administration dans un modèle murin sous-cutané de cancer de la prostate (PC pour prostate cancer), seule une faible accumulation de ces agents est observée dans les tumeurs. Par conséquent, une autre alternative a été envisagée : l'élaboration de conjugués composés cette fois de dérivés neutres de PE (polyéthylène). Cette modification a permis, dans ce même modèle, une nette

amélioration de leur accumulation dans les tumeurs. En effet, une haute sélectivité pour les tumeurs a même été observée 24 heures après injection de la prodrogue lorsqu'elle comporte une chaîne de PEG de 20 kDa ainsi que de multiples chaînes de PEO_8. Cette dernière est aussi bien activée par l'uPA seule *in vitro* que par les cellules du PC l'exprimant et ceci sans aucune action létale en l'absence de lumière. De plus, une accumulation et une activation suffisantes ont été observées au sein des tumeurs *in vivo* ainsi que la guérison de certaines souris traitées par des doses adéquates de prodrogue et de lumière. En ce qui concerne la sélectivité, seule une activation négligeable de la prodrogue a été observée dans les tissus avoisinants la tumeur. Cette étude démontre l'importance de la confection de la prodrogue pour son efficacité et son ciblage.

La recherche présentée dans cette thèse constitue une preuve de principe de la pertinence aussi bien de la mise en œuvre d'une thérapie combinée que de l'administration de médicaments ciblés. En effet, ces travaux ont permis d'améliorer la thérapie par PDT dans le traitement de l'AMD et d'encourager son utilisation pour le traitement du PC.

Ce concept de thérapie combinée et de prodrogues ciblées aux protéases, ainsi que leur utilisation conjointe, peut aussi être appliqué et ajusté à un plus grand nombre de maladies.

Abbreviations

5-ALA	: 5-aminolaevulinic acid
AlS_2Pc	: aluminum phthalocyanine
AMD	: age-related macular degeneration
BCA	: bacteriochlorin a
BCG	: bacillus Calmette-Guerin
bFGF	: basic fibroblast growth factors
BHA	: butyl hydroxyanisole
BPD-MA	: benzoporphyrin derivative monoacid ring A
BSO	: buthionine sulfoximine
CAM	: chorioallantoic membrane model
CNV	: choroidal neovascularization
COX-2	: cyclooxygenase-2
DIPEA	: N-diisopropylethylamine
DMXAA	: 5,6 Dimethylxanthenone-4-acetic acid
DU-145	: prostate cancer cell line
EAC	: Ehrlich ascites carcinoma
EDD	: embryo development day
EGFR	: epidermal growth factor receptor
ECM	: extracellular matrix
EMMPRIN	: extracellular matrix metalloproteinase inducer
G-CSF	: granulocyte-colony-stimulating factor
GM-CSF	: murine granulocyte-colony-stimulating factor
GSH	: glutathione
HATU	: O-(7-azabenzotriazol-1-yl)-*N, N, N, N*-tetramethyluronium hexafluorophosphte
HeLa	: human cervix carcinoma
HIF	: hypoxia inducible factor
HpD	: hematoporphyrin derivative
HPMA	: N-(2-hydroxypropyl) methacrylamide
HPPH	: hexylether pyropheophorbide-a
HT-1080	: human sarcoma cell line
IFN	: interferon
ICG	: indocyanine green
IL	: interleukin
MAPK	: mitogen-activated protein kinase

MC540	: merocyanine 540
Mce$_6$	: meso-chlorin e$_6$ monoethylene diamine
MCWE	: mycobacterium cell-wall extract
MMP(s)	: metalloproteinase(s)
MPM	: malignant pleural mesothelioma
m-THPC	: meso-tetrahydroxyphenylchlorin
m-THPP:	: meso-tetra (*p*-hydroxyphenyl)porphyrin
NF	: nuclear transcription factor
NIR	: near infrared
NK	: natural killer cells
NPe$_6$	: mono-L-aspartyl chlorine e6
OVCAR	: human epithelial ovarian carcinoma
PC	: prostate cancer
PC-3	: prostate cancer cell line
PC-3M-luc-C6	: luciferase transfected prostate cancer cell line
PEG	: poly-ethylene-glycol
PEO	: poly-ethylene-oxide
PDT	: photodynamic therapy
PG	: prostaglandin
PPC	: porphyrin platinum conjugates
PPCII	: porphyrin platinum conjugates second generation
PPP	: polymerc photosensitizer prodrug
PS	: photosensitizer
ROS	: reactive oxygen species
RTK	: tyrosine kinase
sFlt-1	: soluble VEGF receptor 1
TCC	: Transitional cell carcinoma
TIMP	: tissue inhibitor of metalloproteinase
TNF	: tumor necrosis factor
TUR-BT	: transurethral resection of bladder tumor
uPA	: urokinase-like plasminogen activator
VEGF	: vascular endothelial growth factor
VEGFR-1	: vascular endothelial growth factor receptor-1
ZnPC	: zinc phthalocyanine